Cross-reactivity of B and T cells: Desired in influenza vaccine responses, feared in autoimmune diseases

Inauguraldissertation
zur
Erlangung der Würde eines Doktors der Philosophie
vorgelegt der
Philosophisch-Naturwissenschaftlichen Fakultät
der Universität Basel

von

Marc Benjamin E. Bigler

aus Stettlen BE, Schweiz

Basel, 2018

Genehmigt von der Philosophisch-Naturwissenschaftlichen Fakultät

Auf Antrag von

Prof. Dr. Primo Schär, Fakultätsverantwortlicher
PD Dr. Christoph Berger, Dissertationsleiter
Prof. Dr. Christian Brander, Korreferent

Basel, den 26. Juni 2018

Prof. Dr. Martin Spiess
Dekan

Table of contents

FOCUS II: UNRAVELING ANTIGEN-SPECIFIC IMMUNE RESPONSES IN GIANT CELL ARTERITIS

Summary of the doctoral research

In my doctoral studies, I was studying cross-reactive adaptive immune responses in the context of autoimmunity and vaccination. The main focus was initially set on elucidating the mechanisms underlying the pathogenesis of giant cell arteritis. This work resulted in a publication challenging the usefulness of anti-14-3-3 antibodies as biomarkers for diagnosing GCA: A part of these autoantibodies seem to target epitopes revealed during immunopathology while others may be directed against a secreted protein of *T. gondii* (Kistner A & Bigler MB *et al.*, Rheumatology 2017). In a second publication, we showed that T cells recognizing *Varicella zoster virus* antigens are not more frequent in GCA patients. Moreover, we found no evidence for an increased self-reactivity of peripheral blood T cells from GCA patients (Bigler MB & Hirsiger J *et al.*, Arthritis & Rheumatology 2017). These data challenge a disease-triggering role of this virus as suggested by others. Finally, the molecular analysis of the T cell repertoire in the inflamed arteries yielded so far promising preliminary results, suggesting that indeed dominantly expanded clones can be found in the artery. The completion of this project will provide more information about disease-relevant antigens recognized by these expanded T cell receptors.

The main focus for the second part of my PhD-studies shifted to studying the influenza vaccine-induced cross-reactivity of B cell responses. I established a workflow for sorting of influenza-specific B cells, analyzing escape variants, and establishing a BCR sequencing pipeline. The data from this study suggests that a skewed B cell receptor repertoire aggravates escape from the vaccine response upon viral antigenic drift (Bigler MB & Egli SE *et al.*, in preparation). In an international collaboration, I also established a protocol for site-directed mutagenesis and production of influenza escape variants that will be applied in a prospective vaccination cohort that we started in 2017/18.

Finally, in a side project, I analyzed samples of a clinical trial on psychoactive drugs reflecting different types of stress. We found that pharmacological stress hormone release led to an increase of cytotoxic NK cells in the periphery. These NK cells were characterized by a typical surface receptor expression pattern, e.g. high expression of stress-relevant hormone receptors (Bigler MB *et al.*, PLoS One 2015). This paper (and some co-authorships for which I contributed experimental data) was not included in the cumulative thesis but is attached in the appendix.

Aim of the thesis

Innate immune mechanisms are very efficient at mounting rapid immune responses at the site of infection. Complete clearance of a pathogen and long-lasting protection through memory formation requires the adaptive immune system. To be able to cope with the large variety of pathogens we encounter, T and B cells acquire an almost infinite number of specificities by VDJ-recombination and somatic hypermutation. However, not all recombinations are equally likely to occur and the majority of lymphocyte clones will never be released from the thymus or bone marrow due to negative selection. T cells also need to recognize host HLA-proteins, adding further constraints. Therefore, immune cell diversity is more restricted than theoretically possible. A certain redundancy is induced by the fact that a T or B cell clone may recognize multiple epitopes, albeit with different affinities, a feature termed cross-reactivity.

In a vaccine against a genetically diverse pathogen, cross-reactivity of vaccine-induced immune cells is desirable. An ideal vaccine enables the host to mount an immune response not only against the vaccine strain but also against naturally occurring variants that may be antigenically different.
Influenza virus is one of the most prevalent human pathogens and of high economic relevance. The 'success' of influenza virus is tightly linked to its extraordinary ability to evolve – that is, evading the host's immune system – while still maintaining its integrity and virulence. Annually updated influenza vaccines provide some protection against infection. However, vaccine efficacy is strongly reduced when there is an antigenic mismatch between vaccine strain and predominant circulating virus.

We hypothesized that the cross-reactivity of the influenza vaccine response is affected by the individual B cell repertoire and wanted to test whether low cross-reactivity associates with a narrow repertoire. A narrow antibody repertoire could be related to the previous infection history or to repetitive vaccination with very similar influenza vaccine strains. Consequently, this may lead to higher susceptibility to emerging viral variants. The breadth and degree of antigen-specificity of the B cell receptor (BCR) repertoire can be assessed by sequencing the immunoglobulin heavy chains before and after vaccination. We tested this hypothesis by analyzing samples from a previous cohort of influenza-vaccinated healthy subjects and aimed to extend our findings by conducting a prospective clinical influenza vaccination study in individuals with known

vaccination history. Since the composition of the influenza vaccine is an active debate in the field, our results could inform on both strain selection and better vaccination strategies.

Cross-reactivity can be beneficial in the case of vaccination but may be harmful if cross-reactive lymphocytes target self-structures, as it is the case in autoimmunity. While B cells recognize native macromolecular structures, T cells mainly respond towards peptides displayed on MHC of antigen-presenting cells (APC). In Giant Cell Arteritis (GCA), a disease affecting medium-sized and large arteries, considerable infiltration of $CD4^+$ T cells is found in the affected vessels. Several lines of evidence suggest that these T cells are not just merely attracted to a site of inflammation, but rather might recognize a specific antigen. Whether this is a primary response against a microbial or self-protein or infection-induced cross-reactivity to self-proteins is currently unknown. In order to investigate antigen involvement in GCA pathogenesis, we used an antigen-centered approach to screen for T cell reactivity against self- and candidate viral antigens. Complementary, we used a T cell receptor (TCR)-based approach in order to investigate expanded clones and enriched CDR3-motifs in the affected arteries. Finally, taking advantage of our prospective GCA cohort study at the University Hospital Basel, we tested the antibody reactivity in newly diagnosed GCA patients against a self-protein proposed by others to be important in GCA pathogenesis. These results will help us to better understand the (early) disease pathogenesis and to find possible druggable pathways.

General introduction

Immunity and autoimmunity – infections as potential triggers of autoimmune diseases

Somatic recombination in adaptive immune cells provides us with an immense repertoire of antigen-specificities to be able to recognize the enormous range of foreign antigens. This goes along with an increased risk for recognition of antigens derived from self-proteins, thereby enabling autoimmunity. To reduce this risk, mechanisms termed central tolerance have evolved to delete T and B cells that bind too strong to self-antigens. In the medulla of the thymus, T cells are negatively selected by exposing them to self-protein-derived antigens on APCs and specialized mTECs (medullary thymic epithelial cells) [1]. Central tolerance of B cells is taking place in the bone marrow and can induce apoptosis in developing B cells or make them tolerant (non-reactive) to self antigen [2]. However, since these central selection or suppression mechanisms are imperfect, every individual harbors some functional autoreactive lymphocytes. The mechanisms that prevent T and B cells from reacting to self-antigens after their maturation are summarized as peripheral tolerance. These include regulatory T cells that can prevent the action of autoreactive T cells through inhibitory cytokines or surface receptors or by modulating APC-activation [3]. Peripheral B cell tolerance can be induced in the germinal center (GC) reaction in lymph nodes or the spleen [4]. Also, lymphocytes are physically hindered from entering certain zones of potential self-antigen encounter, e.g. through the blood-brain barrier [5]. Importantly, in the absence of an inflammatory response, dendritic cells (DC) are immature, present self-antigen and induce inhibitory signals to binding T cells eventually leading to cell death [6].

Owing to all these immunological checkpoints, the mere presence of autoreactive cells is usually not sufficient to induce an autoimmune disease; additional hereditary and environmental factors are necessary to break tolerance. A frequently reported hereditary factor predisposing to autoimmune disease such as rheumatoid arthritis, psoriasis and GCA is the HLA-locus [7,8]. Some HLA molecules thus might be especially efficient in presenting certain antigens to autoreactive T cells. Further evidence for the importance of the genetic background is coming from monozygotic twin studies. Exemplified, a Danish study reporting disease concordance for type I diabetes mellitus of 53% in monozygotic twins, but only 11% in dizygotic twins [9].

Concerning environmental factors, infections frequently precede onset of autoimmune disease. In some cases of molecular mimicry, that is, a shared epitope between a pathogen protein and a host protein, the immunological targets could be defined. For example, rabbits immunized with a peptide derived from the hepatitis B virus polymerase (HBVP) were shown to generate antibodies against both HBVP and host myelin basic protein (MBP), thereby inducing encephalitis [10]. Before onset of systemic lupus erythematosus (SLE), disease-relevant antibody reactivity against both the RNA-binding protein 60 kDa Ro and the Epstein-Barr virus (EBV) protein EBNA-1 has been reported in some patients [11].

Besides molecular mimicry, other mechanisms of infection-mediated autoimmunity have been proposed. Bystander activation is the accidental triggering of an autoreactive T cell by activated APCs or cytokines during an immune response targeted against an infection [12]. The release of endogenous epitopes through immune-mediated damage can lead to immune responses against these. This process is termed 'epitope spreading' and has been described in a multitude of diseases [12,13]. Intriguingly, allelic exclusion seems to work incompletely and human T cells have been found that co-express two different TCR alpha chains or beta chains [14,15]. These dual TCRs can theoretically possess pathogen-reactivity and autoreactivity. However, this has so far only been addressed in transgenic models [16].

Despite the numerous reports about the presence of autoreactive T and B cells in organs affected by autoimmune diseases, a clear causal link between a pathogen and autoimmunity has rarely been proved. This might be due to the reason that B cells react to antigens released by epitope spreading at the site of infection rather than through molecular mimicry. This would render testing of host-pathogen cross-reactivity impossible. In T cells, cross-reactivity between host and pathogen structures may simply have been missed. An elegant study showed that T cell clones reactive towards an HLA-DR2-restricted MBP-peptide proliferated also upon recognition of some viral peptides predicted to bind to HLA-DR2 [17]. Of note, the amino acid sequences of these peptides were often very different from the original peptide (degenerate), revealing a certain ambiguity in TCR-antigen binding. Thus, autoreactivity cannot be simply predicted by aligning pathogen-derived peptides with host peptides. This T cell degeneracy may on one hand increase the risk for infection-induced autoimmunity, but on the other hand may also increase cross-reactivity against related pathogens.

Generation of immune repertoire diversity: VDJ-recombination

Analyzing immune cell receptor repertoires in the context of B cell cross-reactivity and T cell antigen-recognition is a central part of this thesis. Given that B cell receptors (BCR) have properties beyond antigen-recognition, can undergo affinity maturation but share some basic features with T cell receptors (TCR), this introduction focuses on the generation of mature B cells and their BCR repertoire only. The concept of somatic rearrangement is translatable to the TCR.

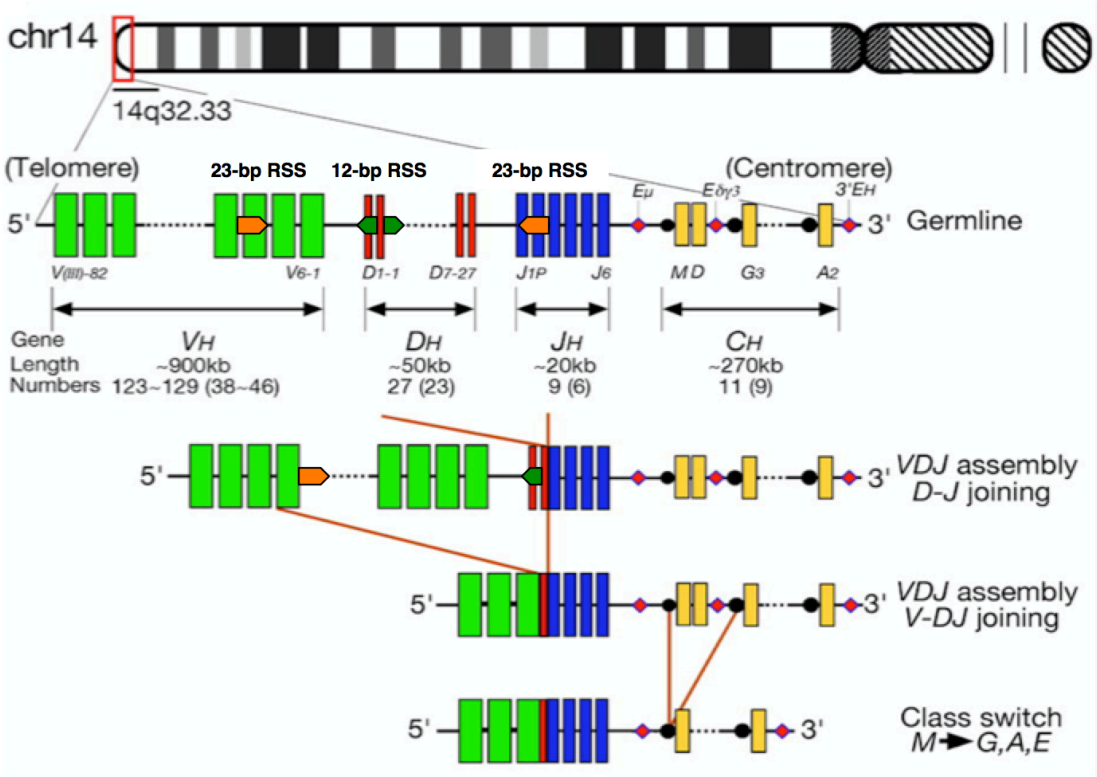

Figure 1: Genomic rearrangements at the IgH locus. The IgH locus is located towards the telomeric end of the long arm of chromosome 14. It harbors multiple variable (V_H, green), diversity (D_H, red) and joining regions (J_H, blue), many of them being non-functional pseudogenes. The D-J and afterwards V-DJ recombination requires the VDJ-recombinase complex, which includes the enzymes RAG-1 and RAG-2. The recombination signal sequences (RSS) include a 12-bp or a 23-bp spacer. A 12-bp RSS (green arrow) can only pair with a 23-bp RSS (orange arrow), thereby ensuring proper recombination. In naïve B cells, only two of the constant regions (C_H, yellow) are attached to VDJ by alternative splicing: Cμ (M) and/or Cδ (D) leading to an IgM and/or IgD isotype. Enhancers (E, pink diamonds) located upstream of the different C regions enable distant "donor" and "acceptor" chromosomal regions to come in close contact and initiate the genomic recombinations resulting in class switch to another isotype (more detailed in main text). Figure adapted from Dyer et al., Blood 2010 [18].

A complete BCR consists of two pairs of an immunoglobulin heavy and light chain. The heavy chain has a V (variable), D (diversity), J (junction) and a C (constant) region, the

light chain only has a V and J region. Each region is encoded by multiple genes that arose from gene duplication and underwent substantial differentiation. The rearrangement of V, D and J genes requires recombination of genomic DNA. This is, among many other proteins, initiated by RAG-1 (recombination activating gene) and RAG-2 resulting in recombination by non-homologous end joining (NHEJ). The importance of this step is clearly illustrated by the severe complications that arise when RAG-genes are mutated: The spectrum encompasses severe combined immunodeficiency (SCID) without T and B cells, immune dysregulation and T cell-mediated autoimmunity. VDJ recombination already induces considerable combinatorial diversity, which is further enhanced by the addition of random nucleotides at the recombination sites (junctional diversity). The C gene (Cμ, leading to an IgM-BCR) is spliced to VDJ on mRNA level [19]. (**Figure 1**: Overview of VDJ-recombination)

The generation of immature B cells takes place in the bone marrow. In order to enter the pre-B cell stage, a complete heavy chain in combination with a surrogate light chain needs to be expressed. This triggers the VJ-recombination of the light chain and eventually leads to the expression of a complete IgM-BCR. If a B cell is not deleted or rendered anergic (non-responsive) due to self-reactivity, it can enter the circulation as an immature B cell. These immature B cells become long-lived naïve B cells once passaged through the spleen where they receive BCR-mediated survival signals [20–22].

B cell affinity maturation and class-switch

Eventually, a naïve B cell may enter the B cell follicle of the spleen or a lymph node and encounter its cognate antigen presented on specialized APCs such as the follicular dendritic cells (FDC). If the B cell receives help from follicular T-helper cells recognizing the same antigen, a germinal center (GC) can form inside the follicle. Within the GC, the B cell is cycling between the dark zone (DZ) and the light zone (LZ). During this time, the activity of the enzyme AID (activation-induced cytidine deaminase) is elevated. AID-mediated deamination of cytosine to uracil takes place in the VDJ-region, increasing the likelihood of inducing mutations during the next round of replication (somatic hypermutation, SHM). The B cells mainly replicate in the DZ; afterwards, they are exposed again to their antigen in the LZ. Clones with mutations increasing their BCR-affinity proliferate faster, have therefore a selective advantage and may undergo further DZ-LZ iterations (and mutations). Finally, they are released and either become memory B cells or antibody-secreting plasma cells [4,21].

B cell class switch, i.e. the replacement of the Cμ or Cδ region by another C region, is a second AID-mediated mechanism promoting B cell diversity. The result is antibodies of other isotypes such as IgG1, IgA1 or IgE that are adapted to different tissue compartments. These can bind with varying avidity to components of the complement system [23] and can attach to Fc-receptors initiating cellular responses such as phagocytosis (ADCP) or antibody-dependent cellular cytotoxicity (ADCC) [24,25].

Class switch can be induced before GC-formation. Depending on the signals received, transcription is initiated upstream of Cμ / Cδ and other C-regions (e.g. Cα1 for IgA1 or Cγ1 for IgG1). A DNA-RNA-hybrid is formed which facilitates the recruitment of AID. As in SHM, subsequent action of uracil DNA glycosylase (UNG) results in an abasic site repaired by an error-prone form of the base excision repair (BER) pathway that may induce double-strand breaks (DSB). Alternatively, the MMR (mismatch repair) pathway recognizes the U:G base mismatches and creates DSBs during repair. The new C-region is then relocated downstream of VDJ by the NHEJ pathway [24]. Summing up, after their release from the bone marrow, B cells are selected for the best possible affinity towards their cognate antigen while also induced to produce the type of antibodies that may be most suitable to a particular type and site of infection.

FOCUS I: BREADTH AND LIMITATIONS OF THE INFLUENZA VACCINE-INDUCED IMMUNE RESPONSE

Introduction

Clinical, epidemiological and economic features of influenza

Influenza is a viral infectious disease of the respiratory tract that occurs seasonally in temperate zones, i.e. from late fall until early spring in the northern hemisphere. The characteristic flu symptoms are fever, cough, muscle and joint pain, sore throat and running nose. While most people recover within one week, the disease course can be very severe and an estimated number of 290'000 to 650'000 people succumb to complications from respiratory disease annually [26].

Risk groups more prone to develop severe disease or complications include the elderly, children younger than five years, pregnant women, patients with chronic diseases and immunosuppressed individuals. Of note, case fatalities due to influenza is highest in those above 65 years in industrialized countries, whereas infant death is much more common in developing countries [27,28].

Additional to the high disease burden, the economic impact due to healthcare costs, loss of workforce and lower workforce productivity is considerable. A model to predict the economic impact in case of an influenza pandemic included the population structure, epidemiology and current vaccine coverage. The estimate ranged from 71.3 billion to 166.5 billion US dollars for the US only [29]. Thus, the socioeconomic impact of the virus is vast and worldwide.

Influenza virus structure and life cycle

Influenza viruses are enveloped spherical viruses belonging to the *Orthomyxoviridae* family. They contain 8 segments of single-stranded, negative-sense RNA that encode up to 16 proteins. The segments PA, PB1 and PB2 encode parts of the viral RNA-dependent RNA polymerase (RdRp). HA is coding for hemagglutinin, the predominant surface protein of influenza virus, important for binding to the host cell and therefore infection. Neuraminidase (NA) is a second transmembrane protein especially important in release

of the virus. The viral ribonucleoproteins (vRNP) consist of vRNA-segments wrapped around NP (nucleoprotein) with the polymerase complex attached to the ends. M encodes the matrix protein M1 and the viral pore protein M2. The NS (non-structural) segment encodes proteins hijacking the host's spliceosome [30] and helping vRNP export [31,32]. Influenza virus structure is displayed in **Figure 2A**.

Influenza virus can attach to epithelial cells of the respiratory tract by binding of hemagglutinin to sialic acids (SA), the outermost structures on surface glycoproteins. The SA-galactose (Gal) bond on glycoproteins is different between mammals and birds and confers specificity for certain influenza viruses [33]. Following endocytosis, the endosome gets more acidic which enables the fusion peptide, a part of the HA, to mediate the fusion of viral envelope with the bilayer of the endosome [34]. Acidification of the virus lumen results in vRNP release [31,35].

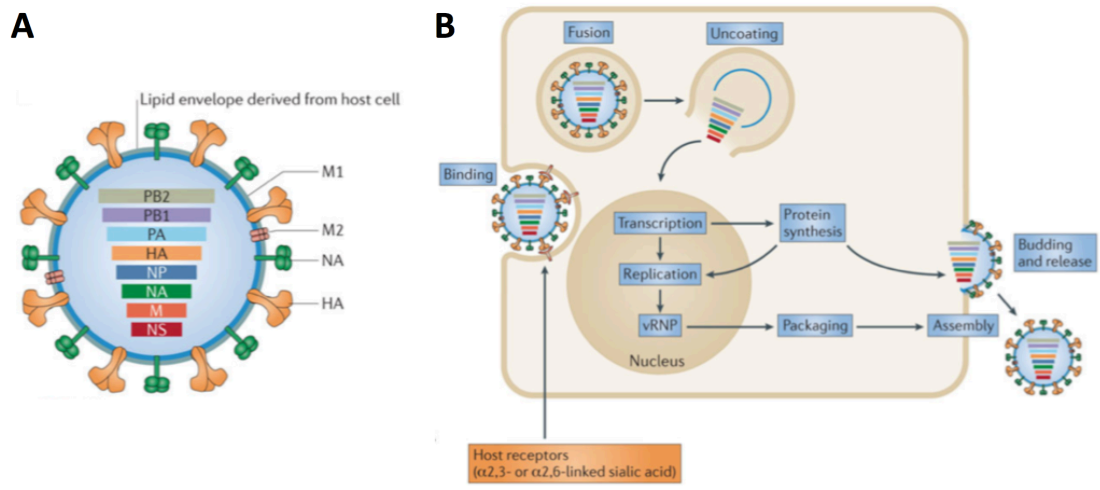

Figure 2: Influenza virus structure and life cycle. A) A schematic representation of an influenza virion. All eight viral RNA (vRNA) segments and all transmembrane proteins present on the virus surface are depicted. **B)** A simplified display of the viral replication cycle. Influenza virus extensively uses the host cellular machinery: Among other, RNA polymerase II synthesizes vRNA, ribosomes in the cytoplasm and the ER translate viral RNA and host proteases generate functional HA in released virions by cleaving it into HA1 and HA2 subunits. Figure adapted from Shi et al., Nat. Rev. Microbiology 2014 [36].

The vRNP contains nuclear localization signals that enable the import into the nucleus [37]. Complementary RNA (cRNA) is generated by RdRp and vRNA is synthesized by cellular RNA polymerase II [38,39]. 5'-capping and splicing is carried out by the host's

machinery, whereas polyadenylation is performed by RdRp [40,41]. The viral mRNAs are exported, translated, return as vRNPs to the nucleus and are re-exported by CRM1-dependent export [37]. The mRNAs of the membrane proteins HA, NA, M1 and M2 are shuttled through the ER – Golgi route and vRNPs and membrane proteins form mature virions at the plasma membrane [32,42].

The release of the virions by budding requires the action of NA: The sialic acids on the surface of the host cells need to be cleaved in order to disrupt the binding of HA to the glycoproteins [43]. HA-cleavage by host proteases into HA1 and HA2 subunits renders the virus infective [44] (Life cycle summary: **Figure 2B**). The humoral immune system can interfere with the viral life cycle by inhibiting viral entry and release, and also by disrupting membrane fusion and HA-cleavage [45].

Taxonomy, serotypes, hosts and strains

The Orthomyxoviruses include, among other genera, the influenza viruses A, B and C. The family is characterized by containing segmented negative-strand ssRNA as genetic material, expressing HA, NP and RdRP and possessing a lipid envelope [46]. Influenza A virus is able to infect a broad range of birds and mammals, including humans. Influenza B virus has only been isolated from humans and seals [47]. Influenza C virus is the rarest form; its hosts are humans and pigs [48].

Influenza A virus is the most abundant species causing influenza in humans. It is categorized into so-called serotypes of which only two are currently present in humans, H1N1 and H3N2. These serotypes are defined by the type of HA and NA expressed by the virus. All influenza A serotypes have their origin in avian influenza viruses [49]. Waterfowl are the main reservoir of Influenza A viruses and harbor mostly low pathogenic avian influenza viruses (LPAIV). Brigde species such as domestic poultry are usually necessary to enable occasional zoonotic spread of LPAIV to swine or humans [50,51]. Crossing of the species barrier happens quite frequently between swine and humans. This can lead to pandemics in case viruses reassort vRNA segments from different species, as it happened in the 2009 H1N1 pandemic [52]. While some viral mutations (e.g. in the HA receptor binding site or in PB2) have been associated with adaptation to another host species, the mechanisms required for bird-to-mammal or mammal-to-mammal host switch and stable transmission within the new host are

largely unknown [53]. Transmission among influenza A virus host species is summarized in **Figure 3.**

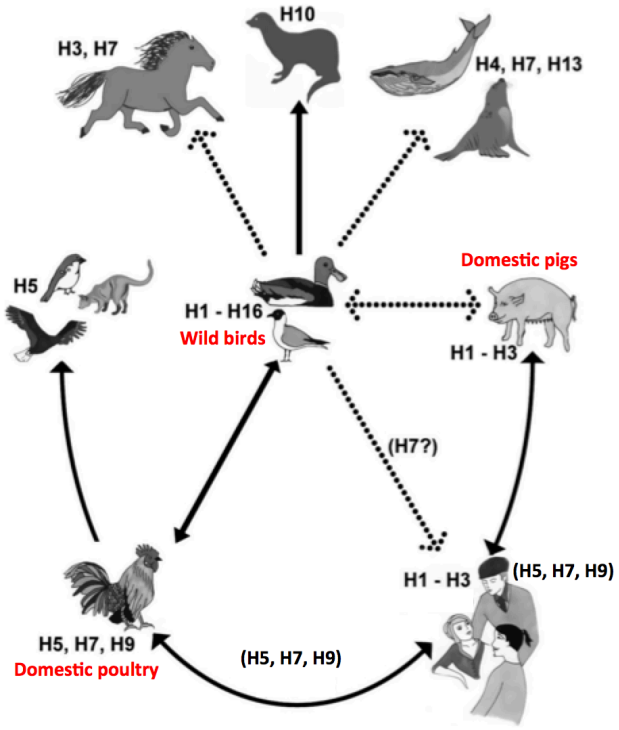

Figure 3: Zoonotic spread of influenza A virus. Waterfowl such as ducks and gulls harbor the broadest range of serotypes and constitute the main virus reservoir. Viruses originating from wild birds have been able to switch to and being transmitted within other wild and domestic mammals and birds. Within humans, only the H1N1 and H3N2 serotypes are currently circulating. Zoonotic spread to humans has been reported for H1N1 and H3N2 strains (from pigs), as well as for H5N1, H9N2 and different H7 serotypes (from poultry, rare). The latter is especially feared due to the occurrence of highly pathogenic influenza viruses (HPAIV). Figure adapted from Wahlgren, Infect Ecol, Epidemiol 2011 [54].

A standardized nomenclature is used to unambiguously name different influenza strains. It includes the genus, the host of origin (if not of human origin), the geographical origin, strain number, year of isolation and optionally the serotype in case of influenza A [55]. Examples below are obtained from the influenza database GISAID [56].

GISAID EPI_ISL_166859: A/Switzerland/9715293/2013(H3N2)
GISAID EPI_ISL_1463: B/Seal/Netherlands/1/99

For better readability, the strains mentioned in manuscript 1 are sometimes referred to as e.g. “Switzerland” instead of A/Switzerland/9715293/2013(H3N2).

The immune response against influenza virus

Influenza virus is directly transmitted from person to person through aerosols and droplets, which are formed e.g. through coughing or sneezing. Touching contaminated

surfaces (fomites), or direct contact with infected individuals can also lead to transmission [57]. The virus can reach the upper respiratory tract through direct contact or large droplets, while small droplets may also be able to reach the lower respiratory tract [58].

Like most pathogens, the virus is first recognized by the innate immune system. Infected cells sense the viral ssRNA by endosomal TLR7 and cytosolic RIG-I as well as NLRP3, a part of the inflammasome, resulting in signaling cascades leading to the production of the pro-inflammatory cytokines IL-1β, IL-6 and TNF-α and type I interferons, especially IFN-β [59,60]. Alveolar macrophages sense the virus through the same receptors and sustain the inflammatory milieu among other with production of nitric oxide [61]. Dendritic cells located below the airway epithelium barrier incorporate antigen through infection, endocytosis or phagocytosis and present it to T cells in the draining lymph nodes [62,63]. In the presence of non-neutralizing antibodies, Natural killer (NK) cells are able to eliminate infected cells by ADCC or directly through recognition of hemagglutinin on the cell surface [64].

One of the first effectors of the adaptive immunity in the antiviral response are IgA antibodies that opsonize the virus or interfere with the viral replication cycle [65]. IgM antibodies have an important function in activating the classical complement pathway [66]. Being located on the viral surface, HA and NA are the viral proteins mostly targeted by antibodies [67]. It is thought that IgG-antibodies with virus-neutralizing capacity, mostly interfering with HA functionality, are the most protective [45,68]. Nevertheless, many non-neutralizing antibodies are key in enabling Fc-mediated macrophage or NK effector function [69]. T cells are also involved in viral containment through conferring B cell help or via cytotoxicity towards infected cells. They recognize a wide variety of MHC-I restricted influenza virus peptides, most of them being derived from the intraviral proteins PB1, NP and M1. The specific peptides targeted, the breadth and the magnitude of recognition strongly varies with different HLA backgrounds [70–72]. Since the immunodominant T cell epitopes belong to highly conserved viral proteins, pre-existing immunity from cytotoxic T cells might be especially important in combating pandemic influenza viruses against which there is no pre-existing humoral immunity [73].

Influenza vaccine composition

Vaccination is an efficient way to reduce the risk for influenza. Currently, most of the marketed vaccines are produced as split vaccines (detergent-inactivated) containing either all viral proteins or only HA with or without neuraminidase [74]. The vaccines are annually updated in order to contain virus strains that were dominating in the previous season. Over the past decades, the vaccine always included a representative of the H1N1 and the H3N2 serotype and at least one influenza B lineage (Yamagata or Victoria), or more recently both of them in the quadrivalent vaccine available since 2014. Stabilizing agents and buffer salts in varying concentrations are included. Traces of detergents, sucrose and chicken egg proteins such as ovalbumin, all related to the vaccine production, may be found.

Compared to other virus or bacteria vaccines, the efficacy of the influenza vaccine is rather low. Estimates range between 20 and 60%, depending on the season and type of the vaccine but the range is even broader when separated by genus and serotype [75]. The low efficacy has been attributed to the high capability of the virus to evolve through antigenic drift and thereby evading the host's immune system [76]. Moreover, most current influenza vaccines are produced in fertilized chicken eggs. This can result in viral variants adapted to binding to avian-type sialic acids [77]. It has been shown that these variants can induce antibodies that are poorly binding to naturally occurring viruses [78–80]. The concept of original antigenic sin states that the antigens encountered earliest in life ("senior" antigens) will be preferentially targeted throughout life due to immunological memory [81,82]. Reduced vaccine efficacy in years where, compared to the previous season, identical or very similar strains were included in the preparation has been reported [83–85].

Hemagglutinin: Main antibody-target

Hemagglutinin (HA) is the most abundant protein on the viral surface usually present as a homotrimer. It is a transmembrane protein, has a molecular weight of around 60 kDa (monomer) and consists of the HA1 subunit (roughly defined as the "head") and the HA2 subunit (partly constituting the "stalk" or "stem") that are covalently attached through a disulfide bond. The receptor-binding site (RBS) on HA1 makes contact with the sialic acids present on the host cell and hence mediates endocytosis of the virus [86]. The HA2 subunit harbors the fusion peptide, a structure activated upon acidification of the

endosome, which enables the release of the virus into the cytosol [34]. Characteristics of Influenza A HA are shown on a surface representation of the protein (**Figure 4**).

Due to its exposed position, HA is the influenza structure that is preferentially targeted by antibodies, the head region much more frequently than the stalk region. Five regions on the head, designated A to E, are especially antigenic [87–89]. Consequently, the selection pressure is higher on the head region resulting in higher sequence variability in this area. From the virus perspective, a successful mutation leads to immune evasion through antigenic drift, while maintaining the fitness of the virus. It has been suggested that major changes in antigenicity (for influenza A H3N2) can be attributed to mutations in only seven amino acids adjacent to the RBS [90]. Due to its importance in viral-endosomal membrane fusion, large parts of HA2 are relatively intolerant to mutations and thus show a high degree of conservation [91]. This is also partly true for the RBS; but given its proximity to antigenic sites, the RBS is a primary target for antibodies and mutations requiring compensatory mutations have been described [91,92].

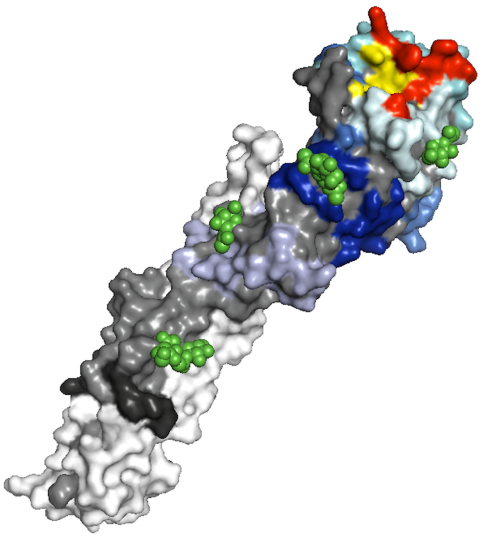

Figure 4: Surface representation of HA monomer from A/Victoria/361/2011 (H3N2). The HA1 subunit is shown in grey, HA2 subunit in white with the fusion peptide highlighted in black. The major antigenic sites (A – E, partly hidden) are depicted in shades of cyan and blue [87–89]. The receptor binding site [93] (yellow) is lined by seven amino acids causing major antigenic changes when mutated (red) [90]. HA is a glycoprotein with many N(Asparagin)-linked glycosylations that may alter antigenic properties. The innermost sugars (GlcNAc, N-Acetylglucosamine) are represented as green spheres. Figure created with Mac PyMol molecular graphics system, version 1.7, Schrödinger LLC. PDB ID: 4O5N

Assays to characterize the antibody response against influenza virus

Neutralizing antibodies mostly target HA and may interfere with any step of the viral replication cycle. They consist of antibodies (i) abrogating the association of the RBS of HA with sialic acids, (ii) inhibiting virus-endosome fusion, iii) block proteolytic HA-cleavage or (iv) interfering with viral release through virion cross-linking or interfering

with Neuraminidase function [45]. Non-neutralizing antibodies do not interfere with viral replication but can exert complement- or Fc-mediated effects to remove infected cells. Broadly neutralizing (bnAbs) or non-neutralizing antibodies in addition are able to target a very wide spectrum of related strains.

The hemagglutination assay and the hemagglutination inhibition assay (HAI) are standard techniques to measure the amount of virus or influenza-specific antibodies in the serum. When influenza virions are mixed in a microtiter plate with erythrocytes, the HA on the viral surface binds to the sialic acids on the erythrocytes' surface, thereby forming a lattice. This process is called hemagglutination. By keeping the amount of erythrocyte fixed and serially diluting the virus, the virus titer can be deduced. The virus titer is defined as the highest dilution, where the amount of virus is sufficient to induce hemagglutination. In higher dilutions, the erythrocytes form a pellet on the bottom of the plate.

HAI is an extension of the hemagglutination assay described above. Here, the amount of erythrocytes and virus are fixed and serum is serially diluted into the plate. The HAI titer is defined as the highest serum dilution where hemagglutination is prevented [94] (**Figure 5**). The higher the HAI titer, the higher is the amount and avidity of HA-specific antibodies. The HAI titer does not give information about all HA-specific and possibly neutralizing antibodies, but is restricted to neutralizing antibodies interfering with the RBS. Nevertheless, since HAI titers above 40 (that is, 40-fold serum dilution or more) were shown to confer protection in more than 50% of experimentally infected individuals, HAI is a very frequently used technique [95].

Since it measures the ability of the virus to infect target cells, the microneutralization assay is a powerful tool to detect all neutralizing antibodies against influenza. Brief, serum is serially diluted in a microplate and fixed amounts of virus are added to the wells. After two hours of incubation, virus-antibody mixtures are added to MDCK cells for over night incubation. Following fixation, the degree of infection is then assessed by ELISA, e.g. by staining for influenza NP. Similar to HAI, titers are calculated based on the highest serum dilution without apparent viral infection [96].

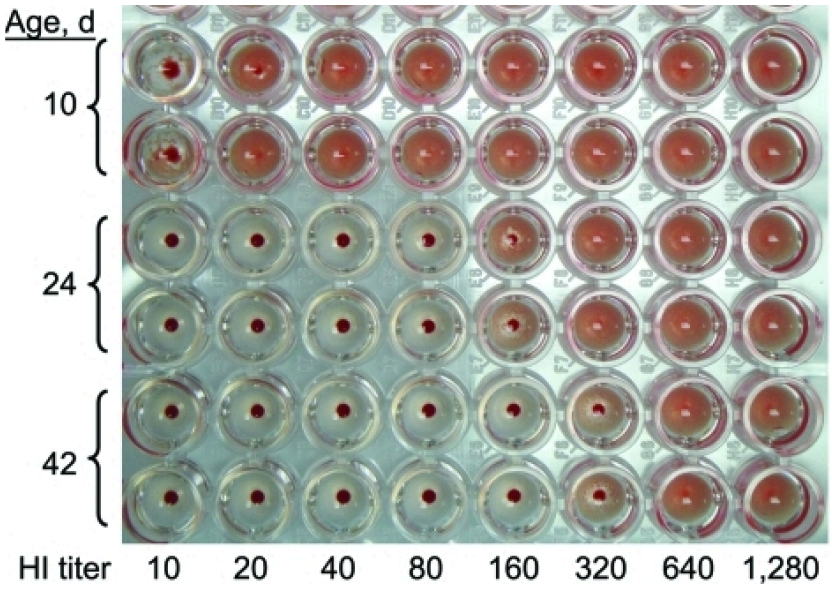

Figure 5: Hemagglutination inhibition assay. Serum stems from a newborn infected with pandemic H1N1 2009 virus 10, 24 and 42 days after birth. First, serial dilutions of HA-depleted serum are given to the microtiter plate, followed by addition of a fixed amount of virus. After 30 minutes of incubation at room temperature, samples are mixed with turkey erythrocytes and incubated for another 30 minutes at room temperature. HAI titers (here: HI titers) are defined as the highest serum dilution (or the reciprocal thereof) where hemagglutination is inhibited. On the plate above, titers are 10 at day 10, 160 at day 24 and 320 at day 42.

In order to characterize breadth of influenza-specific antibodies, the response against multiple viruses has to be tested. This is not feasible with the abovementioned techniques. A multiplexed assay allows to analyze binding of broadly cross-recognizing antibodies. Multiple microspheres (beads) with different fluorescence properties are covalently linked with HA from different strains. These beads are simultaneously exposed to serum antibodies, which are then detected with a fluorescent secondary antibody. The antibody signal per bead type enables the analysis of cross-reactive antibodies against a set of HA [97]. These bead-based assays have been widely used in assessing vaccine-induced antibody cross-reactivity, including the flu vaccine [98–100]. While informing about the breadth of the vaccine-induced antibody response, such multiplexed assays do not measure neutralization capacity of these antibodies.

Influenza virus evolution

The relatedness between two viruses (or any organisms) can be measured by the genetic distance, that is, the amount of mutations or polymorphisms that separate a

specific virus from another one. In the case of influenza virus, it is the HA segment that diverges most between viral isolates. These differences can be represented in phylogenetic trees where each node usually corresponds to a non-synonymous mutation. Isolates of influenza viruses bearing the same amino acid change or set of amino acid changes are clustered into specific clades or subclades (see **Figure 6**).

The genetic distance does not always correlate with antigenic distance. More precisely, two viruses that are phylogenetically separated by many mutations may be equally well recognized by the immune system. On the other hand, a virus variant with a single point mutation may be poorly recognized by the immune system; the antigenic distance is large.

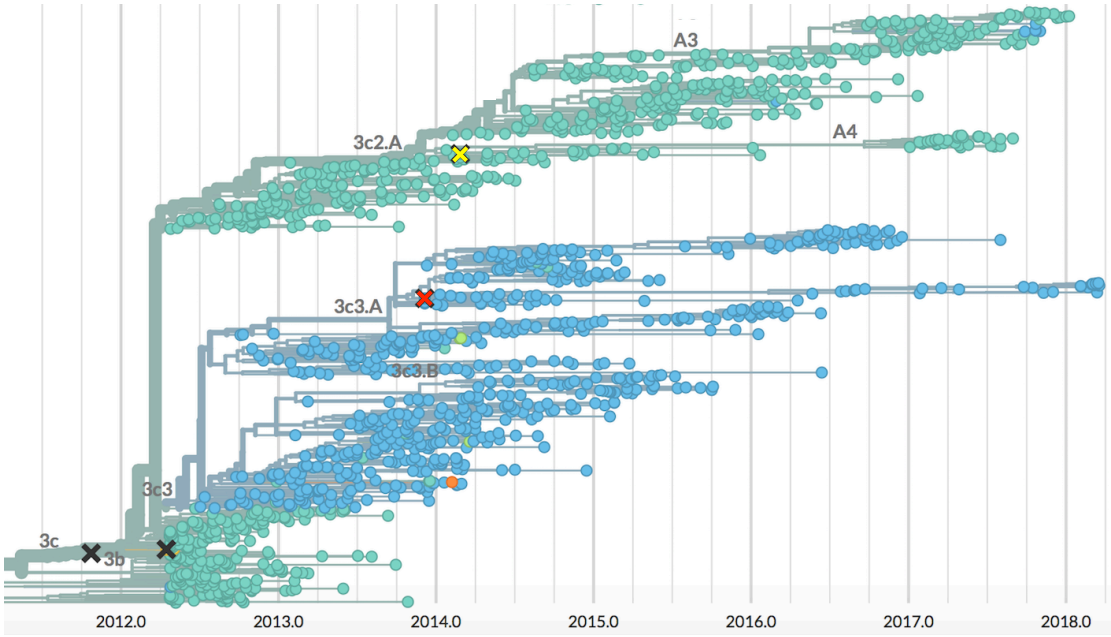

Figure 6: Phylogenetic tree of HA from Influenza A H3N2 virus. Strains (sequence source: GISAID) isolated from all over the world between April 2012 and April 2018 are depicted as colored dots. Strains are colored for amino acid HA1 128, where blue is alanine, turquoise is threonine and other colors represent other rare amino acids. Clades are labeled in grey; the 2015/16 vaccine contained the 3c3.A representative A/Switzerland/9715293/2013, marked with a red cross. The vaccines in the following years contained a genetically different virus, A/Hong Kong/4801/2014 in clade 3c2.A, marked with a yellow cross. Figure created with nextstrain tool [101].

The visualization of antigenic distance in antigenic maps was introduced by Smith and colleagues [102] based on concepts proposed by Lapedes and Farber [103]. The maps are based on one single method to determine antigenic distance, the hemagglutination

inhibition assay. Usually, the sera of infected influenza-naïve ferrets are used. Briefly, the HAI titers against a multitude of e.g. H3N2 viruses derived from matching and non-matching antisera are used to determine antigenic distance between single viruses. An antigenic distance of 1 corresponds to a difference of a twofold dilution of antiserum in the HAI. Viruses are grouped in antigenically distinct clusters with the main antigenic changes being induced by mutations in only 7 residues [90]. An antigenic map for influenza A H3N2 viruses is shown in **Figure 7**.

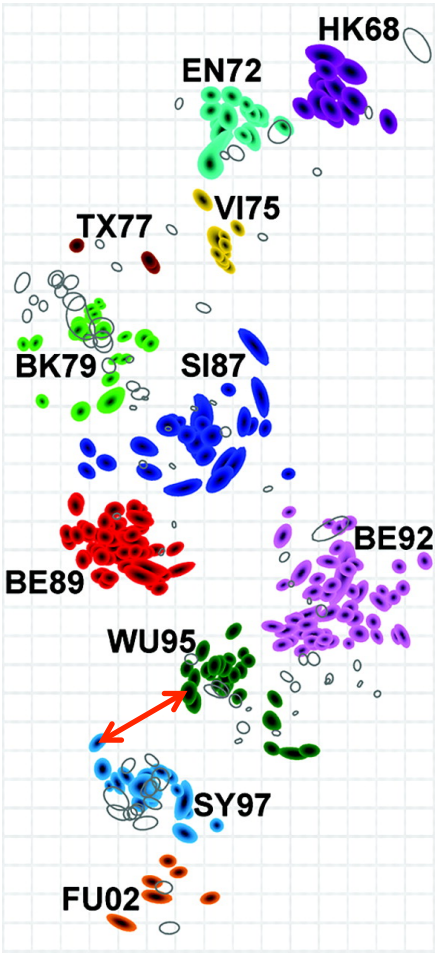

Figure 7: Antigenic map of H3N2. Each color defines a cluster of antigenically similar H3N2 viruses from their emergence in 1968 until 2002. A subset of these viruses was used to infect ferrets in order to retrieve antisera. HAI titers were generated by exposing each virus in the map to antisera derived from the same strain, as well as closely and distantly related strains. Based on the titers, the strains can be placed in a two-dimensional map where the spacing between grid lines corresponds to a twofold difference in HAI-titer. Example: The distance between the viruses connected by the red arrow is approximately 3, corresponding to an eightfold difference in HAI-titer. Open shapes are antisera; shape size depicts the confidence area. Map adapted from Smith et al, Science 2004 [102].

Pre-existing immunity

The exposure history of influenza infections endured and influenza vaccinations obtained, combined with the individual immunological status complicates the analysis of influenza vaccine responses in humans. Consequently, it is very difficult to predict if, and how much an individual would profit from vaccination. Some general observations

are that infections induce more cross-reactive immune responses and longer lasting memory compared to vaccination [104]. Also, antibody affinity and neutralization capacity slightly decrease with age [105]. Finally, in the special setting of infection with a recombined, pandemic virus, most people have no pre-existing humoral immunity but may be partially protected by T cells targeting conserved epitopes [73].

The so far most comprehensive study on the impact of pre-existing immunity on antibody response towards antigenically different viruses shows the extent of cross-reactive antiviral responses (towards H3N2 viruses from 1968 to 2010) in relation to age, vaccination/infection status and longitudinally within individuals [106]. Individual or group data was represented as an antigenic landscape, an extension of the antigenic map and plots human HAI-titers on top of the ferret-derived antigenic distance data (**Figure 8**). Some of the main findings:

- Pre-vaccination titers are usually not highest against the current antigenic cluster, but rather against the one before or the penultimate
- Without vaccination or infection, the antigenic landscape is remarkably stable across six years
- Upon infection with a H3N2-virus, titers increase against recent viruses, but often also against very distant clusters
- Vaccination with a virus belonging to an antigenic cluster to which there has been a few years of exposure leads to a "backboost", similar to infection, but limited cross-reactivity to the most recent cluster
- Vaccination with an antigenically novel virus both increases titers against novel viruses and leads to a backboost
- The latter holds true for two risk groups: The elderly and those with pre-vaccination titers below 40

Summing up, these data suggest that vaccination with antigenically advanced variants is beneficial even if the circulating strains turn out to be of a pre-existing antigenic cluster.

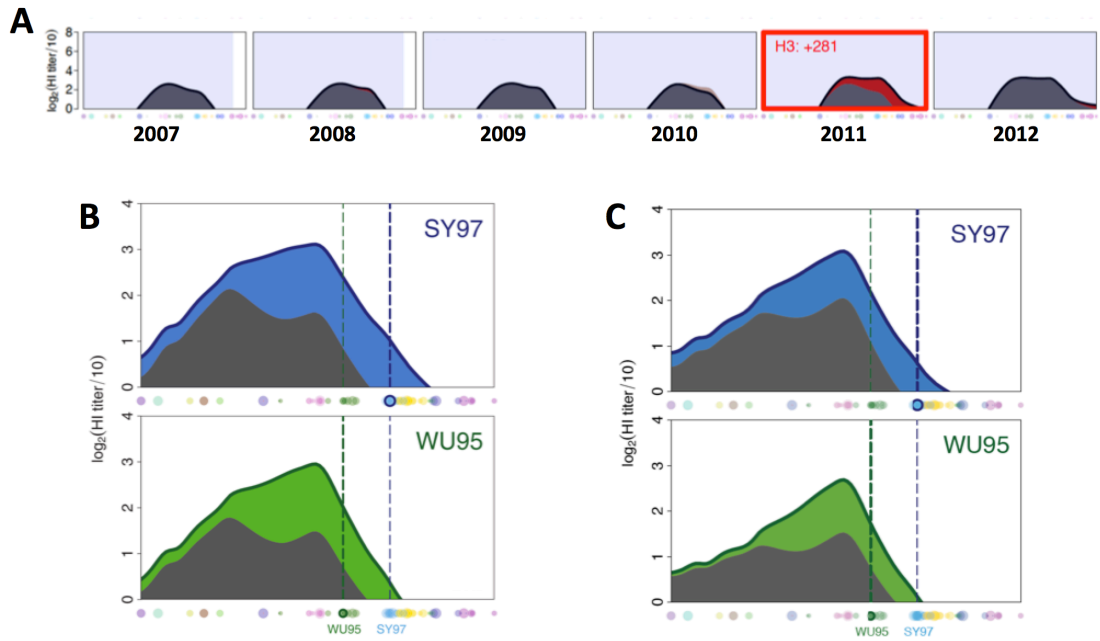

Figure 8: Antigenic landscapes of unvaccinated and vaccinated individuals. A) Antigenic landscapes from 2007 - 2012 of an unvaccinated donor of Vietnamese origin. On the x-axis, H3N2 viruses representing 14 antigenic clusters from 1968 – 2011 are depicted according to their antigenic distance. HAI titers across clusters are shown as grey-shaded area and show a remarkably stable pattern until 2011, when the subject was diagnosed with H3N2-infection (281 days before serum sample was taken). Changes in titers compared to the previous year are shown in red (increase) or brown (decrease). **B)** Summary HAI-data from Australian vaccination cohorts either vaccinated 1998 with a strain from the antigenically advanced "Sydney" cluster (SY97) or 1997 with a strain from the prevailing "Wuhan" (WU95) cluster. A backboost in HAI titers towards older clusters is observed with both vaccines (blue- and green-shaded area), but the titer increase against current and future clusters is higher with the "Sydney"-variant. **C)** The same holds true for cohort participants >60 years old.

Manuscript 1

Escape from the H3N2 influenza vaccine response due to a single amino acid change relates to a restricted memory B cell repertoire

Escape from the H3N2 influenza vaccine response due to a single amino acid change relates to a restricted memory B cell repertoire

Marc B. Bigler[1], Simon B. Egli[1], Julia Hirsiger[1], Chanson Brumme[2], Mohammadyaseen Syedbasha[3], Gideon Hoenger[4], Matthias Mehling[5], Mike Recher[6], Ulrike Menzel[7], Nicholas Sanderson[8], Sai T. Reddy[7], Victor Greiff[9], Christoph T. Berger[1,10]

[1] Translational Immunology, Dep. of Biomedicine, University Hospital Basel, Basel, Switzerland
[2] British Columbia Centre for Excellence in HIV/AIDS, Vancouver, BC, Canada
[3] Applied Microbiology Research, Dep. of Biomedicine, University Hospital Basel, Basel, Switzerland
[4] Transplantation Immunology and Nephrology, University Hospital Basel, Basel, Switzerland
[5] Translational Neuroimmunology, Dep. of Biomedicine, University Hospital Basel, Basel, Switzerland
[6] Immunodeficiency, Dep. of Biomedicine, University Hospital Basel, Basel, Switzerland
[7] Department of Biosystems Science and Engineering, ETH Zürich, Basel, Switzerland
[8] Clinical Neuroimmunology, Dep. of Biomedicine, University Hospital Basel, Basel, Switzerland
[9] Department of Immunology, Faculty of Medicine, University of Oslo, Oslo, Norway
[10] Clinical Immunology, Dep. of Internal Medicine, University Hospital Basel, Basel, Switzerland

Abstract

Background: Rapidly evolving pathogens are prone to evade vaccination-induced immune responses. Individual antibody repertoires may predict susceptibility to viral escape. Here, we aimed at investigating the extent of vaccination-induced antibody cross-reactivity against multiple vaccine strains and its relationship with viral sequence homology and the host's B cell immune repertoire.

Methods: By means of a multiplex immunoassay, we profiled a 2007/08 influenza vaccine cohort for antibody responses targeting the Influenza A hemagglutinin (HA). The response to the strains contained in the respective vaccine and to influenza A viruses with different phylogenetic relatedness (five H1N1, eight H3N2) was assessed to estimate cross-protection. The antibody repertoire was interrogated by BCR sequencing of memory B cells and plasmablasts in a subset of 12 subjects pre- and post-vaccination. Effects of repeated antigen exposure by vaccination were investigated in a second cohort in the 2017/18 influenza season.

Results: HA cross-recognition was partly dependent on the pre-existing antibody levels and the phylogenetic distance. Importantly, however, the T128N mutation resulted in a glycosylation change between the closely related HAs of H3N2 A/Victoria/361/2011 and A/Texas/50/2012 and reduced the antibody response by more than half. This was most pronounced in vaccinated subjects with a skewed antibody repertoire of their pre-vaccination memory B cells. Comparison of different vaccination cohorts between 2008 and 2018 indicated that vaccination with an N128-containing vaccine strain in 2014/15 induced a response targeting this HA region. This recognition was however lost again in 2017/18, indicating that no robust memory against this novel epitope was induced.

Conclusions: Vaccination induces cross-reactivity against influenza strains closely related to the vaccine strains. Low antibody diversity might however make the response prone to escape by mutations at immunodominant sites. We propose an antigenic site that might be poorly recognized at population level if the respective clade expands.

Introduction

Vaccination is a highly effective intervention to reduce infectious diseases at low costs. Mass vaccinations led to the containment or even elimination of pathogens from populations, saving millions of lives [1]. Vaccinations aim at protecting from infection, ideally by inducing pathogen-neutralizing antibodies that interrupt the viral replication cycle [2,3]. In pathogens with a very high replication rate, such as influenza or HIV, mutations in genes encoding for viral surface glycoproteins occur frequently. When such mutations affect antibody-binding sites, this may result in poorer recognition of the virus, a process commonly referred to as antigenic drift. Therefore, pathogens with a high number of related, but antigenically distinct strains remain a challenge to vaccine design [1].

Influenza virus is a highly variable virus, which can cause severe respiratory tract infections. It infects 5 to 10% of all adults and 20 to 30% of all children annually, hence, immunity against the virus is present in most individuals already at a young age [4,5]. Influenza A virus infection accounts for most seasonal influenza epidemics [6]. Based on two surface proteins, hemagglutinin (HA) and neuraminidase (NA), influenza A viruses are subdivided into different serotypes, of which only H1N1 and H3N2 are currently circulating in humans [7].

Regularly updating the influenza vaccine composition to match currently circulating strains and yearly vaccinations aim at counteracting viral escape [6]. Vaccine effectiveness (VE) in an individual is typically estimated by applying an assumed surrogate of protection. For influenza vaccination, a hemagglutination inhibition (HAI) IgG titer >1:40 is considered protective, although specifically it provided 50% protection from experimental infection in young healthy subjects [8]. In a real-life setting, titer-based protection is lower [9]. VE estimates based on the comparison of the odds of vaccination between patients with influenza-like symptoms positive or negative for the virus are more reliable (test-negative design) [10,11]. Such estimates vary strongly between influenza serotypes, but overall effectiveness ranges from 20 to 60% depending on the year [12–17].

Vaccine-induced antibodies generally neutralize homologous strains within a given serotype, but can only provide a certain degree of cross-protection against more distantly related circulating strains [18]. Currently, more than half a year is required from candidate strain selection until vaccine marketing. This substantially increases the risk for a mismatch between the epidemic viruses and the vaccine viruses selected based on

surveillance data from the previous season [19]. Moreover, the viruses included in influenza vaccines are propagated in fertilized chicken eggs. This can result in vaccine virus adaptation to avian-type receptors, which may induce poorly binding antibodies [20,21]. Taken together, fast virus evolution, time lag and mode of vaccine production contribute to the relatively poor clinical efficacy of the seasonal influenza vaccine.

The individual cumulative exposure history of natural influenza contacts and/or vaccination shapes the influenza-specific adaptive memory [22]. While natural infections induce a long-lasting, broad immune response, the influenza vaccine response is skewed and of limited duration [23]. The vaccine-induced memory response is influenced by age, previous infections, vaccinations and vaccine types [24–26]. A 'back-boost' effect of the antibody response towards viral strains encountered early in life has been well characterized [27,28], exemplarily demonstrated in the better ability of elderly people to neutralize the reassorted A(H1N1)pdm09 strain after the 2009 pandemic [29]. This suggests that the benefit of a vaccination depends on the exposure history of the host. High-throughput B cell receptor (BCR) sequencing can be used to assess the antibody repertoire and track the expansion and contraction of B cell lineages (clonotypes) upon influenza vaccination [30,31]. The expanded lineages are constituted of replicating memory B cells and antibody-secreting plasmablasts, both being highly enriched in influenza-specific clonotypes [32,33]. The high degree of somatic hypermutation (SHM) suggest that the majority of influenza-specific B cells derive from the memory pool [32]. However, *de novo* recruitment is critical to control rapidly evolving viruses and probably is especially important in elderly people who tend to have a narrowed BCR repertoire with high levels of SHM [34]. So far, it is unknown whether the degree of cross-reactivity is reflected in the BCR-repertoire. Repeated challenge with very similar antigens may skew the antibody response towards conserved elements and prevent *de novo* responses (concept of the 'original antigenic sin') [35,36]. Indeed, repeated H3N2 vaccination with a low degree of antigenic variation between vaccine strains was reported to reduce VE [37,38] and, irrespective of antigenic variation, reducing HAI titers [39].

In this study, we aimed at characterizing the breadth of B cell responses in vaccinated healthy donors. The degree of antibody cross-reactivity against HA of influenza vaccine and closely related strains was assessed upon vaccination and related to the phylogenetic distance to the vaccine strains. Further, the relationship of cross-reactivity with the individual's antibody repertoire was investigated. Finally, we analyzed an HA variant that escaped vaccine-induced humoral immunity.

Methods

Vaccination cohort and clinical samples

Within prospective influenza vaccination cohorts of the seasons 2007/2008 [40] and 2017/18, samples from healthy adults were analyzed. All subjects gave written informed consent and the study was IRB-approved. Clinical characteristics of both cohorts are summarized in **Supplementary Table S1**. In addition, samples from various other influenza vaccination cohorts at the University Hospital Basel were used as indicated in the respective sections: 2008/2009 [41], 2009/2010 [41], and 2014/15 (*unpublished*). All subjects had no acute illness and no other vaccinations in the previous 30 days. In 2007/08, all participants received vaccination with a trivalent virosomal vaccine (Inflexal V, Berna Biotech, Basel, Switzerland), whereas in the other seasons a non-adjuvanted trivalent (2008/09 and 2009/10, Mutagrip, Sanofi Pasteur SA, Lyon, France) or quadrivalent (2014/15 and 2017/18) split vaccine was used (Agrippal, Seqirus, Maidenhead, UK and Fluarix Quadrivalent, GSK, Philadelphia, PA, USA respectively). For the individuals included in the 2017/18 cohort, vaccination history and influenza-like illness (ILI) back to season 2012/13 were assessed using a standardized questionnaire. Plasma and peripheral blood mononuclear cells (PBMC) were collected immediately prior to vaccination and at day 7 and day 28 post-vaccination. For the 2007/08 cohort, an additional sample from day 14 was available. Samples were cryopreserved until use.

Recombinant Influenza A Virus Hemagglutinin

Full-length (HA0) recombinant hemagglutinin (rHA) reflecting the influenza A H1N1 and H3N2 strains included in the seasonal influenza vaccine from 2000/01 to 2014/15 were ordered (Sino Biological Inc., Bejing, China). Additionally, two pandemic influenza strains, i.e. an H1N1 strain from 1918 (A/Brevig Mission/1/1918) and an H3N2 strain from 1968 (A/Hong Kong/1/1968) were included as comparators resulting in a set of 13 rHA (overview in **Figure 1A**). Based on the commercial availability, the five influenza A H1N1 rHA were expressed in HEK cells and the eight influenza A H3N2 strains in an insect baculovirus expression vector system (BEVS). H3N2 A/Perth/16/2009 was not commercially available at the time of the study design. For specific rescue experiments, HEK-cell produced rHA-proteins (HA1 subunit) of the H3N2 A/Victoria/361/2011 and A/Texas/50/2012 strains, as well as a custom-made Texas N128T HA (reverse mutant) were used (all Sino Biological Inc.). The very same proteins were used to assess escape and rescue in the 2017/18 cohort. Detailed information is available in **Supplementary Table S2**.

Multiplexed immunoassay

The influenza A rHA of the different influenza A strains were coupled to different MagPlex® microspheres (Luminex corporation, Austin, TX, USA), hereafter termed 'beads' throughout the manuscript. Coupling was performed mainly according to xMAP® cookbook (Luminex). An extended protocol and a detailed description of the validation are available in the **Supplementary Methods**. To measure the HA-specific antibodies, plasma samples were first centrifuged at maximum speed and then diluted 1:500 in PBS with 1% BSA (PBS-BSA). 20 µL of diluted plasma was added to 20 µL of the bead mixture containing 13 different HA beads and BSA-coated control beads in a 96-well plate and incubated for 60 minutes at RT on a plate shaker at 800 rpm. The beads were washed twice in 100 µL of PBS-TBN buffer and then incubated with a PE-labeled mouse anti-human IgG Fc antibody (clone JDC-10, 9040-09, SouthernBiotech, Birmingham, AL, USA) for another 30 minutes. Binding of influenza-specific IgG antibodies was measured on a Luminex® 100 analyzer running on xPonent® software (Luminex Corporation). The extent of antibody-binding is represented by the PE median fluorescence intensity (MFI). The vaccine response was calculated as background-corrected (BSA-coated beads) ΔMFI day 28 - day 0. Vaccine response against HA of the H1N1 and H3N2 vaccine strains was set to 1 and responses against the other strains were scaled to the respective vaccine strain response for each subject (negative values were set to 0). Donors with a ΔMFI < 25 against the vaccine strain were considered non-responders and excluded from data analysis. GraphPad Prism v.7 (GraphPad Software, La Jolla, CA, USA) was used for statistical analysis and data presentation.

Influenza virus HA homology and phylogenetic analysis

Influenza nucleotide sequences were accessed through the NCBI's influenza virus resource [42]. The strains and accession numbers are listed in **Supplementary Table S3**. Nucleotide sequences were aligned to Reference H1N1 (GenBank Entry: ACP41105.1) and H3N2 strains (UniProtKB/Swiss-Prot: Q91MA7.1) using MUSCLE (**MU**ltiple **S**equence **C**omparison by **L**og-**E**xpectation) and the alignment was fixed to preserve the reading frame by sweeping together 1- or 2-bp (or any non-divisible-by-3 bp) gaps that occurred in a <20-bp window. Phylogenetic trees were generated using FastTree [43]. The branch support values were generated applying the Shimodaira-Hasegawa test. For each strain, sequence homology was calculated compared to the vaccine strain (i.e. proportion of amino acids exactly matching the amino acid in the same position in the reference sequence). Frequency of clades and mutants were estimated and visualized with nextstrain tool [44]. N-linked glycosylation sites were predicted by analyzing the

sequence context of the Asn-X-Ser/Thr consensus sequence with the NetNglyc algorithm [45,46].

Multidimensional vaccine response vectors and hierarchical clustering

Antibody binding profiles for each subject were generated, encompassing responses at day 0, 7, 14 and 28 post vaccination against all strains of a serotype [26]. Hierarchical clustering of the binding profile with the host factors age, gender, peak IgG and peak avidity against the vaccine strain and pre-existing IgG levels was performed using the complete-linkage algorithm. Avidity reflects the sum total of the binding strength of an antibody to its antigen at multiple sites and high avidity IgG may tolerate more epitope sequence variation, thus have higher cross-reactivity. Avidity of the IgG responses was estimated calculating the avidity index following urea challenge (raw data not shown) [47]. Heatmaps were generated using either the R packages ComplexHeatmap [48] or NMF [49].

Fluorescence-activated cell sorting of B cell subsets

Cryopreserved PBMC from healthy donors before (day 0) and after vaccination (day 7), were thawed and rested over night. Cells were then stained with antibodies against CD14 (FITC, clone MϕP9, 345784), CD16 (FITC, clone NKP15, 335035) and CD27 (PE, clone L128, 340425), all from BD Biosciences, Franklin Lakes, NJ, USA and against CD3 (Alexa Fluor 488®, clone UCHT1, 300415), CD19 (Alexa Fluor 700®, clone HIB19, 302226), CD20 (Brilliant Violet 510TM, clone 2H7, 302340), CD38 (APC, clone HIT2, 303510) and IgD (PE-Cy7, clone IA6-2, 348210), all from Biolegend, San Diego, CA, USA. Compensation was performed using single stained Antibody Capture Beads (VersaComp, B22804, Beckman Coulter, Brea, CA, USA). All B cell subsets were sorted into medium on a FACSAria® III (BD Biosciences) using a 70 µM nozzle. The gating strategy is indicated in **Supplementary Figure S1**. Cells were pelleted and kept at -80°C until RNA extraction.

IgG-BCR-sequence library preparation

IgG heavy chain libraries compatible for sequencing with the MiSeq platform (2x300bp paired-end, Illumina, San Diego, CA, USA) were prepared similarly to a previously described two-step primer extension method for mouse Ig heavy chains [50]. Total RNA from memory B cells (day 0 and 7) and plasmablasts (day 7) was isolated with the RNeasy® Plus Micro kit (74034, Qiagen, Hilden, Germany, without column-based gDNA elimination but with adding 200 ng of carrier RNA according to manufacturer's 'Animal and Human Cells' protocol. Subsequently, the complete RNA was depleted from genomic

DNA with RQ1 RNAse-Free DNAse (M6101, Promega, Madison, WI, USA). First-strand cDNA was synthesized from total RNA by using AccuScript Hi-Fi Reverse Transcriptase (200820, Agilent Technologies, Santa Clara, CA, USA) with oligo(dT) primers according to manufacturer's protocol in triple volume. Following RT, a bead-based nucleic acid clean-up was carried out: The complete RT product (60 µL) was mixed with 48 µL of SPRIselect magnetic beads (B23318, Beckman Coulter) on a custom-made magnet in order to perform a 0.8x left-sided cleanup (i.e. remove smaller DNA fragments up to a certain threshold). The supernatant with the small fragments was discarded and bead-bound DNA washed twice with 85% ethanol and finally eluted in 20 µL of water.

For PCR amplification of the rearranged heavy chain locus, a set of eight forward primers containing an overhang and annealing to framework region 1 [51] and reverse primers binding to Cγ1-4, containing another overhang, were used in PCR 1 (complete primer list in **Supplementary Table S4**). In a reaction volume of 25 µL with 5% DMSO, half of the purified cDNA was amplified with Q5® High-Fidelity DNA Polymerase (M0491, New England Biolabs, Ipswich, MA, USA) by using the following settings: Activation at 98°C for 30s followed by 4 cycles of 98°C for 20s, 48°C for 40s, 72°C for 60s; 4 cycles of 98°C for 20s, 53°C for 40s, 72°C for 60s; 12 cycles of of 98°C for 20s, 60°C for 40s, 72°C for 60s and 2 minutes of extension at 72°C. A bead-based 0.8x left-sided cleanup was performed again followed by elution in 20 µL of water. PCR 2 was used to add Illumina adapter sequences and population-specific Illumina indices. Complete PCR 1 product was amplified with Q5® DNA Polymerase in two parallel reactions of 25 µL volume with 5% DMSO and the following conditions: Activation at 98°C for 30s followed by 4 cycles of 98°C for 20s, 40°C for 40s, 72°C for 60s; 12 cycles of 98°C for 20s, 65°C for 40s, 72°C for 60s and 2 minutes of extension at 72°C. After 0.8x SPRIselect left-sided size selection and elution in 20 µL of water, the complete product of PCR 2 was loaded onto a 1% agarose gel and purified with MinElute® Gel Extraction Kit (28604, Qiagen). DNA concentration of all purified PCR products was assessed with a Quantus™ Fluorometer using the QuantiFluor® ONE dsDNA System (E4870, both Promega). Regardless of concentration, 2 µL per sample was added to the final library. Before sequencing, DNA quality and quantity was verified on a Fragment Analyzer™ (Advanced Analytical Technologies Inc., Ankeny, IA, USA) using DNF-473 Standard Sensitivity NGS fragment analysis kit.

BCR repertoire analysis

Clonotype formation by CDRH3 and error correction was performed as described previously [52,53]. For downstream analyses, functional clonotypes were only retained if: (i) they were composed of at least 4 amino acids, and (ii) had a minimal read count of 2 [50,54]. Clonal overlap was defined as $\frac{A \cap B}{(A+B)/2}$, with the number of shared clonotypes between subjects A and B in the numerator and the mean of total clonotypes of subjects A and B in the denominator [55]. In a group of e.g. four subjects, six (3+2+1) clonal overlaps are calculated. Statistical analysis was performed using R. Graphics were generated using the R packages ggplot2 [56] and RColorBrewer [57]. For all repertoire analyses, clones were defined by 100% amino acid sequence identity of CDRH3 regions [53,54,58]. CDRH3 regions were annotated and defined by the MiXCR software [52] according to IMGT nomenclature [59]. Using Euclidean distance as a distance metric, hierarchical clustering was performed using the complete-linkage clustering algorithm performed by the R function hclust(). Hierarchical clustering was visualized using the NMF [49]. Statistical significance was tested using the Wilcoxon rank-sum test if not indicated otherwise. P values lower than 0.05 were required for stating significant differences between groups. BCR sequencing data will be made freely available upon publication.

Results

Vaccine response and cross-recognition of non-vaccine strains

Broad variant recognition defines a powerful vaccine against fast mutating viruses. Using a multiplexed, bead-based immunoassay, we tested the vaccination-induced IgG response (ΔMFI day 28 - day 0) against the 2007/2008 influenza A vaccine strains and their cross-binding of strains that were included in previous and subsequent vaccine preparations, covering a period from 2000/01 – 2014/15 (**Figure 1A**). Given the way vaccine strains are selected, these represent the antigenic variants of the viruses circulating in the human population during this time span. Additionally, we included two historic controls, H1N1 A/Brevig Mission/1/1918 and H3N2 A/Hong Kong/1/1968, strains responsible for the Spanish flu and Hongkong flu pandemics. Together, this covered variable degrees of phylogenetic relatedness (**Figure 1B**). For each of the 24 subjects, we tested reactivity against 13 different influenza A strains on four time-points (pre-vaccination = day 0, and day 7, 14 and 28 post-vaccination), yielding a total of 1248 data points. Vaccination induced a significant increase of the vaccine strain-specific MFI at day 7, 14 and 28 with peak intensities at day 14 and 28 in most vaccinated subjects ($p < 0.001$ for H1N1 and H3N2 at all time points, **Supplementary Figure S2**). While not changing the statistic outcome, a few individuals (H1N1: four; H3N2: three) were excluded from subsequent analysis due to vaccine non-response, defined as ΔMFI < 25 against the vaccine strain. To assess the degree of cross-reactivity, we normalized the IgG vaccine response against each strain to the vaccine strain response (**Figure 1C**). While both the historic (1918) and future (2009) pandemic H1N1 viruses were poorly cross-recognized (<25% of the vaccine strain response), the response to the previous and subsequently circulating H1N1 strains (i.e. A/New Caledonia/20/99 and A/Brisbane/59/2007) was comparable to the vaccine strain. H3N2 cross-binding was significantly lower against two previous vaccine strains (A/Fujian/411/2002 and A/Moscow/10/1999) and the 1968 pandemic strain (A/Hong Kong/1/1968), while responses to vaccine viruses of the previous and two subsequent years were comparable to the vaccine strain response. A striking drop in cross-recognition was observed to A/Texas/50/2012, the most recent of the strains tested (**Figure 1C**). Taken together, our multiplexed, bead-based assay reliably captured expected cross-reactivity patterns and discovered putative escape variants.

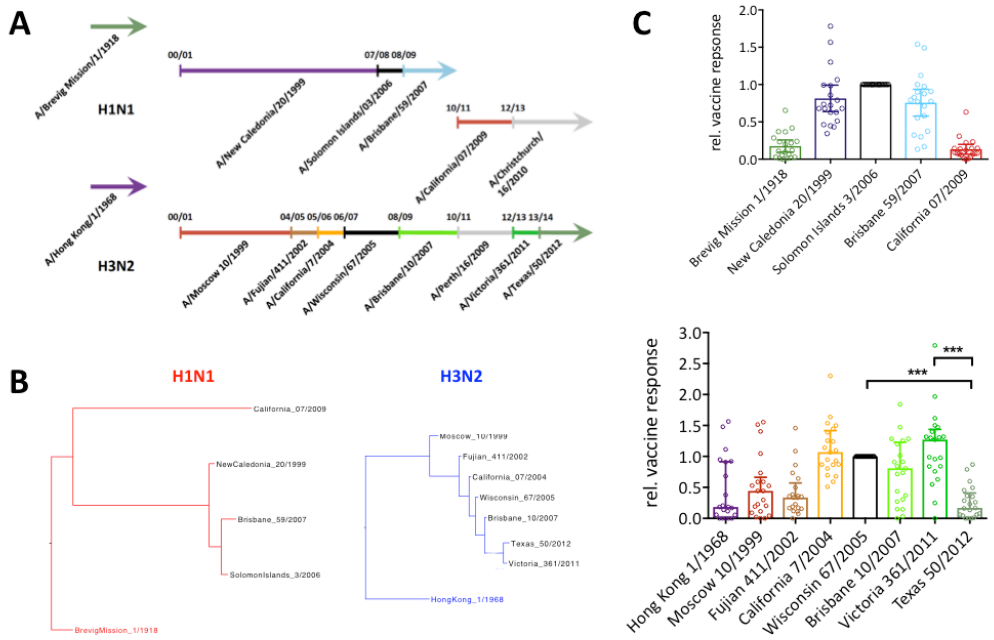

Figure 1: Influenza A vaccine strains included in the analysis. A) Timeline of all H1N1 and H3N2 strains included in vaccines between 2000/01 and 2014/15 including distantly related pandemic strains. The gap in H1N1 in season 2010/11 accounts for vaccine adaptation to the pandemic 2009 swine flu. **B)** Phylogenetic trees based on HA amino acid sequences of all strains included in our analyses were generated with FastTree. **C)** Cross-reactivity of the vaccine response for H1N1 (top) and H3N2 (bottom) 28 days after administration. Vaccine strains are shown in black. Statistical analysis with Wilcoxon signed rank test is selectively indicated (*** $p < 0.001$).

Impact of host factors on cross-reactivity patterns

To investigate whether specific host factors affect cross-reactivity patterns, we generated individual antibody binding profiles for each subject [26]. The impact of predefined factors (age, gender, preexisting IgG / peak response against the vaccine strain and IgG avidity) on the response profile was then assessed using hierarchical clustering. Individuals loosely clustered for preexisting IgG and peak response against the vaccine strain, both for H1N1 (**Figure 2A**) and H3N2 (**Figure 2B**). Thus, the cross-recognition profile was to some extent related to the quantity of antibody available. However, irrespective of IgG levels being high or low, some strains were poorly recognized by most individuals. This is exemplified by the very moderate response against the H3N2 strains A/Fujian/411/07 and A/Texas/10/2012 including in subjects with robust vaccine responses (**Figure 2C**).

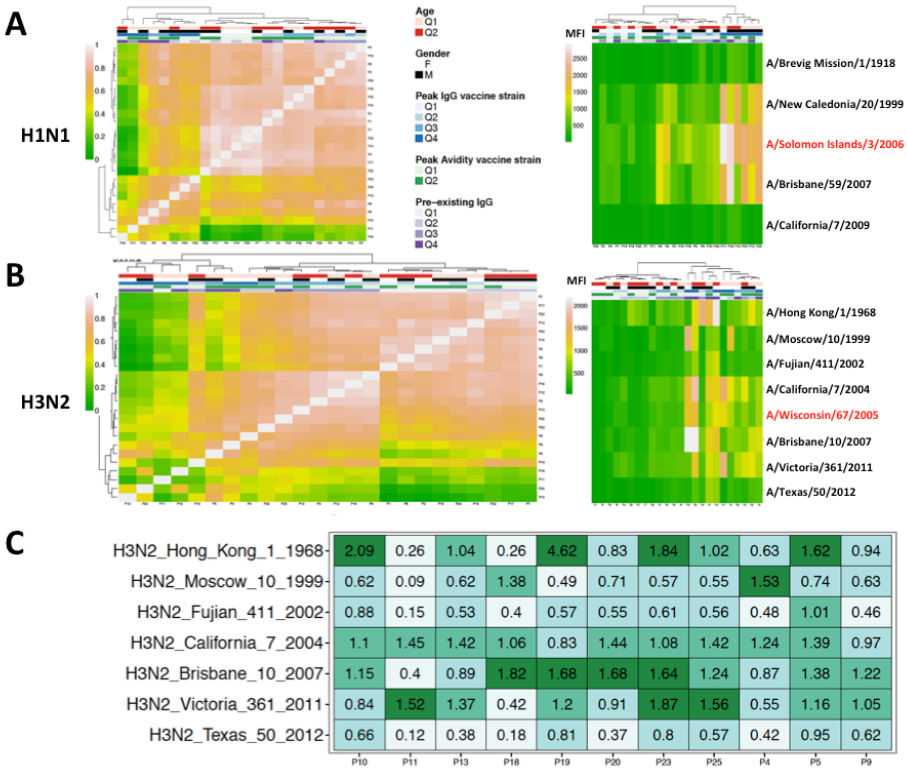

Figure 2: High IgG levels predict broad antibody binding profiles. A, B) Hierarchical clustering based on antibody-binding profiles according to IgG-levels at day 0, 7, 14 and 28 across all investigated H1N1 (A) and H3N2 (B) strains (left panels). Low quantiles of the investigated host factors are shown in light colors, high quantiles in dark colors. The cluster analysis reveals a group defined by high pre-existing and peak IgG. The individuals in this group are characterized by quite broad and strong recognition of different strains, as shown in the strain-resolved clusters (right panels, d28 post vaccination, vaccine strains highlighted in red). **C)** Relative vaccine responses against all measured H3N2 strains in a subset of donors with high and broad vaccine response. Dark colors indicate a high, light colors indicate a low response against the respective strain. The Texas and Fujian strains are quite consistently poorly cross-recognized.

Low antibody cross-reactivity is associated with a narrower memory BCR repertoire

The acute response to inactivated influenza vaccination in adults is characterized by rapid proliferation of antibody-secreting plasmablasts. In humans, the number of plasmablasts circulating in the periphery peaks 7 days post-vaccination and is dominated by a recall of IgG memory responses [33]. Analyzing the B cell receptor repertoire of plasmablasts in this short window of opportunity offers a possibility to map the vaccine response on a clonal level [33]. We hypothesized that serum antibodies with high cross-recognition capability are clonally more diverse. To test this, memory B cells (CD3/14/16$^-$ CD19$^+$ CD20$^+$ IgD$^-$ CD27$^+$ CD38$^-$) at day 0 and 7 and plasmablasts (CD3/14/16$^-$ CD19$^+$ CD20$^-$ IgD$^-$ CD38^{++}) at day 7 post-vaccination were sorted from a subset of 12 vaccine-responding individuals from the 2007/08 cohort and sequenced

for CDRH3. 'High' and 'low' cross-reactivity groups were defined by median split of the loss in cross-recognition (day 28 post-vaccination) of A/Texas/50/2012. Texas cross-recognition was chosen as the criterion, since it represented a future strain at the time of the vaccination.

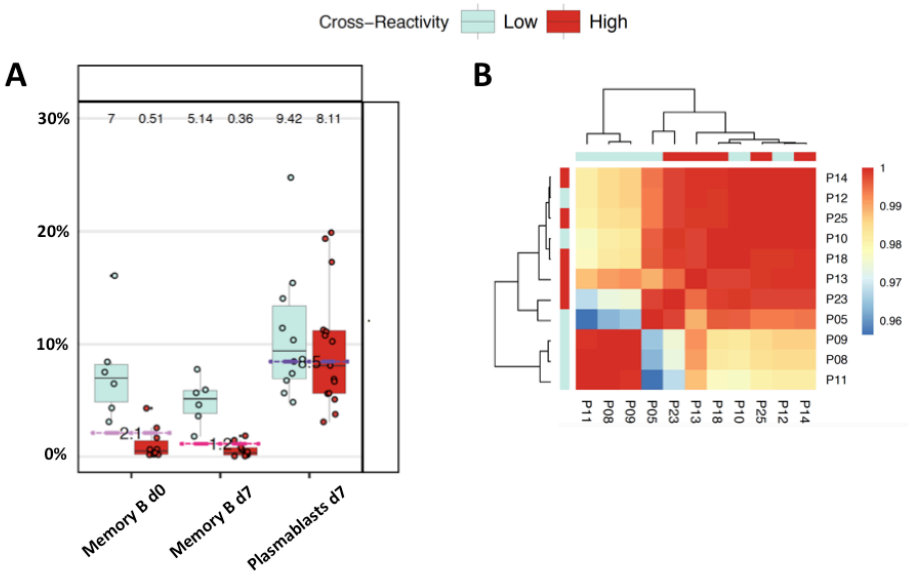

Figure 3: Lower BCR repertoire breadth may predispose to poorer cross-reactivity.
A) Clonal overlap within highly (red) and poorly (turquoise) cross-reactive groups (as defined in the main text) are shown for all sequenced B cell populations. Being enriched in influenza-specific B cells, the clonal overlap is highest within plasmablast populations. It is only within the memory B cells (d0 and d7) of the 'low' group though, were the overlap is significantly higher than in the 'high' group. Median (value on top), IQR and mean per cell population (dashed line) are shown. **B)** Hierarchical clustering of plasmablast evenness profiles according to cross-reactivity group. While clonal overlap among plasmablasts is similar between the groups, the structure of the BCR-repertoire seems to be altered.

V-gene usage and degree of somatic hypermutation was similar between groups and cell subsets (**Supplementary Figure S3**). High clonal overlap within a group is indicative of a narrow or more precisely skewed repertoire. Clonal overlap was highest among plasmablasts. This was irrespective of whether they belonged to the 'high' or 'low' cross-reactivity group. In contrast, in the low cross-reactivity group, clonal overlap within memory B cells (day 0 and 7) was significantly higher than in the 'high' cross-reactivity group (**Figure 3A**). Evenness profiles [60] for the plasmablast repertoires tended to cluster together with cross-reactivity (**Figure 3B**). High evenness is indicative of clonal expansion. While clonal overlap between plasmablast populations was comparable between the cross-reactivity groups, the evenness profiles suggested a difference in the

structure of the BCR repertoire. For the low-crossreactivity group, this could e.g indicate less clonal expansion or also more clonal expansion, but the expanded clonotypes would produce poorly cross-recognizing antibodies based on or measurements. Combined, this suggests that subjects with low cross-reactivity recruited their B cell vaccine response from a less diverse pool, eventually resulting in poorer responses against future antigenically novel strains (i.e. Texas).

Antigenic variation dictates cross-reactivity on the population level

Besides the individual antibody repertoire, antigenic similarity between two strains can explain strong cross-recognition by the immune response. While overall Influenza A HA homology correlated strongly with the median relative response score of the 21 healthy subjects ($r=0.76$, $p=0.003$), this was biased by the few H1N1 strains ($r=1$, $p=0.02$), two of which are pandemic strains (**Figure 4A**). For H3N2 overall sequence, homology and cross-recognition were disconnected ($r=0.5$, $p=0.2$). Specifically, Texas and Fujian were poorly recognized (see also **Figure 1C**) despite differing in only very few amino acids from the vaccine strain Wisconsin. However, overall sequence homology is an unreliable comparator, as the region of sequence variability, i.e. antigenically relevant structures, are more important [61–63].

Since Texas is the closest relative of the Victoria strain (**Figure 1B**), which was strongly cross-recognized in our vaccination cohort, we focused for further analyses on the antigenic differences between Victoria and Texas. The HA of the two strains only differ by seven amino acids (i.e. 1.2 % or 7/566 AA) (**Figure 4B**). Five out of seven point mutations were located in close proximity to the receptor binding site. These regions are enriched for glycan attachment sites; N-linked glycosylations are well known to alter the antigenicity of influenza viruses. Indeed, a T128N mutation between Victoria and Texas disrupted the Asn-X-Ser/Thr consensus sequence, thereby potentially disabling N-linked glycosylation at N126 (**Figure 4B**). PAGE showed higher electrophoretic mobility of the Texas compared to Victoria HA, indicating that Texas indeed lost a glycan structure (**Figure 4C**). Analysis with the phylogenetic tool nextstrain revealed that T128N is a very rare mutation but, based on sequence context analysis, is alike to the 3c3 clade-defining mutation T128A in causing a glycosylation loss at N126. Clade 3c3 emerged end of 2012 and dominated the years 2013 and 2014 (**Supplementary Figure S4**). To test whether this T128N mutation, and the resulting structural change, could be responsible for the reduced recognition of Texas, we compared the antibody response to Victoria, Texas and a Texas variant with a reverted mutation restoring the glycosylation site (N128T).

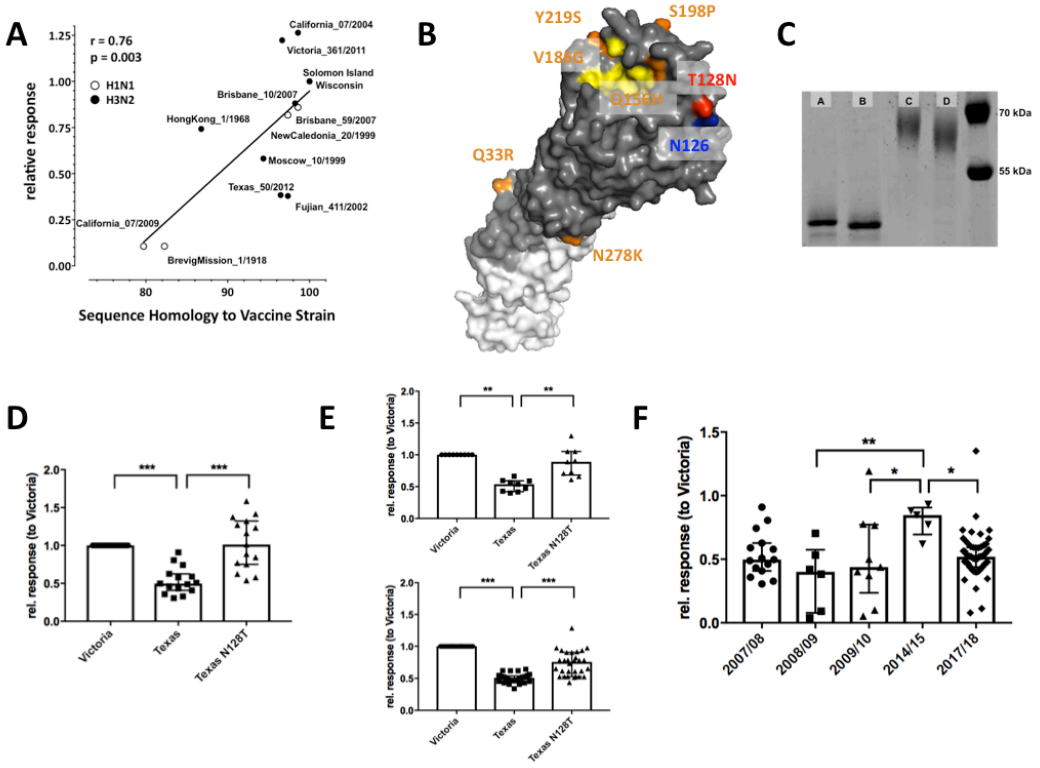

Figure 4: Reduction of HA-specific antibody response by a single glycosylation change. **A)** Correlation between sequence homology and median antibody response relative to the H1N1 and H3N2 vaccine strains of 2007/08. Antibody-binding against H3N2 strains Fujian and Texas is poor despite very high sequence homology **B)** Amino acid changes (orange) between the Victoria and Texas strain HA depicted on a surface representation of the Victoria HA monomer (PBD ID: 4O5N). The T128N-mutation (red) potentially leads to a loss of glycosylation at N126 (blue). Yellow: HA receptor binding site **C)** Enzymatic cleavage of all N-linked oligosaccharides results in similar PAGE migration patterns between recombinant HA1 of Victoria and Texas (lanes A and B). When not modified, Texas HA migrates faster indicating loss of a glycan structure (lanes C and D). **D)** Vaccine response at day 28 was assessed both against Texas relative to Victoria and upon insertion of the N128T-mutation (T128 as in Victoria) into the Texas HA1. Antibody-binding is significantly increased in Texas N128T (2007/08 cohort, n = 15, Wilcoxon signed rank test). **E)** Same setting as in D but with subjects of a 2017/18 vaccine cohort never (n = 9) or 3x vaccinated with Texas-like strains (n = 19). **F)** Analysis of Texas cross-recognition including 3 seasons in between (08/09 n = 6; 09/10 n = 9; 14/15 n = 5). While being low until 2009/10, the relative response increased significantly upon vaccination with a Texas-like strain in 2014/15 (Friedman Test with Dunn's correction). *** $p < 0.001$, ** $p < 0.01$, * $p < 0.05$

Indeed, antibody escape could be rescued, suggesting that the mutation at position 128 might affect the cross-recognition (**Figure 4D**). Next, we tested whether vaccination with a Texas-like variant improves its recognition. In a vaccine cohort from 2017/18, individuals that were always vaccinated between 2013/14 and 2015/16 were compared to those who received no vaccine in that period. In these three years, the H3N2 vaccine strain was either A/Texas/50/2012-like or

A/Switzerland/9715293/2013-like, bearing an N-W-N-motif (N126/N128, Texas) or an N-W-A-motif (N126/A128, Switzerland) both abrogating glycosylation at N126. However, we found no difference in the cross-reactivity between these two groups (**Figure 4E**). Finally, we analyzed Texas cross-recognition in vaccination cohorts of years in between (**Figure 4F**). In 2008/09 and 2009/10, when the H3N2 strain contained an N-W-T-motif (N126/T128, Victoria-like), the lower antibody-binding to Texas (N128) compared to Victoria (T128) was sustained. In contrast, in 2014/15, where the vaccine contained a Texas-matched N-W-N-motif, the drop in Texas recognition was substantially reduced. Therefore, following the adaptation of the vaccine strain, the response against the escaped epitope could be rescued. Based on the data of 2017/18 (**Figure 4E**), the durability of the Texas-adapted response was limited though, turning back to the levels before emergence of the 3c3 clade.

Discussion

In our 2007/08 cohort, vaccination generally induced a broad antibody response targeting not only the vaccine strain, but also closely related strains of the same serotype. As expected, cross-reactivity waned against strains separated by decades of antigenic drift (e.g. A/Hong Kong/1/1968) or reassorted variants (antigenic shift, e.g. A/California/7/2009). The variability in the intensity and breadth of cross-reactivity within the cohort accounts for the individual influenza infection and vaccination history.

There was, however, HA of strains that were poorly recognized despite high overall homology to the vaccine strain. We focused on A/Texas/50/2012, being a novel strain at that time and also not being integrated into a known antigenic cluster yet [27,64]. Being located within an antigenic site close to the receptor-binding site, a mutation from threonine to asparagine at position 128 was suspected to induce an antigenic shift [61,65]. Indeed, T128N seemed to disrupt glycosylation at position 126 and was responsible for the loss of recognition. Those individuals with especially poor cross-reactivity against Texas recruited their antigen-specific B cells from a more narrow pool of memory B cells generating a plasmablast population with altered BCR repertoire structure. So far, BCR-repertoires have been used to trace vaccine responses, also at the level of antigen-specificity, but not in the context of cross-reactivity [30,32,66]. Overlaying HA-specific BCR-repertoires with plasmablast BCR repertoires would be highly informative about the numbers of lineages targeting HA and whether these numbers are reduced in individuals mounting poorly cross-reactive responses.

T128N probably also mimics the T128A mutation with regard to glycan loss at N126. T128A defines H3N2 clade 3c3 that emerged end of 2012 and constituted the majority of H3N2 viral isolates in the years 2013 and 2014 (**Supplementary Figure S4**). The idea that immune evasion due to loss of a glycosylation site was enabling the fast expansion of the clade is intriguing. Moreover, our measurements from 2017/18 show, that despite being exposed to viruses of the 3c3-clade by repetitive vaccination or infection, the population responds again poorly towards the Texas strain carrying T128N. We suggest that upon B cell memory recall, "Texas-specific" B cells to the region around N(126)-W-N(128) cannot access their cognate epitope anymore due to glycosylation at N126 and are consequently not positively selected. This glycan-mediated masking of an antigenically relevant site could prepare the ground for another expansion of clade 3c3.

While our immunoassay quantifies antibody-binding to HA, it does not inform about the neutralization capacity of these antibodies. Since we used recombinant HA monomers rather than stabilized HA-trimers, a proportion of binding antibodies might moreover have been missed or led to false-positive signals. However, it is established that ELISA IgG binding titers correlate with neutralizing antibody titers and since binding is a prerequisite for neutralization, the reduced binding to T128N-mutants likely translates to poor neutralization in an infection setting [67].

The 2017/18 cohort was designed to further investigate effects of repetitive vaccination with similar epitopes on the evolution of the immune response. This allowed to test whether repetitive exposure to the H3N2 N-W-N/N-W-A-motif might have affected the variant recognition, which was however not the case in this setting. For H1N1, the other influenza A strain included in the vaccine, the 2017/18 vaccine provided a unique opportunity to test the influence of exposure history: In the five previous seasons, vaccines included HA of an A/Christchurch/16/2010-like virus that was changed to HA from an A/Michigan/45/2015-like virus in 2017/18. We did not find preferential targeting of the former in subjects repeatedly vaccinated with the Christchurch-like strain (data not shown). However, detecting effects of repetitive exposure depends on alterations in the antigenicity between the two strains, which we did not assess in the H1N1 setting. Moreover, effects may have been disguised by vaccinations and infections preceding our time window from 2012/13 until 2017/18. Preferential reactivity to antigenically senior strains (i.e. encountered early in life) upon vaccination, concomitant with good recognition of novel variants when using antigenically advanced vaccine strains [27], has been reported in many settings [27,29,68].

Concluding, we established a multiplexed, high-throughput method to screen for and

validate viral immune escape variants. Our data highlights the importance of testing and considering emerging influenza variants with glycosylation changes for vaccine inclusion.

References

1. Nabel, G. J. Designing tomorrow's vaccines. *N Engl J Med* **368,** 551–560 (2013).
2. Plotkin, S. A. Vaccines: correlates of vaccine-induced immunity. *Clin Infect Dis* **47,** 401–409 (2008).
3. Knossow, M. & Skehel, J. J. Variation and infectivity neutralization in influenza. *Immunology* **119,** 1–7 (2006).
4. Thompson, W. W. *et al.* Influenza-associated hospitalizations in the United States. *JAMA* **292,** 1333–1340 (2004).
5. Nair, H. *et al.* Global burden of respiratory infections due to seasonal influenza in young children: a systematic review and meta-analysis. *Lancet* **378,** 1917–1930 (2011).
6. Glezen, W. P. Prevention and Treatment of Seasonal Influenza. *N. Engl. J. Med.* **359,** 2579–2585 (2008).
7. Bouvier, N. M. & Palese, P. The biology of influenza viruses. *Vaccine* **26 Suppl 4,** D49-53 (2008).
8. Hobson, D., Curry, R. L., Beare, A. S. & Ward-Gardner, A. The role of serum haemagglutination-inhibiting antibody in protection against challenge infection with influenza A2 and B viruses. *J Hyg* **70,** 767–777 (1972).
9. Tsang, T. K. *et al.* Association between antibody titers and protection against influenza virus infection within households. *J Infect Dis* **210,** 684–692 (2014).
10. CDC. Seasonal Influenza Vaccine Effectiveness, 2005-2018. (2018). at <https://www.cdc.gov/flu/professionals/vaccination/effectiveness-studies.htm>
11. Belongia, E. A. *et al.* Variable influenza vaccine effectiveness by subtype: a systematic review and meta-analysis of test-negative design studies. *Lancet Infect Dis* **16,** 942–951 (2016).
12. Nichol, K. L. The efficacy, effectiveness and cost-effectiveness of inactivated influenza virus vaccines. *Vaccine* **21,** 1769–1775 (2003).
13. Monto, A. S. *et al.* Comparative efficacy of inactivated and live attenuated influenza vaccines. *N Engl J Med* **361,** 1260–1267 (2009).
14. Petrie, J. G., Ohmit, S. E., Johnson, E., Cross, R. T. & Monto, A. S. Efficacy studies of influenza vaccines: effect of end points used and characteristics of vaccine failures. *J Infect Dis* **203,** 1309–1315 (2011).
15. DiazGranados, C. A., Denis, M. & Plotkin, S. Seasonal influenza vaccine efficacy and its determinants in children and non-elderly adults: a systematic review with meta-analyses of controlled trials. *Vaccine* **31,** 49–57 (2012).
16. Osterholm, M. T., Kelley, N. S., Sommer, A. & Belongia, E. A. Efficacy and effectiveness of influenza vaccines: a systematic review and meta-analysis. *Lancet Infect Dis* **12,** 36–44 (2012).
17. Beck, C. R. *et al.* Influenza vaccination for immunocompromised patients: systematic review and meta-analysis by etiology. *J Infect Dis* **206,** 1250–1259 (2012).
18. Tricco, A. C. *et al.* Comparing influenza vaccine efficacy against mismatched and

matched strains: a systematic review and meta-analysis. *BMC Med* **11,** 153 (2013).
19. CDC. Selecting Viruses for the Seasonal Influenza Vaccine. (2016).
20. Ito, T. *et al.* Differences in sialic acid-galactose linkages in the chicken egg amnion and allantois influence human influenza virus receptor specificity and variant selection. *J. Virol.* **71,** 3357–3362 (1997).
21. Wu, N. C. *et al.* A structural explanation for the low effectiveness of the seasonal influenza H3N2 vaccine. *PLoS Pathog.* **13,** 1–17 (2017).
22. Andrews, S. F. *et al.* Immune history profoundly affects broadly protective B cell responses to influenza. *Sci Transl Med* **7,** (2015).
23. Kim, J. H. *et al.* Prior infection with influenza virus but not vaccination leaves a long-term immunological imprint that intensifies the protective efficacy of antigenically drifted vaccine strains. *Vaccine* **34,** 495–502 (2016).
24. Andrews, S. F. *et al.* High preexisting serological antibody levels correlate with diversification of the influenza vaccine response. *J. Virol.* **89,** 3308–17 (2015).
25. Reber, A. J. *et al.* Preexisting Immunity, More Than Aging, Influences Influenza Vaccine Responses. *Open Forum Infect Dis* **2,** (2015).
26. Berger, C. T. *et al.* Influenza vaccine response profiles are affected by vaccine preparation and preexisting immunity, but not HIV infection. *Hum Vaccin Immunother* **11,** 391–396 (2015).
27. Fonville, J. M. *et al.* Antibody landscapes after influenza virus infection or vaccination. *Science* **346,** 996–1000 (2014).
28. Yu, X. *et al.* Neutralizing antibodies derived from the B cells of 1918 influenza pandemic survivors. *Nature* **455,** 532–536 (2008).
29. Hancock, K. *et al.* Cross-reactive antibody responses to the 2009 pandemic H1N1 influenza virus. *N Engl J Med* **361,** 1945–1952 (2009).
30. Vollmers, C., Sit, R. V, Weinstein, J. a, Dekker, C. L. & Quake, S. R. Genetic measurement of memory B-cell recall using antibody repertoire sequencing. *Proc. Natl. Acad. Sci. U. S. A.* **110,** 13463–8 (2013).
31. Jiang, N. *et al.* Lineage Structure of the Human Antibody Repertoire in Response to Influenza Vaccination. **5,** 1–16 (2013).
32. Ellebedy, A. H. *et al.* Defining antigen-specific plasmablast and memory B cell subsets in human blood after viral infection or vaccination. *Nat. Immunol.* **17,** 1226–1234 (2016).
33. Wrammert, J. *et al.* Rapid cloning of high-affinity human monoclonal antibodies against influenza virus. *Nature* **453,** 667–71 (2008).
34. Siegrist, C. & Aspinall, R. B-cell responses to vaccination at the extremes of age. *Nat. Rev. Immunol.* **9,** 185–194 (2009).
35. Francis Jr., T. On the Doctrine of Original Antigenic Sin. *Proc. Am. Philos. Soc.* **104,** 572–578 (1960).
36. Zarnitsyna, V. I., Lavine, J., Ellebedy, A., Ahmed, R. & Antia, R. Multi-epitope Models Explain How Pre-existing Antibodies Affect the Generation of Broadly Protective Responses to Influenza. *PLoS Pathog* **12,** (2016).
37. Smith, D. J., Forrest, S., Ackley, D. H. & Perelson, A. S. Variable efficacy of repeated annual influenza vaccination. *Proc Natl Acad Sci U S A* **96,** 14001–14006 (1999).
38. Skowronski, D. M. *et al.* Serial vaccination and the antigenic distance hypothesis: Effects on influenza vaccine effectiveness during A(H3N2) epidemics in Canada, 2010-2011 to 2014-2015. *J. Infect. Dis.* **215,** 1059–1069 (2017).
39. Thompson, M. G. *et al.* Effects of Repeated Annual Inactivated Influenza Vaccination among Healthcare Personnel on Serum Hemagglutinin Inhibition Antibody Response to A/Perth/16/2009 (H3N2)-like virus during 2010-11. *Vaccine* **34,** 981–988 (2016).
40. Fritz, S. *et al.* Virosomal influenza-vaccine induced immunity in HIV-infected individuals with high versus low CD4+ T-cell counts: clues towards a rational

vaccination strategy. *AIDS* **24,** 2287–2289 (2010).
41. Mehling, M. *et al.* Antigen-specific adaptive immune responses in fingolimod-treated multiple sclerosis patients. *Ann Neurol* **69,** 408–413 (2011).
42. Bao, Y. *et al.* The influenza virus resource at the National Center for Biotechnology Information. *J Virol* **82,** 596–601 (2008).
43. Price, M. N., Dehal, P. S. & Arkin, A. P. FastTree : Computing Large Minimum Evolution Trees with Profiles instead of a Distance Matrix. *Mol Biol Evol.* **26,** 1641–1650 (2009).
44. Neher, R. A. & Bedford, T. nextflu: real-time tracking of seasonal influenza virus evolution in humans. *Bioinformatics* **31,** 3546–3548 (2015).
45. Mellquist, J. L., Kasturi, L., Spitalnik, S. L. & Shakin-Eshleman, S. H. The amino acid following an Asn-X-Ser/Thr sequon is an important determinant of N-linked core glycosylation efficiency. *Biochemistry* **37,** 6833–6837 (1998).
46. Nikolaj, B., Thomas, S., Ramneek, G., Steen, G. & Søren, B. Prediction of post-translational glycosylation and phosphorylation of proteins from the amino acid sequence. *Proteomics* **4,** 1633–1649 (2004).
47. Mehling, M. *et al.* Avidity of vaccine-induced influenza IgG fails to increase in fingolimod-treated patients with MS. *Neurol Neuroimmunol Neuroinflamm* **1,** (2014).
48. Gu, Z., Eils, R. & Schlesner, M. Complex heatmaps reveal patterns and correlations in multidimensional genomic data. *Bioinformatics* **32,** 2847–2849 (2016).
49. Gaujoux, R. & Seoighe, C. A flexible R package for nonnegative matrix factorization. *BMC Bioinformatics* **11,** 367 (2010).
50. Menzel, U. *et al.* Comprehensive evaluation and optimization of amplicon library preparation methods for high-throughput antibody sequencing. *PLoS One* **9,** e96727 (2014).
51. Krebber, A. *et al.* Reliable cloning of functional antibody variable domains from hybridomas and spleen cell repertoires employing a reengineered phage display system. *J Immunol Methods* **201,** 35–55 (1997).
52. Bolotin, D. A. *et al.* MiXCR: software for comprehensive adaptive immunity profiling. *Nat. Methods* **12,** 380–381 (2015).
53. Greiff, V. *et al.* Systems Analysis Reveals High Genetic and Antigen-Driven Predetermination of Antibody Repertoires throughout B Cell Development. *Cell Rep.* **19,** 1467–1478 (2017).
54. Greiff, V. *et al.* Quantitative assessment of the robustness of next-generation sequencing of antibody variable gene repertoires from immunized mice. *BMC Immunol* **15,** 40 (2014).
55. Greiff, V. *et al.* Systems Analysis Reveals High Genetic and Antigen-Driven Predetermination of Antibody Repertoires throughout B Cell Development. *Cell Rep* **19,** 1467–1478 (2017).
56. Wickham, H. *ggplot2: Elegant Graphics for Data Analysis*. (Springer, 2009). doi:10.1007/978-0-387-98141-3_1
57. Brewer, C. A., Hatchard, G. W. & Harrower, M. A. ColorBrewer in Print: A Catalog of Color Schemes for Maps. *Cartogr. Geogr. Inf. Sci.* **30,** 5–32 (2003).
58. Greiff, V., Miho, E., Menzel, U. & Reddy, S. T. Bioinformatic and Statistical Analysis of Adaptive Immune Repertoires. *Trends Immunol.* **36,** 738–749 (2015).
59. Lefranc, M. P. *et al.* IMGT, the international ImMunoGeneTics database. *Nucleic Acids Res* **27,** 209–212 (1999).
60. Greiff, V. *et al.* A bioinformatic framework for immune repertoire diversity profiling enables detection of immunological status. *Genome Med.* **7,** 3–5 (2015).
61. Wiley, D. C., Wilson, I. A. & Skehel, J. J. Structural identification of the antibody-binding sites of Hong Kong influenza haemagglutinin and their involvement in antigenic variation. *Nature* **289,** 373–378 (1981).
62. Gerhard, W., Yewdell, J., Frankel, M. E. & Webster, R. Antigenic structure of

influenza virus haemagglutinin defined by hybridoma antibodies. *Nature* **290,** 713–717 (1981).
63. Skehel, J. J. *et al.* A carbohydrate side chain on hemagglutinins of Hong Kong influenza viruses inhibits recognition by a monoclonal antibody. *Cell* **81,** 1779–1783 (1984).
64. Smith, D. J. Mapping the Antigenic and Genetic. *Science (80-.).* **305,** 371–376 (2004).
65. Wilson, I. C. N. Structural Basis of Immune Recognition of Influenza Virus Hemagglutinin. *Annu. Rev. Immunol.* **Vol. 8,** 737–787 (1990).
66. Galson, J. D. *et al.* B-cell repertoire dynamics after sequential hepatitis B vaccination and evidence for cross-reactive B-cell activation. *Genome Med.* **8,** 1–13 (2016).
67. Pedersen, G. K. *et al.* Serum IgG titres, but not avidity, correlates with neutralizing antibody response after H5N1 vaccination. *Vaccine* **32,** 4550–4557 (2014).
68. Henry, C., Palm, A. K. E., Krammer, F. & Wilson, P. C. From Original Antigenic Sin to the Universal Influenza Virus Vaccine. *Trends Immunol.* **39,** 70–79 (2018).

Supplementary information to 'Escape from the H3N2 influenza vaccine response due to a single amino acid change relates to a restricted memory B cell repertoire'

Supplementary methods

Bead coupling

The influenza A rHA of the different influenza A strains was coupled to MagPlex® microspheres (Luminex corporation, Austin, TX, USA), carboxylated polystyrene microparticles (hereafter termed 'beads' throughout the manuscript), mainly following the manufacturer's instructions (xMAP® cookbook, 3rd edtion, chapter 4.2) with some alterations and amendments: MES buffer instead of sodium phosphate buffer was used to activate the carboxylic acids on the beads. Generally, 1.25 µg of HA protein was coupled onto 5M of beads in a volume of 500 µL of MES buffer, since it showed to generate the strongest signals in the immunoassay. For the rHA-beads exposed to plasma from 2017/2018, beads were downscaled to 1.25M with the same volume and amount of protein used. In order to adjust protein load per bead between bead types (see next paragraph), also amount of protein and coupling volume had to be altered in some cases.

Coupling validation

In experiments where signals were compared between different types of beads (i.e. against different rHA), equal protein load between bead types had to be assured. This was accomplished by incubating beads with a broadly cross-reactive antibody against stem (1 µg/mL, 86001-RM01, Sino Biological) (HA0 rHA only) and an anti-His antibody (1 µg/mL, A00174, GenScript) (all rHA) followed by incubation with a PE-labeled anti-rabbit IgG antibody (1 µg/mL, 406421, Biolegend) according to the protocol in the next paragraph.

Multiplexed immunoassay: Extended protocol

Three multiplexed bead sets were prepared to measure i) cross-reactivity in the 2007/08 cohort (13 HA-coupled bead types, together with BSA-coupled and uncoupled beads), ii) cross-reactivity in the 2017/18 cohort (2 bead types) and iii) viral escape in all investigated cohorts (3 bead types). Human plasma samples were centrifuged for 10 min at 4 °C in a microcentrifuge at maximum speed prior to use and then diluted 1:500 in PBS with 1% BSA (PBS-BSA). 20 µL of diluted plasma were added to 20 µL of bead mixture (50 beads/µL of each type) in a 96-well plate and incubated for 60 minutes at RT on a plate shaker at 800 rpm. The beads were washed twice in 100 µL PBS-TBN buffer (0.1% BSA, 0.02% TWEEN®-20, 0.05% sodium azide, pH 7.4). A PE-labeled mouse anti-human IgG Fc antibody (clone JDC-10, 9040-09, SouthernBiotech, Birmingham, AL, USA) was added at 1 µg/mL in PBS-BSA and incubated for 30 min. at RT and 800 rpm. Binding of influenza-specific IgG antibodies was measured on a Luminex® 100 analyzer running on xPonent® software (Luminex Corporation). The extent of antibody-binding is represented by the PE median fluorescence intensity (MFI). The vaccine response was calculated as background-corrected (BSA-coated beads) ΔMFI day 28 - day 0. Vaccine response against HA

of the H1N1 and H3N2 vaccine strains was set to 1 and responses against the other strains were scaled to the respective vaccine strain response for each subject. Donors with a ΔMFI < 25 against the vaccine strain were considered non-responders and excluded from data analysis. GraphPad Prism v.7 (GraphPad Software, La Jolla, CA, USA) was used for statistical analysis and data presentation.

Fluorescence-activated cell sorting of B cell subsets and antigen-specific B cells

Cryopreserved PBMC from healthy donors before (day 0) and after vaccination (day 7), were thawed and rested over night. The next morning, cell count and viability was determined and cells were stained with antibodies against CD14 (FITC, clone MϕP9, 345784), CD16 (FITC, clone NKP15, 335035) and CD27 (PE, clone L128, 340425), all from BD Biosciences and against CD3 (Alexa Fluor 488®, clone UCHT1, 300415), CD19 (Alexa Fluor 700®, clone HIB19, 302226), CD20 (Brilliant Violet 510TM, clone 2H7, 302340), CD38 (APC, clone HIT2, 303510) and IgD (PE-Cy7, clone IA6-2, 348210), all from Biolegend. For HA-specific staining, d7 PBMC were first incubated in PBS with 100 mU/mL of Neuraminidase (N5631-1UN, Sigma Aldrich, St. Louis, MO, USA) for 1 hour at 37°C to reduce non-specific HA-binding [1]. Then, cells were stained with antibodies against CD3 (Alexa Fluor 700®, clone OKT3, 317340) and CD19 (PE-Cy7, clone HIB19, 302216), FITC-coupled HA from H1N1 A/Michigan/45/2015 and PE-coupled HA from H3N2 A/Hongkong/4801/2014. Conjugation was performed with Lightning-Link Fluorescein/R-PE antibody labeling kit (707-0030 and 703-0030, Expedeon, San Diego, CA, USA) according to manufacturer's instructions (protein concentration 4x lower than recommended). Before HA-staining, sialic acids on PBMC were removed with 100 mU/mL neuraminidase (N5631, Sigma Aldrich) at 37°C for one hour in order to reduce unspecific staining. Compensation was performed using single stained Antibody Capture Beads (VersaComp, B22804, Beckman Coulter). All B cell subsets were sorted into medium on a FACSAria® III (BD Biosciences) using a 70 µM nozzle. The gating strategy is indicated in ***Supplementary Figure S1***. Cells were pelleted and kept at -80°C until RNA extraction.

IgG-BCR-sequence library preparation: Extended protocol

IgG heavy chain libraries compatible for sequencing with the Illumina MiSeq platform (paired-end 2x 300 bp) were prepared similarly to a previously described two-step primer extension method for mouse Ig heavy chains [2]. This method proved to enable high amplification efficiency and broad capture of repertoire diversity. Due to the extended scope and in order to increase yield, some procedures were different in the 2017/18 cohort and are depicted in [brackets]. Total RNA from [naïve B cells (day 0)], memory B cells (day 0 and 7 (only 07/08) and plasmablasts, [H1- and H3-specific B cells (day 7)] was isolated with the RNeasy® Plus Micro kit (74034, Qiagen, without column-based gDNA elimination but with adding 200 ng of carrier RNA (in the 2007/08 cohort only) according to manufacturer's 'Animal and Human Cells' protocol. Subsequently, the complete RNA was depleted from genomic DNA with RQ1 RNAse-Free DNAse

(M6101, Promega) according to protocol. First-strand cDNA was synthesized from total RNA by using AccuScript Hi-Fi Reverse Transcriptase (200820, Agilent Technologies) with oligo(dT) primers according to manufacturer's protocol in triple volume. Following RT, a bead-based nucleic acid clean-up was carried out: The complete RT product (60 µL) was mixed with 48 µL of SPRIselect magnetic beads (B23318, Beckman Coulter) on a custom-made magnet in order to perform a 0.8x left-sided clean-up (i.e. remove smaller DNA fragments up to a certain threshold). The supernatant with the small fragments was discarded and bead-bound DNA washed twice with 85% Ethanol and finally eluted in 20 µL of water.

For PCR amplification of the rearranged heavy chain locus, a set of eight forward primers containing an overhang and annealing to framework region 1 [3] and reverse primers binding to Cγ1-4 [and Cµ (for naïve and memory B cells)], containing another overhang, were used in PCR 1 (complete primer list in ***Supplementary Table S2***). In a reaction volume of 25 µl with 5% DMSO [and 100 ng of the ssDNA-stabilizing enzyme ET SSB (M2401, New England Biolabs, Ipswich, MA, USA)], half [a third] of the purified cDNA was amplified with Q5® High-Fidelity DNA Polymerase (M0491, New England Biolabs) by using the following settings: Activation at 98°C for 30s followed by 4 [6] cycles of 98°C for 20s, 48°C for 40s, 72°C for 60s; 4 [6] cycles of 98°C for 20s, 53°C for 40s, 72°C for 60s; 12 [14] cycles of of 98°C for 20s, 60°C for 40s, 72°C for 60s and 2 minutes of extension at 72°C. After this overall 20 [26] cycles, a bead-based 0.8x left-sided clean-up was performed again followed by elution in 20 µL of water [separation on a 1% agarose gel stained with SYBR® Safe (S33102, Invitrogen) was carried out followed by purification of the appropriately sized bands (around 500 bp). MinElute® Gel Extraction Kit (28604, Qiagen) was used, elution in 10 µL of water]. PCR 2 was used to add Illumina adapter sequences and population-specific Illumina indices (TruSeq index reverse primers, RPI1-16, 18-37). Complete PCR 1 product was amplified with Q5® DNA Polymerase in two parallel [one] reaction(s) of 25 µL volume with 5% DMSO with the following conditions: Activation at 98°C for 30s followed by 4 [6] cycles of 98°C for 20s, 40°C for 40s, 72°C for 60s; 12 [16] cycles of 98°C for 20s, 65°C for 40s, 72°C for 60s and 2 minutes of extension at 72°C. After 0.8x SPRIselect left-sided size selection and elution in 20 µL of water (only 07/08), the complete product of PCR 2 was mixed with 6 µL of 30% glycerol and gel-purified as described above. DNA concentration of all purified PCR products was assessed with a Quantus™ Fluorometer using the QuantiFluor® ONE dsDNA System (E4870, both Promega). Regardless of concentration [concentration of individual libraries were diluted to account for input cell number while aiming at a minimal sequencing depth of 10 and highest possible concentration of the final library], 2 µL per sample was added to the final library and its quality and quantity was verified on a Fragment Analyzer™ (Advanced Analytical Technologies Inc., Ankeny, IA, USA) using DNF-473 Standard Sensitivity NGS fragment analysis kit. The number of successful paired-end reads in the 2007/08 run ranged from 346 to 373'695 (memory B cells) and 99'666 to 1'080'549 (plasmablasts).

ELISpot for antigen-specific B cells

PVDF plates (3654-WP-10, Mabtech, Nacka Strand, Sweden) were activated with 20 µL of 35% ethanol per well for one minute. Subsequently, plates were washed five times with water and supplied with 50 µL/well of antigen in PBS at a concentration of 2.5 µg/mL. HA0 of A/Michigan/45/2015 (H1N1) and A/Hong Kong/4801/2014 (H3N2) were used, as well as anti-human IgG (clone MT91/145, 3850-3-250, Mabtech) as a positive control. Plates were coated over night at 4°C. Afterwards, plates were washed five times with PBS and blocked by addition of 200 µL of RPMI with 10% FCS (incubation at 37°C for 2 hours).

H1- and H3-specific and HA-negative B cells were sorted into RPMI (+ 10% FCS) and activated at 37°C for three days in the presence of 25'000 autologous $CD19^-$ feeder cells, IL-21 (200-21, Peprotech, London, UK) and CD40L (SRP8044, Sigma Aldrich) at a concentration of 100 ng/mL. Then, antigen-specific B cells were thoroughly washed and around 100 B cells (based on counts by flow cytometry) in 200 µL of RPMI were added per well to the coated and blocked PVDF plates. Incubation for six hours at 37°C. Subsequently, the plates were washed twice with PBS, twice with PBS containing 0.05% Tween (PBS/Tween) and again twice with PBS. 100 µL (1 µg/mL) of biotinylated anti-human IgG antibody (clone MT78/145, 3850-6-250, Mabtech) was added for 90 minutes at room temperature (RT). After five times washing with PBS/Tween, 100 µL of Streptavidin-ALP (alkaline phosphatase, 12100018, Lophius Biosciences, Regensburg, Germany) at 1 µg/mL was added for one hour at RT. Then, plates were three times washed with PBS/Tween, three times with PBS, plate bottom cover was removed and membranes rinsed with deionized water. Afterwards, 50 µL of filtered BCIP/NBT (ALP-substrate, 3650-10, Mabtech) was added. Incubation for 7 minutes at RT in the dark. After extensively rinsing with deionized water, plates were dried and analyzed on an AID EliSpot Reader System ELR07 (AID GmbH, Strassberg, Germany) with EliSpot Reader software (v.7, AID GmbH).

	2007/2008	2017/2018
Study participants (n)	24	48
Age: median + (range)	34 (22 - 76)	43 (25 - 85)
% female	46%	N.A.
No vaccine response H1N1	4	10
No vaccine response H3N2	3	5
0x vaccinated (12/13 – 16/17)	N.A.	7
1x vaccinated (12/13 – 16/17)	N.A.	4
2x vaccinated (12/13 – 16/17)	N.A.	7
3x vaccinated (12/13 – 16/17)	N.A.	7
4x vaccinated (12/13 – 16/17)	N.A.	6
5x vaccinated (12/13 – 16/17)	N.A.	17

Supplementary Table S1: Characteristics of the 2007/08 and 2017/18 vaccination cohorts. Data for the healthy subjects included into the cohorts is shown. Vaccination history was only established in the 2017/18 cohort. N.A: not available.

Strain (H1N1)	HA0/HA1	Expression	Provider	Article Nr.
A/Brevig Mission/1/1918	HA0	HEK cells	Sino Biological Inc.	11068-V08H
A/New Caledonia/20/1999	HA0	HEK cells	Sino Biological Inc.	11683-V08H
A/Solomon Islands/3/2006	HA0	HEK cells	Sino Biological Inc.	11708-V08H
A/Brisbane/59/2007	HA0	HEK cells	Sino Biological Inc.	11052-V08H
A/California/07/2009	HA0	HEK cells	Sino Biological Inc.	11085-V08H
A/California/07/2009	HA0	HEK cells	eEnzyme LLC	IA-SW-12P
A/Michigan/45/2015	HA0	HEK cells	eEnzyme LLC	IA-H1-M15WP

Strain (H3N2)	HA0/HA1	Expression	Provider	Article Nr.
A/Hong Kong/1/1968	HA0	BEVS	Sino Biological Inc.	40116-V08B
A/Moscow/10/1999	HA0	BEVS	Sino Biological Inc.	40154-V08B
A/Fujian/411/2002	HA0	BEVS	Sino Biological Inc.	40120-V08B
A/California/7/2004	HA0	BEVS	Sino Biological Inc.	40118-V08B
A/Wisconsin/67/2005	HA0	BEVS	Sino Biological Inc.	11972-V08B
A/Brisbane/10/2007	HA0	BEVS	Sino Biological Inc.	11056-V08B
A/Victoria/361/2011	HA0	BEVS	Sino Biological Inc.	40145-V08B
A/Texas/50/2012	HA0	BEVS	Sino Biological Inc.	40354-V08B
A/Victoria/361/2011	HA1	HEK cells	Sino Biological Inc.	40145-V08H1
A/Texas/50/2012	HA1	HEK cells	Sino Biological Inc.	40354-V08H1
A/Texas/50/2012 N128T	HA1	HEK cells	Sino Biological Inc.	Custom-made
A/H3N2/Hongkong/4801/2014	HA1	HEK cells	Sino Biological Inc.	40555-V08H

Supplementary Table S2: List of recombinant hemagglutinin from H1N1- and H3N2-strains used in the study. HA was either used in the multiplexed immunoassay or for labeling antigen-specific B cells. HA0: Full-length, uncleaved HA. HA1: Only HA1-subunit. BEVS: Baculovirus expression vector system.

Strain (H1N1)	Accession number
A/Brevig Mission/1/1918	AF116575
A/New Caledonia/20/1999	CY033622
A/Solomon Islands/3/2006	EU124177
A/Brisbane/59/2007	CY058487
A/California/07/2009	FJ969540

Strain (H3N2)	Accession number
A/Hong Kong/1/1968	CY033996
A/Moscow/10/1999	DQ487341
A/Fujian/411/2002	CY112933
A/California/7/2004	EU103820
A/Wisconsin/67/2005	CY034116
A/Brisbane/10/2007	Y035022
A/Victoria/361/2011	KJ942680
A/Texas/50/2012	KC892248

Supplementary Table S3: List of strains included to calculate sequence homology and phylogenetic relatedness. Accession numbers are indicated for HA amino acid sequences. The strains correspond to those included in the multiplexed immunoassay.

PCR 1

IgH forward	**Overhang Fw + VH 5'-specific Region**
huVH1-GLUE-fw1	CCC TCC TTT AAT TCC CCA GGT CCA GCT KGT RCA GTC TGG
huVH157-GLUE-fw2	CCC TCC TTT AAT TCC CCA GGT GCA GCT GGT GSA RTC TGG
huVH2-GLUE-fw3	CCC TCC TTT AAT TCC CCA GRT CAC CTT GAA GGA GTC TG
huVH3-GLUE-fw4	CCC TCC TTT AAT TCC CGA GGT GCA GCT GKT GGA GWC Y
huVH4-GLUE-fw5	CCC TCC TTT AAT TCC CCA GGT GCA GCT GCA GGA GTC SG
huVH4-DP63-GLUE-fw6	CCC TCC TTT AAT TCC CCA GGT GCA GCT ACA GCA GTG GG
huVH6-GLUE-fw7	CCC TCC TTT AAT TCC CCA GGT ACA GCT GCA GCA GTC A
huVH3N-GLUE-fw8	CCC TCC TTT AAT TCC CTC AAC ACA ACG GTT CCC AGT TA
IgG isotype reverse primer	**Overhang Rv + IgH/L 3'-specific region (reverse complement)**
hu-IgGall-GLUE-rv	GAG GAG AGA GAG AGA GCW GAT GGG CCC TTG GTG GAR G

PCR 2

	TruSeq Universal Adapter + Required Diversity region + Overhang Fw
PE-IgALL-Univ-Fw	AAT GAT ACG GCG ACC ACC GAG ATC TAC ACT CTT TCC CTA CAC GAC GCT CTT CCG ATC TNN NNC CCT CCT TTA ATT CCC
	TruSeq Adapter Index (reverse complement) + Required Diversity region + Overhang Rv
PE-Index-Rv	CAA GCA GAA GAC GGC ATA CGA GAT (Index) GTG ACT GGA GTT CAG ACG TGT GCT CTT CCG ATC TNN NNG AGG AGA GAG AGA GAG

Illumina Index Sequences (contained in primer PE-Index-Rv)

Idx 1	CGTGAT	**Idx 13**	TGTTGACT	**Idx 26**	GCTCAT
Idx 2	ACATCG	**Idx 14**	ACGGAACT	**Idx 27**	AGGAAT
Idx 3	GCCTAA	**Idx 15**	TCTGACAT	**Idx 28**	CTTTTG
Idx 4	TGGTCA	**Idx 16**	CGGGACGG	**Idx 29**	TAGTTG
Idx 5	CACTGT	**Idx 18**	GTGCGGAC	**Idx 30**	CCGGTG
Idx 6	ATTGGC	**Idx 19**	CGTTTCAC	**Idx 31**	ATCGTG
Idx 7	GATCTG	**Idx 20**	AAGGCCAC	**Idx 32**	TGAGTG
Idx 8	TCAAGT	**Idx 21**	TCCGAAAC	**Idx 33**	CGCCTG
Idx 9	CTGATC	**Idx 22**	CGTACG	**Idx 34**	GCCATG
Idx 10	AAGCTA	**Idx 23**	CCACTC	**Idx 35**	AAAATG
Idx 11	GTAGCC	**Idx 24**	GCTACC	**Idx 36**	TGTTGG
Idx 12	TACAAG	**Idx 25**	ATCAGT	**Idx 37**	ATTCCG

Supplementary Table S4: List of primers for generation of IgG heavy chain libraries. Our primer extension method was adapted from a previously published report for mouse IgG [2]. The primers specific for the variable region were published by Ippolito et al. [4]

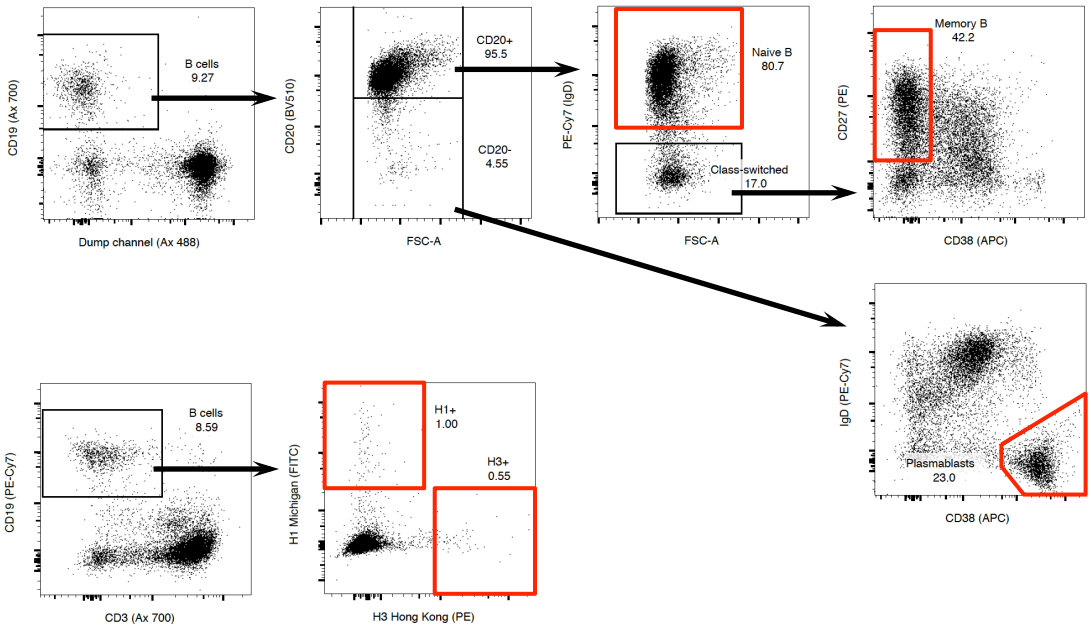

Supplementary Figure S1: Gating strategy for FACS. One flow-panel (upper part) was used to stain for naïve and memory B cells (d0) and plasmablasts (d7), the second panel (lower part) to stain for H1- and H3-specific B cells (d7). Gates are shown in red within doublet-negative lymphocytes. 10'000 events per image are shown, hence events per gate are not representative for proportions of B cell subsets. Figure created with FlowJo v.10, FlowJo, LLC.

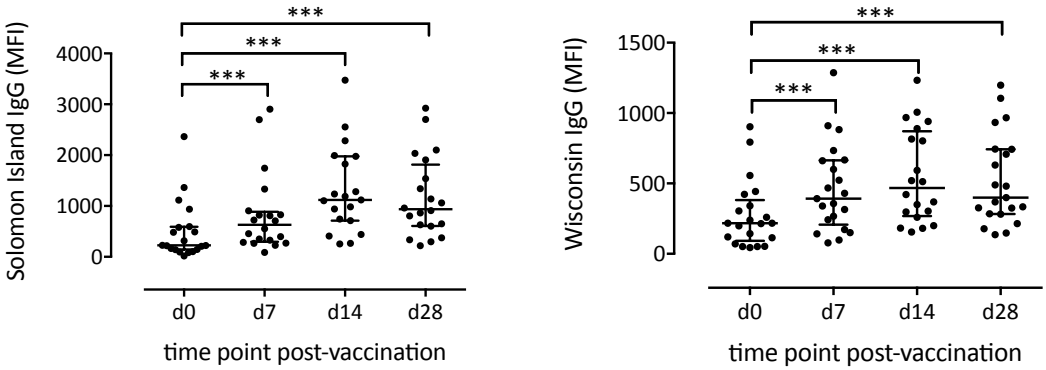

Supplementary Figure S2: Subjects included into the 2007/08 react towards the influenza A components of the vaccine. Vaccine responses are shown as background corrected MFI-values before and at three time points post-vaccination. Four donors did not respond to the H1N1 component (left panel) of the 2007/08 vaccine, three not to the H3N2 component (right panel). Median with IQR is indicated. Antibody levels are slightly higher at day 14 compared to day 28. P values were estimated with Wilcoxon signed rank test (*** $p > 0.001$)

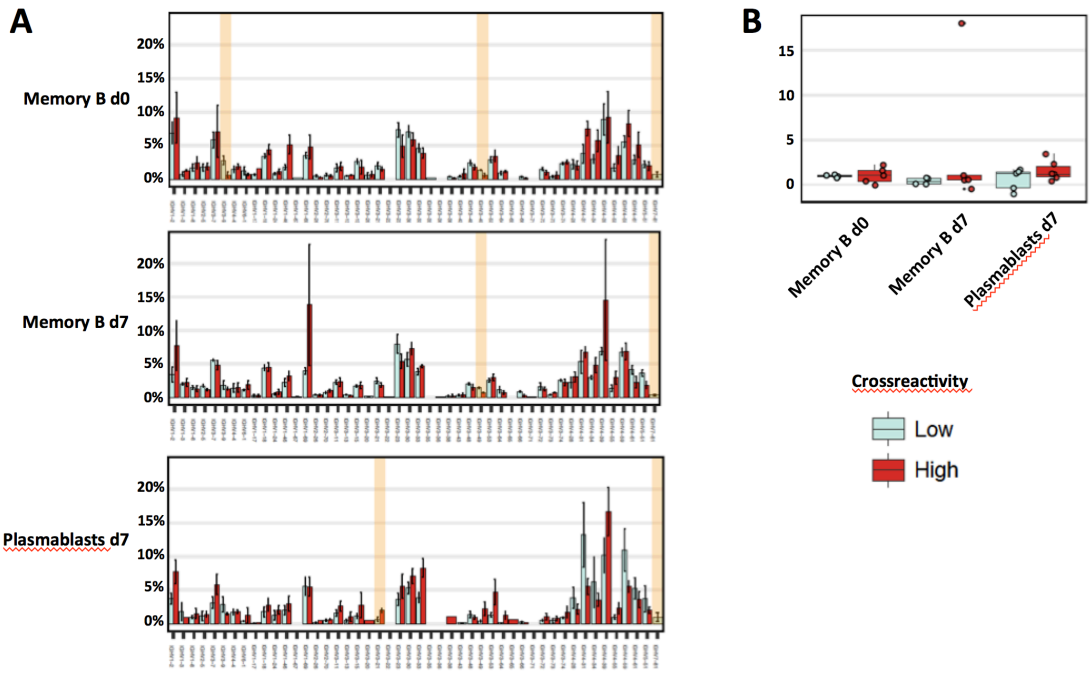

Supplementary Figure S3: V gene usage and somatic hypermutation in B cell subsets. A) Frequency of V genes present in the sequenced BCR between cell populations and reactivity groups. Yellow bars indicate significantly different usage but further analysis was not pursued since usage was never higher for the high-crossreactivity group (which might have indicated broadly cross-reactive antibodies). **B)** Degree of somatic hypermutation (SHM, amino acids changed compared to germline sequence across the sequenced region) between B cell populations and reactivity groups.

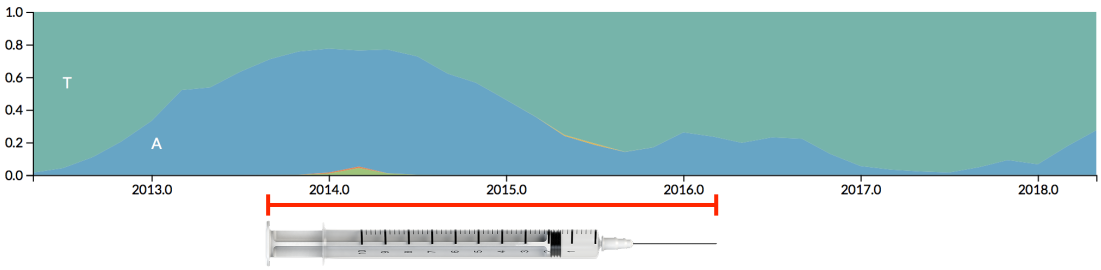

Supplementary Figure S4: Frequency of viral isolates belonging to H3N2 clade 3c3. Clade 3c3-strains are defined by the T128A-mutation. The frequency of 128A is shown in blue from April 2012 until April 2018 based on HA-sequences from 2084 viral isolates worldwide. After its emergence in 2012, 3c3 was the most abundant clade in the following two years. Vaccination period (northern and southern hemisphere) using a clade-matched strain based on the motif surrounding position 128, i.e. N-W-N128 (Texas-like) or N-W-A128 (Switzerland-like) is indicated with the syringe. Figure made with nextstrain tool [5] based on HA sequence data deposited in the GISAID database [6].

References

1. Bardelli, M. *et al.* Ex Vivo Analysis of Human Memory B Lymphocytes Specific for A and B Influenza Hemagglutinin by Polychromatic Flow-Cytometry. *PLoS One* **8,** (2013).
2. Menzel, U. *et al.* Comprehensive evaluation and optimization of amplicon library preparation methods for high-throughput antibody sequencing. *PLoS One* **9,** 1–12 (2014).
3. Krebber, A. *et al.* Reliable cloning of functional antibody variable domains from hybridomas and spleen cell repertoires employing a reengineered phage display system. *J Immunol Methods* **201,** 35–55 (1997).
4. Ippolito, G. C. *et al.* Antibody Repertoires in Humanized NOD-scid-IL2Rcnull Mice and Human B Cells Reveals Human-Like Diversification and Tolerance Checkpoints in the Mouse. *PLoS One* **7,** (2012).
5. Neher, R. A. & Bedford, T. nextflu: real-time tracking of seasonal influenza virus evolution in humans. *Bioinformatics* **31,** 3546–3548 (2015).
6. Shu, Y. & Mccauley, J. GISAID : Global initiative on sharing all influenza data – from vision to reality. *Eurosurveillance* **22,** (2017).

Discussion

Complementary comments

In our manuscript, the focus was set on analyzing the breadth of the vaccine-induced B cell response against influenza A and determining possible gaps representing putative escape variants. This was done by retrospectively harnessing a 2007/08 vaccination cohort and measuring vaccine responses against HA, the main antibody target, from multiple strains in a multiplexed antibody-binding assay. This approach had the advantage that we could not only test strains that were previously circulating in the population, but also antigenically drifted strains that emerged in the years following vaccination. The reactivity against most of the tested strains was quite heterogeneous across the whole cohort, implying factors beyond the antigenic properties of the virus affecting cross-reactivity. High pre-existing IgG levels had a positive effect on antibody cross-reactivity, as previously described [107]. Beyond that and not specifically assessed, it is plausible that age, number and type of vaccinations and infections contributed to the observed heterogeneity [104,106,108].

In contrast, the antigenic properties of A/Texas/50/2012, a future strain at time point of vaccination, outbalance the effects of pre-existing immunity. Specifically, its hemagglutinin was poorly recognized by most subjects due to the T128N mutation leading to a loss of glycosylation at position N126. Sequence context analysis suggests a likewise loss of glycosylation in all strains of the 3c3 clade (A128) [109], potentially contributing to its fast expansion in 2013. We showed recognition of the Texas variant to be increased in 2014/15, after inclusion of a matched strain into the vaccine, only to drop back to pre-vaccination levels in 2017/18. This lack of memory formation could indicate inaccessibility to the epitope for N128(Texas)-specific B cells. Shielding of epitopes by emergence of N-linked glycosylation is well known for influenza HA [89,110]. In contrast, the proportion of antibodies targeting preceding strains (e.g. Victoria) but not Texas must have been at least partially directed against carbohydrates. Anti-carbohydrate antibodies are not so frequent, but they can be of high affinity and are well studied in the HIV field [111,112].

BCR-repertoires and repetitive vaccination

The 2017/18 cohort was a pilot study to prospectively investigate effects of repetitive vaccine exposure to antibody cross-reactivity and the structure of the B cell repertoire. Since vaccine history was inquired back until season 2012/13, i.e. vaccinations of the five seasons before 2017/18 were known; we were already able to address some points relating to vaccination history. Indeed, the situation for H1N1 was very interesting: from 2012/13 on, vaccines included HA of an A/Christchurch/16/2010-like virus that was altered to HA from an A/Michigan/45/2015-like virus in 2017/18. We did, however, not find preferential targeting of Christchurch in subjects repeatedly vaccinated with this strain, probably reflecting the lack of antigenicity of the sites altered between the two strains. After 2012/13, the H3N2 strain was adapted three times until 2017/18. Between 2013/14 and 2015/16, vaccinations included strains very likely lacking glycosylation at position N126. Again, in those subjects vaccinated in all three respective seasons, we could not find differences in the response to these strains (precisely: Texas). Possible reasons were discussed above.

We adapted our protocol that we used for preparing the BCR sequencing libraries from 2007/08 in a way to increase the yield of the PCR-products (see **Supplementary Methods**). By using this altered protocol, we generated BCR-repertoire libraries from sorted naïve and memory B cells (day 0) and plasmablasts (day 7) from 23 subjects included in the 2017/18 cohort with especially few or many vaccinations in the last five years. From 16 of them, we also produced libraries from sorted HA-specific B cells. These were labeled and sorted according to a strategy we based on a previously published protocol [113]. Specifically, we coupled recombinant HA from A/Michigan/45/2015 and A/Hong Kong/4801/2014, the current H1N1 and H3N2 vaccine strains to PE and FITC respectively (**Supplementary Methods**). Enrichment for antigen-specific B cells was confirmed by EliSpot (**Supplementary Methods** and **Figure 9**). Brief, HA-specific B cells were activated for 3 days in the presence of 100 ng/mL of IL-21 and CD40L. Around 100 B cells were then incubated for six hours on plates coated with H1 (Michigan), H3 (Hong Kong) or anti-human IgG Fc antibodies as a positive control.

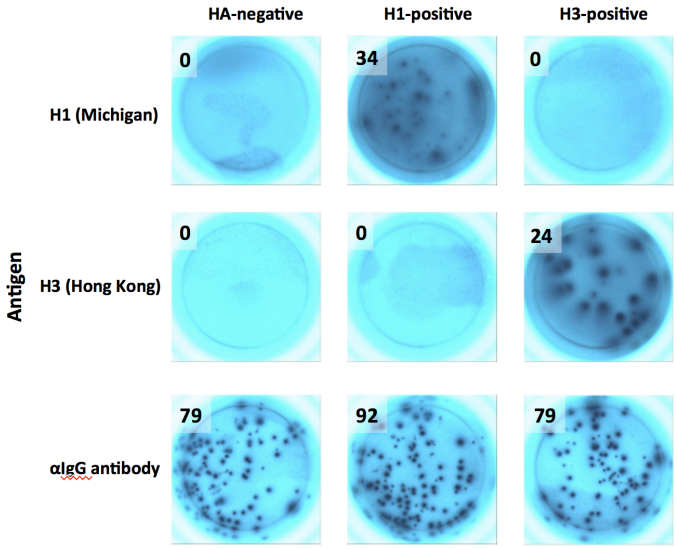

	Mean spot number	
	H1-positive	H3-positive
H1 (Michigan)	34	2.5
H3 (Hong Kong)	0	23
αIgG antibody	89.5	61.5
Specificity	**38%**	**37.4%**

Figure 9: Sorted HA-positive B cells produce IgG antibodies against their cognate antigen. EliSpot data is shown for one vaccinated donor (d21 post-vaccination). One well per condition is depicted with the respective spot number indicated. Samples were tested in duplicates; the specificity of HA-positive B cells is calculated as the proportion of H1/H3-specific spots of total αIgG spots.

At time point of thesis submission, the BCR sequencing is still pending for the 2017/18 cohort. If successful, it will allow us to track the extent of B cell lineage recruitment from the memory or naïve B cell pool to the plasmablast population. We would also be able to confirm whether those individuals with poor cross-reactivity (again against A/Texas/50/2012 or novel putative escape variants, ongoing project not discussed here) present with a narrower BCR repertoire. Finally, the availability of HA-specific BCR sequences would allow us to validate the expanded B cell lineages and investigate whether e.g. repeated vaccination has an effect on the HA-specific repertoire composition.

Vaccine preparations

If confirmed in a prospective setting over several influenza vaccination seasons, our finding of altered antigenicity due to glycosylation changes may inform vaccine design regarding viral strain selection. Since influenza A viruses frequently change their glycosylation pattern [110,114], it might be beneficial to include multiple current variants per serotype in the vaccine to account for potential escape variants. The possibility to elicit vaccine-induced immune responses against several strains in parallel has been

demonstrated e.g. against HIV-1 or *Streptococcus pneumoniae* [115,116]. However, since the vast majority of all influenza vaccine doses administered are currently produced in the conventional way in fertilized chicken eggs, controlled generation of multiple strains per serotype at once is not possible [74]. While being safe and involving low production costs, these vaccines have a second limitation: The propagation of virus in eggs can lead to adaptive mutations for avian-type sialic acid to galactose linkage (SAα2,3Gal) present on cells in the amniotic fluid [77]. This can alter antigenicity against viruses adapted to human sialic acid linkage (SAα2,6Gal) resulting in lower protection [78,80]. Third, around 8 months are required from evaluating the surveillance data over deciding and testing candidate vaccine viruses until marketing of a vaccine in sufficient quantities [117]. Therefore, efforts have been undertaken to produce alternative vaccines.

There are now two FDA-approved seasonal influenza vaccines available that use recombinant technology and therefore circumvent the need for eggs [118]. One is a split vaccine that is produced in MDCK cells. The other one contains only hemagglutinin, which is produced in an insect cell line with help of a Baculovirus expression vector. Hence, problems with egg-adapted variants do not arise anymore and production speed is increased. These technologies would also allow the production of multiple strains for vaccine inclusion, however, only the WHO-proposed variants are included in the vaccines currently.

Besides altering the production mode, a lot of research has been invested in directing the vaccine response against highly conserved structures. One strategy is to induce broader and maybe even heterosubtypic (across serotypes) B cell protection. Conventional vaccination, and also infection, induces undetectable or very low amounts of antibodies targeting NA, NP, M or the very conserved HA stem [119,120]. Nevertheless, bnAbs targeting the HA stalk have been described, some even recognizing all known HA subtypes [121,122]. They often seem to act through Fc-mediated effector functions [123]. A stable trimeric form of the H1 HA2-domain could be engineered for potential vaccination use, showed binding of known stem-targeting monoclonal antibodies and reduced infection-induced fever in non-human primates [124,125]. Interestingly, following the 2009 pandemic with reassorted H1N1 virus, the production of stem-specific antibodies, even with neutralizing capacity, was boosted in infected individuals [126]. This led to the assumption that the antigenicity of the HA-stem can be augmented if there is no memory recall for the head region, i.e. that the head region consists of a protein not yet encountered by the immune system such as in the 2009 pandemic. Indeed,

vaccination with an H5N1 virus, where the head region was unknown to the host's immune system, showed to boost the level of anti-stem antibodies [127]. Unfortunately, upon re-vaccination with H5N1, the humoral response against the head region dominated again. This phenomenon might be due to the lower capability of stem-specific memory B cells to bind to their target during recall due to steric hindrance [108]. Probably also because they do not work optimally in individuals with preexisting influenza virus immunity (i.e. the majority of people), stalk-based vaccines are not evaluated in clinical trials yet.

The development of a broadly applicable T cell vaccine is particularly challenging, given the varying distribution of HLA-genotypes across populations. Nevertheless, since T cells seem to be responding to very conserved viral targets [70–72], a vaccine inducing cytotoxic T cells would likely be very useful against pandemic viruses and have the potential as a universal vaccine [128]. Live-attenuated vaccines increase the proportion of influenza-specific T cells to some extent [129]. A vector-based vaccine enabling synthesis of influenza NP and M1 showed an increase in lytic virus-specific T cells and conferred some protection against viral challenge in a small cohort [130,131]. A peptide-based vaccine covering highly conserved regions of multiple influenza A protein showed a negative correlation between T cell responses and viral shedding but did not confer protection [132].

Taken together, broader protection against antigenically different viruses – emerging clades or antigenically shifted pandemic variants – may be gained by the induction of bnAbs against conserved structures such as the HA-stalk. However, the memory B cell response is predominantly targeted towards the HA-head region, likely also due to sterical reasons. The possibility for simultaneous production of multiple strains in mammalian cell lines could increase the breadth of neutralizing head-specific antibodies. T cell help might be increased with live-attenuated vaccines or vector-based vaccines.

FOCUS II: UNRAVELING ANTIGEN-SPECIFIC IMMUNE RESPONSES IN GIANT CELL ARTERITIS

Introduction

Clinical and epidemiological features

Giant cell arteritis (GCA) is an inflammatory disease affecting medium-sized and large arteries. Patients typically present with a systemic inflammation in combination with strong headaches, jaw pain when chewing ('jaw claudication') and scalp tenderness together with polymyalgia rheumatica (PMR, muscle pain of the shoulders). Less frequent symptoms depend also on the localization of the arteritis; these include ocular symptoms such as transient ('amaurosis fugax') or permanent vision loss, stroke or limb claudication. Such ischemic events are the most feared complications of GCA. They are caused by intima (innermost artery layer) hyperplasia induced by the local immune response [133,134].

The disease is almost exclusively occurring in people above 50 years of age and women are more often affected than men. Incidence is highest in Caucasians, especially in people of Northern European descent, going up to 27/100'000 in those older than 50 years [135,136]. In Japan, incidence was reported to be only 1.47/100'000 [137].

Disease diagnosis relies on the clinical presentation, imaging findings showing inflamed large arteries and most importantly on the histology of an affected artery, typically the temporal artery (TA). For study purposes, classification criteria have been established. These include age above 50 at disease onset, new onset of localized headache, temporal artery tenderness, elevated erythrocyte sedimentation rate and positive TA biopsy. At least three out five criteria should be fulfilled. A positive TA biopsy shows transmural infiltrates of $CD4^+$ T cells and presence of multinucleated giant cells that gave the disease its name [138]. Arterial wall layers and characteristic GCA histopathology are shown in **Figure 10A-C.**

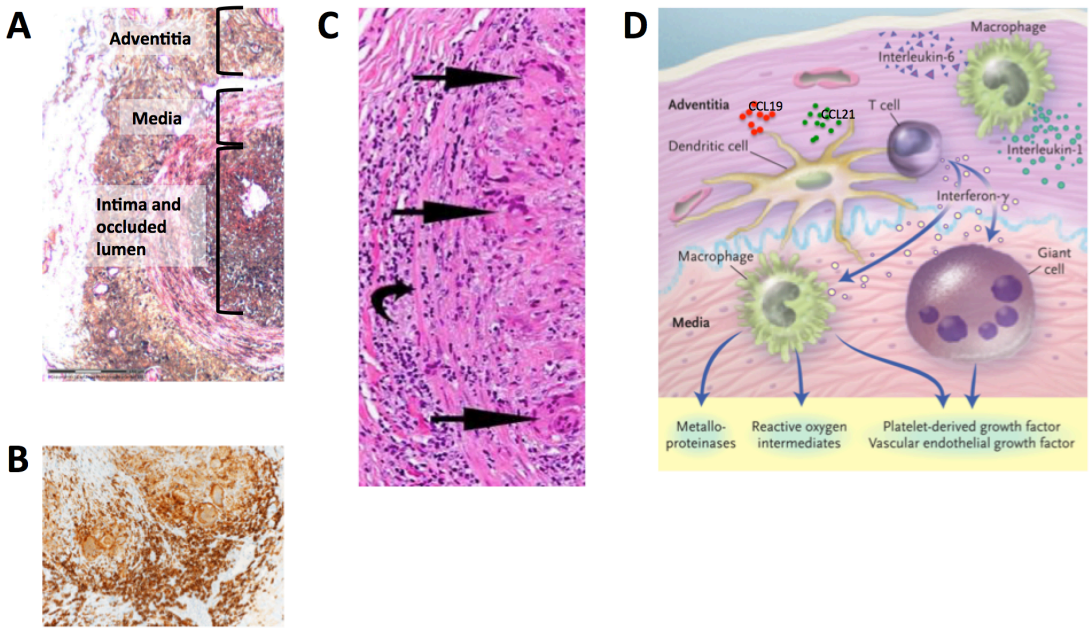

Figure 10: Arterial wall pathology in GCA. A) H&E-staining of a cross-sectional slide from a temporal artery with almost complete luminal occlusion. The names of the wall layers are indicated. **B)** GCA-TA staining with an antibody against CD4 showing a high degree of T cell infiltration. **C)** TA H&E-staining showing the GCA-typical giant cells, multinucleated structures of fused macrophages (indicated with black arrows). **D)** Summary of the interplay of innate and adaptive immune response leading to the observed immunopathology. Figures A and B show histological slides of our own, C is from an online pathology picture deposit [139] and figure D is adapted from Weyand et al., NEJM 2003 [134].

Disease pathogenesis

Blood vessels are indispensable for delivering oxygen, nutrients, electrolytes, immune effectors etc. to all organs throughout the body. Consequently, damage to arteries especially of larger size absolutely needs to be prevented. In this context, the media (muscular layer of an artery) is often spared from inflammatory processes; it is considered an immunoprivileged zone due to tolerogenic dendritic cells [140]. This is not the case in GCA.

The external elastic lamina that separates the adventitia from the media is lined with vascular dendritic cells, a tissue-resident APC. Under homeostatic conditions, they are in an inactivated state and send inhibitory signals upon encounter with T cells. However, in case of PMR and GCA, those DCs become activated and produce the chemokines CCL19 and CCL21 that attract T cells through the vasa vasorum, small blood vessels pervading the adventitia and media layers of larger arteries [140,141].

The attracted T cells are of the Th1- and Th17-type; they mainly produce IFN-γ and IL-17, respectively, which have pleiotropic effects. For example, IFN-γ is a potent inducer of macrophage activation and can trigger apoptosis in vascular smooth muscle cells (VSMC) or mediate their migration towards the vessel lumen. Activated macrophages produce IL-1β and IL-6, which may induce Th17-polarization. Further, macrophages contribute to vessel wall damage by the production of reactive oxygen species (ROS) and matrix metalloproteinases (MMP) [134,141] (**Figure 10D**).

GCA is treated with high doses of glucocorticoids, which usually leads to a pronounced amelioration of acute disease manifestations. Before onset of treatment, both Th1 and Th17 cells can be found in the TA lesions. Glucocorticoids are potent in shutting down the Th17-response, but Th1 cells persist in TA during treatment, remaining a threat for ischemic events [142]. In an experimental model of GCA involving transplantation of human TAs to SCID-mice, it has been found that NOTCH-signalling is important in keeping T cells in the artery [143]. Moreover, by blocking the immune-inhibitory PD-1/PD-L1 checkpoint, disease was exacerbated. Artery-infiltrating T cells show high expression of PD-1 concomitant with low expression of PD-L1 of the surrounding cells, resulting in a lack of inhibitory signals [144]. Combined, these data suggest that both a local and systemic immune dysregulation and a breakdown of tolerance in the artery are prerequisites for developing GCA.

Evidence for involvement of specific antigens

While the chain of events leading to the GCA phenotype is quite well described, it is poorly understood what triggers the immunopathology observed in the affected vessels. Further, the strict tissue confinement of the disease suggests tissue-specific microenvironments to be important.

Infiltration of $CD4^+$ T cells in affected vessels is a hallmark of GCA [141]. $CD4^+$ T cells recognize antigen that is presented in peptide form on HLA class II proteins. Possibly, the infiltrating T cells recognize a tissue-restricted antigen. Numerous HLA alleles are present in the general population, and not all of them are able to present the same peptides [145]. Several HLA class II alleles have been found to be overrepresented in GCA patients compared to controls, most significantly an allele of the HLA-DR beta-chain defined by a histidine at position 13 (HLA-DRB1*04) [8,146]. Comparing GCA-patients with controls, HLA-DRB1*04 showed an odds ratio of 1.92 in a pan-European cohort [8]. This

supports the idea of a specific antigen being presented. Early work has shown that the same expanded T cell clonotypes can be found in temporal artery specimens at different foci of the lesions and occasionally are also shared between different patients [147,148]. Clonal expansion is indicative of recent antigen encounter.

All this evidence cannot explain why the respective T cells have been activated. In artery-engrafted SCID mice, it was shown that T cells could be attracted from a GCA-TA to a previously not infiltrated PMR-TA. This effect was mediated by the activation of vascular dendritic cells, as shown by abrogating DC-activation with an anti-CD83 antibody [140]. Vascular DCs have an inactivated phenotype in healthy arteries and, opposed to GCA-arteries, do not express HLA-DR [149]. Therefore, vascular DC activation likely followed by antigen presentation seems to be an early event of GCA pathogenesis. Moreover, transplantation of a healthy temporal artery followed by LPS injection and adoptive T cell transfer not only attracted T cells to the TA but fully mimicked a typical GCA-artery phenotype [150].

Since especially TLR4-stimulation through LPS induced a GCA phenotype, TLR expression analysis was carried out on a series of medium-sized and large human arteries from different locations. The expression profile was very heterogeneous, but TLR4 expression was ubiquitous, supporting its role in vascular DC activation but still not explaining why small vessels are never affected by GCA [151]. The vasa vasorum are required for blood supply to the vessel wall once a critical vessel diameter has been reached [152]. It has been shown that the adventitial vascular DCs, but not the intimal vascular DCs, are required for TLR4-induced DC-activation [151]. This could partially explain GCA tissue tropism to medium-sized and large arteries only, since delivery of microbial particles through the vasa vasorum to activate adventitial DCs might be required.

All this findings together with the strongly differing disease prevalence among ethnicities suggest that specific antigens are being presented and might be relevant in disease pathogenesis. Several infectious agents have been suggested as candidates; Parvovirus B19 due to similar cyclic fluctuations in incidence like GCA [153], *Chlamydia pneumoniae* due to overlapping symptoms with GCA and serological findings [154] and *Varicella zoster virus* (VZV) because of its ability to induce vasculitides [155]. Although the respective authors show PCR- or histology-based proof for presence of VZV in the GCA

TAs, these findings have been challenged by others [156,157]. Functional proof for T cell reactivity towards any microorganism is lacking so far.

This part of the thesis is dedicated to the investigation of antigen-specific adaptive immune responses in GCA. Specifically, this included the following steps

A) Assessing the reactivity of peripheral T cells against self- and viral proteins, specifically from VZV being epidemiologically and histologically implicated in GCA pathogenesis (Bigler MB *et al.*, Arthritis & Rheumatology 2018)
B) Sequencing the TCR-repertoire directly at the site of inflammation (TA, aorta) to investigate the presence of expanded clones that are indicative of antigen-induced proliferation (Bigler MB *et al.*, unpublished data)
C) Defining the role of autoantibodies against 14-3-3 protein that have been implicated in complicated large vessel vasculitis (LVV), a disease-entity including also and most frequently GCA (Kistner A and Bigler MB *et al.*, Rheumatology 2017)

Given the importance of TLR4-signalling in inducing the GCA phenotype, we also investigated the LPS plasma levels and, as a consequence, immune responses against gram-negative bacteria in our cohort. These results are presented in the appendix.

A) Manuscript 2

Varicella zoster virus-specific T cell responses in untreated giant cell arteritis

A. Faiz Karim, MD
Laura E. M. Eurelings, BS
P. Martin van Hagen, MD, PhD
Jan A. M. van Laar, MD, PhD
Erasmus Medical Center
Rotterdam, The Netherlands

1. Perugino CA, Mattoo H, Mahajan VS, Maehara T, Wallace ZS, Pillai S, et al. IgG4-related disease: insights into human immunology and targeted therapies. Arthritis Rheumatol 2017;69:1722–32.
2. Wallace ZS, Deshpande V, Mattoo H, Mahajan VS, Kulikova M, Pillai S, et al. IgG4-related disease: clinical and laboratory features in one hundred twenty-five patients. Arthritis Rheumatol 2015;67:2466–75.
3. Lachmann HJ, Goodman HJ, Gilbertson JA, Gallimore JR, Sabin CA, Gillmore JD, et al. Natural history and outcome in systemic AA amyloidosis. N Engl J Med 2007;356:2361–71.
4. Bunker D, Gorevic P. AA amyloidosis: Mount Sinai experience, 1997–2012. Mt Sinai J Med 2012;79:749–56.
5. Karim F, Clahsen-van Groningen M, van Laar JA. AA amyloidosis and IgG4-related disease. N Engl J Med 2017;376:599–600.
6. Carruthers MN, Stone JH, Deshpande V, Khosroshahi A. Development of an IgG4-RD Responder Index. Int J Rheumatol 2012; 2012:259408.

DOI 10.1002/art.40362

Reply

To the Editor:

We thank Dr. Karim and colleagues for their thoughtful comments on our article, including their mention of a patient with longstanding IgG4-RD who developed secondary (AA) amyloidosis, presumably as a consequence of well-established, untreated inflammation (Karim F, Clahsen-van Groningen M, van Laar JA. AA amyloidosis and IgG4-related disease. N Engl J Med 2017;376:599–600). We completely agree with Karim et al regarding the destructive nature of IgG4-RD that goes undiagnosed, particularly its ability to cause both endocrine and exocrine failure of the pancreas, end-stage liver disease from the effects of biliary tract disease, chronic renal failure from the effects of tubulointerstitial nephritis, vision loss and deleterious cosmetic issues from orbital disease, chronic pain from retroperitoneal fibrosis, and so on.

Indeed, because IgG4-RD has been recognized as a unique disease entity for less than 15 years, the full toll from this condition in terms of damage from both the disease itself and its therapy is still being described. We note that IgG4-RD patients with elevated levels of serum CRP are the exception rather than the rule (Wallace ZS, Deshpande V, Mattoo H, Mahajan VS, Kulikova M, Pillai S, et al. IgG4-related disease: clinical and laboratory features in one hundred twenty-five patients. Arthritis Rheumatol 2015;67:2466–75). The more common scenario is the finding of an extremely high ESR—the effect of hypergammaglobulinemia of both IgG4 and IgG1 (and sometimes all 4 IgG subclasses)—in the setting of normal CRP levels.

Because any indolent and chronic inflammatory state can result in secondary amyloidosis, we agree that IgG4-RD in the case reported by Karim and colleagues was likely related to the subsequent development of amyloidosis. The current rarity of secondary amyloidosis and the growing, but still inadequate, awareness of IgG4-RD may partially explain why this was the first published connection between these entities. To our knowledge, serum amyloid A concentrations have not been measured systematically in other cohorts, including in our own. The case reported by Karim and colleagues underscores the importance of early recognition of IgG4-RD and control of the associated inflammation as early and as effectively as possible. The utility of serum amyloid A as a biomarker of interest in IgG4-RD requires further investigation.

Cory A. Perugino, DO
John H. Stone, MD, MPH
Massachusetts General Hospital
Boston, MA

DOI 10.1002/art.40363

Varicella zoster virus–specific T cell responses in untreated giant cell arteritis: comment on the article by England et al

To the Editor:

Giant cell arteritis (GCA) is a large vessel vasculitis of unknown cause. Although infections have long been suspected to be potential disease triggers, a disease-causing pathogen has not been identified to date (1). Recently, investigators in several studies reported varicella zoster virus (VZV) particles in artery biopsy specimens (2). Similar to other herpesviruses, VZV has a very high prevalence and remains dormant in a latent stage controlled by the immune system. Loss of T cell–mediated virus control results in herpes zoster (shingles).

The study by England et al (3) now provides epidemiologic evidence for a potential association between VZV and GCA. The authors used 2 independent health care provider data sets (Medicare and MarketScan). In these databases, prior herpes zoster events were associated with a diagnosis of GCA (hazard ratios 2.16 and 1.99 in the 2 data sets, respectively) (3). Use of antiviral drugs or vaccination did not alter the risk of GCA.

T cells are important in the pathogenesis of GCA (4). Genetic association studies and strict tissue tropism suggest that it is an antigen-driven disease (4,5). The antigen could be either a self antigen or a pathogen-derived antigen that is expressed only in the large arteries. The immunopathology and epidemiologic data implicate VZV as a potential immune target. We hypothesized that cross-reactive VZV-specific T cell immunity may contribute to the pathogenesis of GCA. If our hypothesis were shown to be true, we expected the number of VZV-reactive T cells to be increased in patients with GCA compared to control patients.

We compared the frequency of VZV-specific peripheral blood T cells in 32 patients, all of whom provided informed consent to participate in our prospective GCA cohort study. These patients included the following: 15 patients with newly diagnosed GCA (all of whom had received prednisone treatment for < 5 days at the time of sample collection [median 0 days, mean 1 day]), 60% with biopsy-proven GCA, mean age 74.4 years), 10 control patients with inflammatory disease (5 with polymyalgia rheumatica, 2 with autoinflammatory disease, 1 with aortitis, 1 with myelodysplastic syndrome, and 1 with antineutrophil cytoplasmic antibody–associated vasculitis (mean age 66.5 years), and 7 control

patients with noninflammatory disease (mean age 72.0 years). We quantified antigen-specific T cells using an interferon-γ (IFNγ) enzyme-linked immunospot (ELISpot) assay. Live attenuated varicella vaccine (200 plaque-forming units/ml) and the immunodominant glycoprotein E (1 μg/ml) were used as VZV antigens (6).

Additionally, we stimulated T cells with an aortic explant–derived protein extract from a patient with GCA. This represented a source for potential self and/or VZV antigens. Aortic wall proteins were fractionated in phosphate buffered saline by size-exclusion chromatography (Superdex 200 column; GE Healthcare) into 5 pools (P1–P5), each of which was separately added to the cells (range >500 kd [P1] to <10 kd [P5]; 10 μg/ml). Influenza vaccine antigen (0.4 μg/ml) was used as an unrelated comparator. Staphylococcal enterotoxin B (0.5 μg/ml)–treated wells served as a positive control. Preliminary experiments indicated high reactivity with the aortic wall protein extracts. To exclude nonspecific stimulation, we adapted the standard IFNγ ELISpot protocol (7) as follows: peripheral blood mononuclear cells (PBMCs) (75,000/well) were preincubated with the antigen overnight. On day 2, we added autologous PBMCs (50,000/well), followed by incubation for 36 hours on the ELISpot plates. This procedure reduced nonspecific IFNγ production. The response against viral antigens was not affected (data not shown).

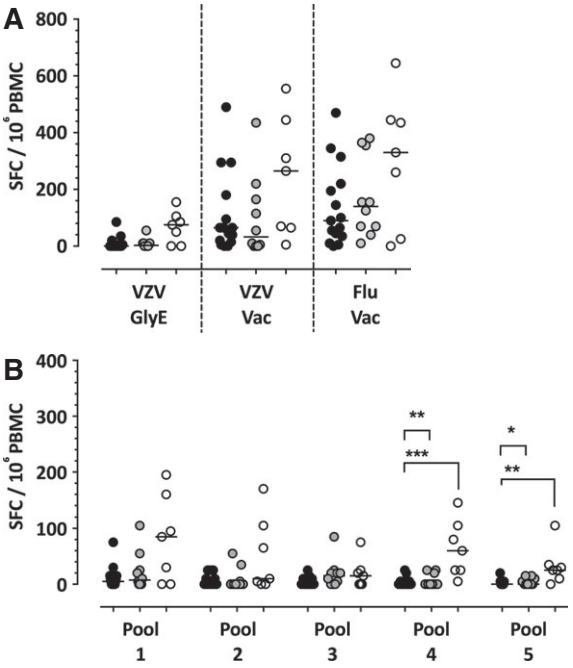

Figure 1. Varicella zoster virus (VZV) T cell reactivity in patients with giant cell arteritis (solid circles), control patients with inflammatory disease (shaded circles), and control patients with noninflammatory disease (open circles). **A,** T cell reactivity against VZV and influenza vaccine, assessed by interferon-γ enzyme-linked immunospot assay. **B,** T cell responses to aortic wall proteins. Aortic wall proteins were fractionated into 5 pools, and each pool was added separately to the cells. Cells treated with medium alone were used for background correction. Each data point represents a single patient. Horizontal lines show the median. * = $P < 0.05$; ** = $P < 0.01$; *** = $P < 0.001$. SFC = spot-forming cell; PBMC = peripheral blood mononuclear cell; GlyE = glycoprotein E; Flu = influenza vaccine (vac) antigen.

The median VZV (glycoprotein E, vaccine) and Flu- (TIV) T cell reactivity was higher in patients with noninflammatory disease compared to those with GCA, with no statistically significant differences (Figure 1A). Control patients with noninflammatory disease had stronger T cell responses to aortic extract ($P = 0.0006$ and 0.0036 for pools 4 and 5, respectively) (Figure 1B). Such reduced peripheral T cell reactivity could reflect immunosenescence or exhaustion, which may result in loss of VZV control. The responses in control patients with inflammatory disease were, however, comparable to those in GCA patients. This suggested that systemic inflammation might blunt the reactivity. However, strong antigen-independent T cell stimulation with phorbol myristate acetate resulted in comparable IFNγ and interleukin-17 effector functions in all 3 study groups (data not shown).

In conclusion, we observed no GCA-specific alterations in VZV- or aortic protein–specific T cell reactivity. Our results provide evidence against involvement of VZV-specific (or cross-reactive) effector T cells in the pathogenesis of GCA. We focused only on IFNγ-producing T cells; other effector cells might be present at different frequencies. It is further possible that VZV- or aortic tissue–specific T cells concentrate at the site of inflammation. Thus, assessment of the peripheral blood compartment may miss these cells. This would, however, not explain the comparable VZV- and aortic protein–reactive T cell frequencies in GCA and other inflammatory conditions.

In the study by England et al, only a minority (<6%) of the GCA patients had a herpes zoster event in the year prior to GCA diagnosis. Such patients may show T cell reactivity profiles distinct from those observed in our study population but the differences might have been missed due to our small sample size. However, based on the studies showing the presence of VZV in almost all GCA biopsy specimens, we expected to observe a signal even when studying a small patient population. Notably, several other groups of investigators observed no VZV, antigen, or genome in temporal arteries (8–10). The truth probably lies somewhere in between, and as stated in the England article, VZV (and other viruses) may be a trigger for GCA but is not the only one.

Supported by the Swiss National Science Foundation (SNSF) (grant PZ00P3-173517 to Dr. Berger). Dr. Recher's work is supported by SNSF grant PP00P3_144863. Dr. Mehling's work is supported by SNSF grant PZ00P3_154733.

Marc B. Bigler, MSc
Julia R. Hirsiger, BSc
Mike Recher, MD
Matthias Mehling, MD
Thomas Daikeler, MD
University Hospital Basel
Christoph T. Berger, MD
University of Basel and University Hospital Basel
Basel, Switzerland

1. Van Timmeren MM, Heeringa P, Kallenberg CG. Infectious triggers for vasculitis. Curr Opin Rheumatol 2014;26:416–23.
2. Gilden D, Nagel MA. Varicella zoster virus triggers the immunopathology of giant cell arteritis. Curr Opin Rheumatol 2016;28:376–82.
3. England BR, Mikuls TR, Xie F, Yang S, Chen L, Curtis JR. Herpes zoster as a risk factor for incident giant cell arteritis. Arthritis Rheumatol 2017;69:2351–8.

4. Weyand CM, Goronzy JJ. Immune mechanisms in medium and large-vessel vasculitis. Nat Rev Rheumatol 2013;9:731–40.
5. Carmona FD, Vaglio A, Mackie SL, Hernandez-Rodriguez J, Monach PA, Castaneda S, et al. A genome-wide association study identifies risk alleles in plasminogen and P4HA2 associated with giant cell arteritis. Am J Hum Genet 2017;100:64–74.
6. Malavige GN, Jones L, Black AP, Ogg GS. Rapid effector function of varicella-zoster virus glycoprotein I-specific CD4+ T cells many decades after primary infection. J Infect Dis 2007; 195:660–4.
7. Berger CT, Carlson JM, Brumme CJ, Hartman KL, Brumme ZL, Henry LM, et al. Viral adaptation to immune selection pressure by HLA class I-restricted CTL responses targeting epitopes in HIV frameshift sequences. J Exp Med 2010;207:61–75.
8. Alvarez-Lafuente R, Fernandez-Gutierrez B, Jover JA, Judez E, Loza E, Clemente D, et al. Human parvovirus B19, varicella zoster virus, and human herpes virus 6 in temporal artery biopsy specimens of patients with giant cell arteritis: analysis with quantitative real time polymerase chain reaction. Ann Rheum Dis 2005; 64:780–2.
9. Procop GW, Eng C, Clifford A, Villa-Forte A, Calabrese LH, Roselli E, et al. Varicella zoster virus and large vessel vasculitis, the absence of an association. Pathog Immun 2017;2:228–38.
10. Muratore F, Croci S, Tamagnini I, Zerbini A, Bellafiore S, Belloni L, et al. No detection of varicella-zoster virus in temporal arteries of patients with giant cell arteritis. Semin Arthritis Rheum 2017. E-pub ahead of print.

DOI 10.1002/art.40370

Reply

To the Editor:

We thank Dr. Bigler and his colleagues for their interest in our study and for sharing the results from their laboratory. The authors proposed evaluating a biologic mechanism linking VZV to GCA through assessment of cross-reactive VZV-specific T cell immunity, hypothesizing that the number of VZV-reactive T cells would be increased in GCA patients relative to controls. Using a small sample of GCA and control patients (with inflammatory or noninflammatory disease), the authors tested this hypothesis through the quantification of VZV-specific T cells and T cell reactivity (in response to stimulation with a protein extract from an aortic tissue specimen obtained from a single GCA patient) in vitro, finding no significant differences between GCA and control patients.

In our study, prior herpes zoster reactivation was observed in only a minority of GCA patients, which led to our interpretation that despite our finding of a significant association between GCA and herpes zoster, there was a low population-attributable risk. Thus, one possible explanation for the null findings by Bigler et al is that the protein extract from the single GCA patient did not contain VZV or VZV cross-reactive antigens.

As Bigler and colleagues point out (and we acknowledged in our article), there have been conflicting reports on the presence of VZV in the temporal arteries of GCA patients. Given the epidemiologic associations observed in our study, we look forward to additional translational research studies investigating potential mechanistic links between VZV and GCA.

Bryant R. England, MD
Ted R. Mikuls, MD, MSPH
University of Nebraska Medical Center and Veterans Affairs Nebraska–Western Iowa Health Care System Omaha, NE
Jeffrey R. Curtis, MD, MS, MPH
University of Alabama at Birmingham

DOI 10.1002/art.40332

Single-strain versus multistrain probiotic supplementation treatment strategy for rheumatoid arthritis: comment on the article by Marietta et al

To the Editor:

We read with interest the recent article by Marietta et al on gut microbial dysbiosis as a key factor in the pathogenesis of inflammatory diseases such as rheumatoid arthritis (RA) (1). Altered microbiota, well described in RA patients, seem associated with perturbation of certain metabolic pathways, and the therapies addressed to correct gut microbiome dysbiosis could help in the maintenance of immune homeostasis of the host (1).

In particular, the authors discussed the ability of *Prevotella histicola* to modulate the systemic and mucosal immune response (by suppression of antigen-specific Th17 responses and increased transcription of interleukin-10) in an animal model. On this basis, they suggested a possible role of this human gut commensal in treatment strategies for RA (1).

According to the authors, a "single bacterium" is what seems to make the "difference" in the balance of microbiota; in our opinion, however, this should be a subject of discussion. In fact, what they observed could just be the "readjustment of the microbiota," and the concept of *Prevotella* "monotherapy" is potentially misleading, since the administration of this microorganism as well as others could be just a way to induce a shift in the balance of flora from proinflammatory to antiinflammatory. In fact, even in the different setting of HIV disease, but notably in human subjects, it has been shown that supplementing antiretroviral therapy with *Prevotella*-free multistrain probiotics (*Streptococcus faecium* and *Streptococcus salivarius* subspecies *thermophilus*; bifidobacteria—represented by *Bifidobacterium breve*, *Bifidobacterium infantis*, and *Bifidobacterium longum*; *Lactobacillus acidophilus*, *Lactobacillus plantarum*, *Lactobacillus casei*, and *Lactobacillus delbrueckii* subspecies *bulgaricus* [Alfa-sigma]) reduces the levels of immune activation on CD4+ T lymphocytes for both of the markers CD38 and HLA–DR and their simultaneous expression, with plasma levels of lipopolysaccharide binding protein and high-sensitivity C-reactive protein normalizing to values comparable to those in controls (2). Multistrain probiotic supplementation (*L plantarum* [De Simone Formulation {DSM} 24730], *S salivarius* subspecies *thermophilus* [DSM 24731], *B breve* [DSM 24732], *Lactobacillus paracasei* [DSM 24733], *L delbrueckii* subspecies *bulgaricus* [DSM 24734], *L acidophilus* [DSM 24735], *B longum* [DSM 24736], *B infantis* [DSM 24737] [DuPont]) is also associated with a reduction of enterocyte apoptosis and density of intraepithelial lymphocytes,

B) Unpublished data

Sequencing the TCR-repertoire in the inflamed artery

Introduction

The histological findings of $CD4^+$ T cell infiltration and vascular DC activation in combination with the repeated detection of identical T cell clones in arteries at different locations and the disease association of HLA-alleles highlight the relevance of $CD4^+$ T cells to disease pathogenesis. The seminal studies identifying identical clones in TA biopsies date back more than 20 years [147,148]. We hypothesized that, if specific antigens were recognized in the inflamed areas, dividing antigen-specific T cells should be present. By means of high-throughput sequencing, expanded dominant T cell clones could be detected and the presence of public clones investigated. This would inform subsequent analyses on both screening for antigens that may be targeted by the respective T cell clones and tracking disease-associated TCRs in the peripheral blood as a biomarker for disease activity. We aimed at sequencing the TCR beta chain repertoire from TA biopsies or aorta explants from newly diagnosed GCA patients. Complementary, we performed TCR sequencing on matched bulk peripheral blood $CD4^+$ T cells and $CCR6^+/CD161^+/$ $CD4^+$ T cells that have been found enriched in the affected vessels as well in the peripheral blood of GCA patients [158].

Methods

OCT-embedded TA samples were cut into slices of 20 µM thickness. Granulomatous infiltration and the histological diagnosis of GCA had been confirmed previously by an experienced pathologist on H&E stainings. Isolation of gDNA was performed with QIAamp DNA micro kit (56304, Qiagen, Hilden, Germany - protocol: Isolation of genomic DNA from tissues) including removal of OCT in the lysate supernatant with QIAshredder columns before ethanol precipitation. $CD4^+/CCR6^-/CD161-$ ("bulk") and $CD4^+/CCR6^+/CD161^+$ ("specific") T cells were sorted by FACS (FACSAria™, BD biosciences, Franklin Lakes, NJ, USA). Antibodies were against CD3 (PE, clone UCHT1, 555333, BD biosciences), CD4 (APC, clone OKT4, 317416), CCR6 (PE-Cy7, clone G034E3, 353418) and CD161 (Alexa Fluor 488, clone HP-3G10, 339924, all three Biolegend, San Diego, CA, USA). Genomic DNA from bulk T cells were isolated with QIAamp DNA blood mini kit (51106, Qiagen - protocol: DNA purification from blood or body fluids), from specific T cells with QIAamp DNA micro kit (protocol: Isolation of genomic DNA from small volumes of blood).

Amplification and sequencing of TCRB CDR3 regions was performed using the immunoSEQ® Platform (Adaptive Biotechnologies, Seattle, WA). The immunoSEQ

Platform combines multiplex PCR with high-throughput sequencing and a sophisticated bioinformatics pipeline for recombination analysis [159,160].

A *candida*-specific T cell line used to establish the clonal tracking PCR was a gift from C. Stühler. RNA was isolated with QIAamp RNA blood mini kit (52304, Qiagen) and cDNA was generated with GoScript™ reverse transcriptase (A5003, Promega, Madison, WI, USA). To determine the TCR beta chain sequence / confirm that it is a clone, 5'-RACE-PCR (5'/3' RACE kit, 03 353 621 001, Roche, Basel, Switzerland) was performed with the following primers targeting TRBC: Primer 1: 5'-TTCCCATCAGCCGCCCAAACCTAA-3' Primer 2: 5'-ATCTGGAGTCATTGAGGGCG-3'. VDJ-recombination was assessed with the IMGT V-Quest tool [161] and confirmed with primers TRBV04_fw 5'-CCTGAATGCCCCAACAGCTCTCTC-3' , TRBV07_fw 5'-TCTCAGGTGTGATCCAAATTCGGG-3' and primer 1. *In vitro* clonal tracking was performed by spiking 1 million down to 1 cell of the clonal cell line into 1M PBMC of non-related donors. Genomic DNA was isolated as described and clone gDNA amplified with GoTaq® qPCR master mix (A6001, Promega). Primers: K1_SYBR_F 5'-CCCAGTGATCGCTTCTCTGC-3'; K1_SYBR_R 5'-GTCTCTCCCAATGAGAGGCTG-3'.

TCR-sequencing indicates recent antigen encounter in GCA-affected arteries

Due to the limited T cell number in the biopsies, it was not feasible to investigate antigen-specific T cell responses at the site of inflammation, and these analyses were carried out on peripheral T cells (see part A). We tried to circumvent this limitation by a TCR-centered approach. We could access OCT-embedded (optimal cutting temperature, a synthetic resin) TA-tissue to perform TCR analysis. Diagnostic TA-biopsies of patients with suspected GCA are formalin-fixed and paraffin-embedded (FFPE). Attempts to perform TCR sequencing on such samples were impeded by too low DNA quality. Therefore, we adapted the protocol: if the patient gives informed consent, a part of the biopsy is embedded in OCT. Once the diagnosis of GCA is definite on the FFPE material, we can access the OCT tissue for research, containing far less damaged nucleic acids (**Figure 11A**).

The TCR beta chain repertoire of inflamed arteries (4 TAs, 1 aorta), matched bulk peripheral $CD4^+$ T cells ("bulk") and CD161+/CCR6+ $CD4^+$ T cells ("specific") was sequenced from five biopsy-proven GCA-patients (Gating strategy: **Figure 11B**).

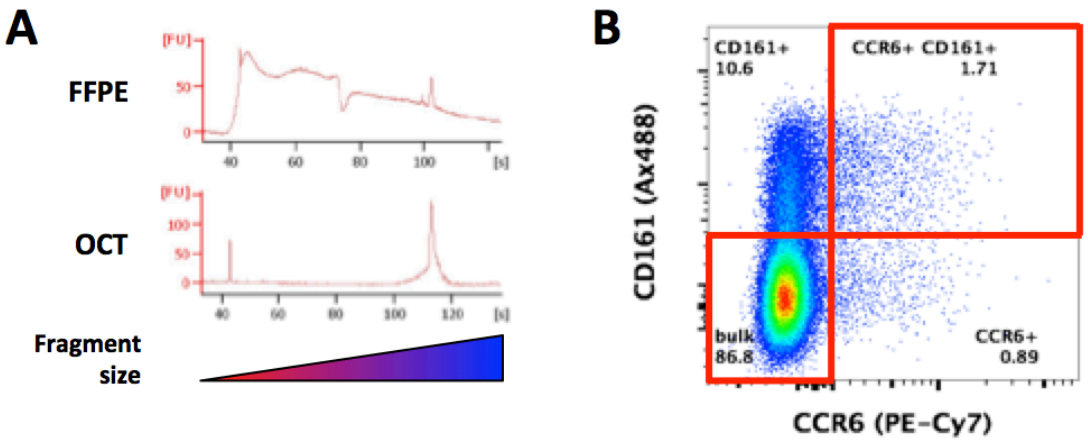

Figure 11: Preparation of genomic DNA from artery and peripheral T cells. A) Bioanalyzer profiles for gDNA fragments isolated from FFPE- or OCT-embedded temporal artery samples. The prominent peaks are DNA length markers. **B)** Gating strategy to sort for bulk and CCR6⁺/CD161⁺ CD4⁺ T cells for subsequent gDNA-isolation. Cells were obtained before onset of glucocorticoid treatment. Gates are shown in red within doublet-negative CD3⁺ CD4⁺ T cells. Figure created with FlowJo v.10, FlowJo, LLC.

The proportion of clonally expanded T cells, indicative of recent or ongoing antigen encounter, is highest in the artery compartment in 4 out of 5 patients with the most expanded clone constituting between 2.6% and 7.2% of total TA/aorta TCR-sequences. Some expanded clones in the TA are unique to this compartment, while others could also be found expanded in the CD161+/CCR6+ and/or in the bulk CD4⁺ T cells (see **Figure 12A**). Therefore, the clonal repertoire found in the TA does not simply mirror expanded clones in the bulk population but rather suggests a tissue-specific expansion of T cells. Finally, we did find 21 public clones that were shared between a maximum of two donors, but none of them was expanded in both (**Figure 12B**).

A direct application of the detection of a patient-specific expanded T cell clone could be to monitor such potentially harmful T cell clones over the disease course. To establish peripheral clonal T cell tracking, 1 million of PBMC of an unrelated donor were spiked with decreasing amounts of cells from a candida-specific T cell clone. Across a range of one cell to a million, we could establish a detection sensitivity of 1:100'000 (**Figure 13**).

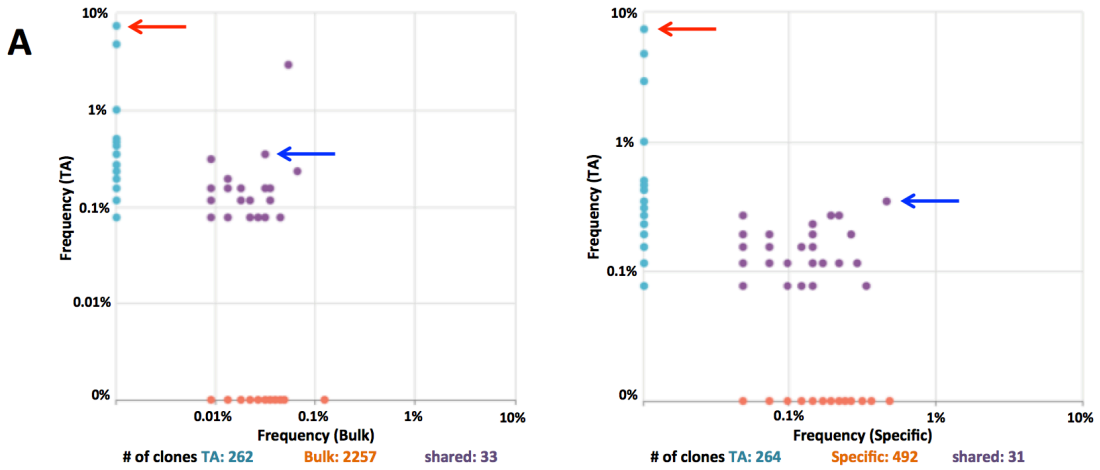

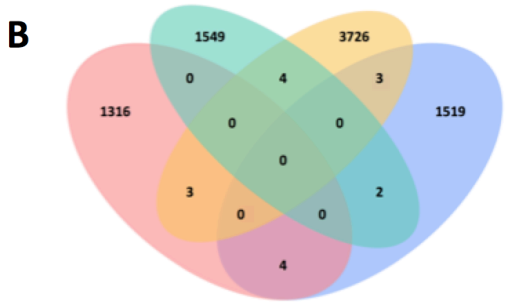

Figure 12: T cell clonal overlap among compartments and patients. A) Scatter plots showing frequency of expanded clones (at least two sequences) in the TA vs. bulk or specific compartments of a representative donor. The number and frequencies of clonotypes unique to the TA (blue), unique to the bulk or specific population (orange) or shared between two (purple) are depicted. Reading examples: The top expanded TA clone (red arrow) constitutes 7.2% of total sequences, but is not expanded in the bulk or specific population. Another clone (blue arrow) is considerably expanded in all three compartments (Ranks: 8 (TA), 2 (specific), 11(bulk). **B)** Venn diagram showing clonal overlaps between the four TA samples (aorta sample not shown due to space reasons). Expanded and not expanded clones are included. Reading example: GCA-patient "red" shares seven out of 1316 clones: three with "yellow", four with "blue" and none with "green". All overlaps are on amino acid level with productive rearrangements only (= functional TCRs). Figures were made with immunoSEQ analyzer.

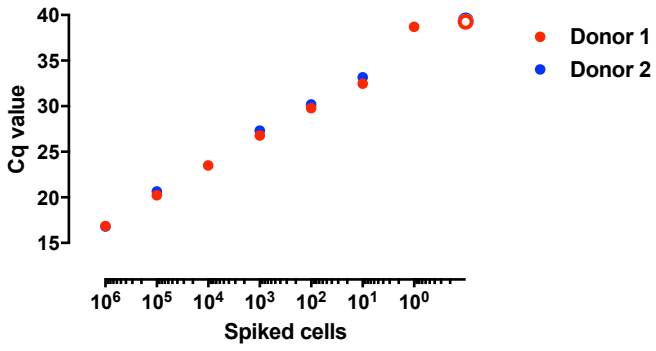

Figure 13: A specific T cell clone can be reliably detected at very low concentrations. 1 million PBMC of two unrelated donors were spiked each with 1M down to 1 cell of a $CD4^+$ T cell clone. Cq-values of clone-specific amplified gDNA is plotted against number of spiked cells. Clone detection is in the linear range down to 10 cells (Spearman's correlation coefficient in the background of both donors: r = 0.998), leading to a detection sensitivity of 1:100'000. Open circles: Donor PBMC only, no unspecific amplification could be detected.

C) Manuscript 3

Characteristics of autoantibodies targeting 14-3-3 proteins and their association with clinical features in newly diagnosed giant cell arteritis

RHEUMATOLOGY

Concise report

doi:10.1093/rheumatology/kew469

Characteristics of autoantibodies targeting 14-3-3 proteins and their association with clinical features in newly diagnosed giant cell arteritis

Anne Kistner[1,*], Marc B. Bigler[1,*], Kathrin Glatz[2], Simon B. Egli[1], Fabian S. Baldin[3], Florian A. Marquardsen[3], Matthias Mehling[4], Katharina M. Rentsch[5], Daniel Staub[6], Markus Aschwanden[6], Mike Recher[3,7], Thomas Daikeler[8] and Christoph T. Berger[1,9]

Abstract

Objectives. Autoantibodies are useful biomarkers for diagnosing and monitoring treatment in some autoimmune diseases. Antibodies against isoforms of 14-3-3 protein have been proposed as biomarkers for the presence of aortic aneurysm in large-vessel vasculitis (LVV). Here, we aimed to evaluate the diagnostic role and potential immunopathological involvement of anti–14-3-3 antibodies in newly diagnosed LVV patients.

Methods. Antibodies against three isoforms of 14-3-3 (γ, ε and ζ) were measured in 90 subjects: 48 GCA and 3 Takayasu's arteritis (TA) patients, and 39 controls (non-inflammatory and inflammatory diseases), using a multiplexed bead-based immunoassay and immunoprecipitation studies. The positive cut-off value was defined based on young healthy controls. Anti–14-3-3 IgG antibodies in LVV patients were compared with those in controls in order to assess their diagnostic performance, and the relationship of anti–14-3-3 IgG antibodies to the immunohistopathology of artery explants was assessed.

Results. Antibodies against all three 14-3-3 isoforms were detected in LVV patients as well as in age-matched inflammatory and non-inflammatory controls. Among LVV patients, detection of antibodies targeting 14-3-3 ε and ζ was associated with more severe disease. Detection of antibodies against 14-3-3 γ was linked to latent *Toxoplasma gondii* infection, a parasite that secrets a 14-3-3 homologue, suggesting potential cross-reactivity.

Conclusion. Detection of antibodies against 14-3-3 proteins at the time of LVV diagnosis is not disease-specific. Their presence at high levels in LVV patients with stroke, aortitis and—in a previous study—aneurysm formation may indicate an association with extensive tissue destruction. The relevance of 14-3-3 antibodies in non-LVV patients needs to be investigated in larger cohorts.

Key words: large-vessel vasculitis, giant cell arteritis, Takayasu's arteritis, autoantibodies, 14-3-3 proteins, aortic aneurysm, multiplex, protein pulldown, toxoplasmosis, stroke

BASIC SCIENCE

Rheumatology key messages

- Antibodies against 14-3-3 isoforms are detectable in newly diagnosed GCA, but also in age-matched disease controls.
- Antibodies against human 14-3-3γ and 14-3-3 secreted by *Toxoplasma* might cross-react in GCA.
- Presence of anti–14-3-3ε and anti–14-3-3ζ in large-vessel vasculitis is associated with aortitis and stroke.

[1]Translational Immunology, Department of Biomedicine, [2]Department of Pathology, [3]Department of Biomedicine, Immunodeficiency Laboratory, [4]Translational Neuroimmunology, Department of Biomedicine, [5]Laboratory Medicine, [6]Department of Angiology, [7]Immunodeficiency Clinic, [8]Rheumatology Clinic and [9]Medical Outpatient Clinic, Department of Internal Medicine, University Basel Hospital, Basel, Switzerland

Submitted 11 July 2016; revised version accepted 18 November 2016

*Anne Kistner and Marc B. Bigler contributed equally to this study.

Correspondence to: Christoph T. Berger, Translational Immunology, Department of Biomedicine, University Basel Hospital, Hebelstrasse 20, 4031 Basel, Switzerland.
E-mail: christoph.berger@usb.ch

Introduction

Several autoimmune diseases are defined by autoantibodies in the context of agreeing clinical presentations. SLE and ANCA-associated vasculitis (AAV) are paradigmatic diseases, where the presence of anti-DNA antibodies and ANCA, respectively, are useful in diagnosis, patient stratification or treatment decisions [1]. To date, no such biomarker exists in large-vessel vasculitis (LVV) syndromes, that is, Takayasu's arteritis (TA) and GCA. LVV patients present with a systemic inflammatory syndrome and variable ischaemic symptoms induced by vascular occlusion [2]. The aetiology remains unknown, but both innate and adaptive immune dysregulation has been implicated in the immunopathogenesis [3]. Diagnosing LVV can be challenging; hence, there is a strong need for biomarkers as diagnostic tools and for guiding clinical decisions.

Recently, Chakravarti *et al.* [4] reported autoantibodies against 14-3-3 proteins in sera of LVV patients who underwent surgical aortic aneurysm repair. Thoracic aortic aneurysm formation is a late complication of GCA, often manifesting years after diagnosis [5]. In the majority (78%) of these selected LVV patients, antibody reactivity against a protein of the aortic wall, identified as the ε, ζ and—to a lesser extent—γ isoforms of the 14-3-3 protein was detected. Since these autoantibodies were largely absent in controls (non-inflammatory aortic aneurysms and inflammatory disease controls such as SLE or AAV), the authors concluded that anti–14-3-3 antibodies could be used as biomarkers and might be involved in LVV pathogenesis or aneurysm formation. Whether anti–14-3-3 antibodies are causally involved in aneurysm formation, or a consequence of immune damage in LVV-associated aneurysms, was not addressed in this study. Here we explored the diagnostic potential of anti–14-3-3-IgG antibodies in LVV, and assessed their potential role in disease pathogenesis.

Methods

Clinical cohort and controls

This study was IRB approved (Ethics Committee of Northwest and Central Switzerland 239/09), and all participants gave informed consent in accordance with the Declaration of Helsinki. A total of 90 subjects were investigated: 48 GCA and 3 TA patients; 20 inflammatory disease controls (mostly patients with initial suspicion of LVV that was not confirmed), 9 age-matched non-inflammatory disease controls and 10 healthy volunteers $<$40 years old. Detailed patient characteristics are given in supplementary Tables S1 and S2, available at *Rheumatology* Online.

Multiplexed fluorescent bead-based immunoassay

Anti–14-3-3 isoform IgGs [4] were measured with a customized multiplexed bead-based immunoassay. The 14-3-3 isoforms γ (Abcam, ab166880), ε (Sigma-Aldrich, E2033; and Abcam, ab73802) and ζ (Sigma-Aldrich, Z3402) were coated on Magnetic MagPlex-microspheres (Luminex). Beads coated with an influenza haemagglutinin [Wisconsin 67/2005 (Sino Biologicals, 11972-V08H)] served as a non-related antigen control, and BSA-coated beads as negative controls. Multiplexed bead assays were performed with 10-fold-diluted plasma according to the *Luminex xMAP Cookbook*. Anti-human IgG-phycoerythrin (PE) (SouthernBiotech, #1030-09) was used for detection, and a polyclonal pan-anti–14-3-3 [Cell Signaling Technology (CST), #8312] as a positive control on a Luminex-200 system (xPONENT software). Results were expressed as background-corrected median fluorescence intensities (MFIs): $[MFI_{experimental}] - [MFI_{BSA}]$. For the correlations with clinical findings, the positive cut-off was defined as $>$(mean + 3 S.D.) of the young healthy controls. In selected samples with anti–14-3-3 antibodies detectable above threshold, plasma was serially diluted to determine the antibody titre, defined as the last dilution at which 14-3-3 antibodies were detectable.

Immunoprecipitations of 14-3-3 antibodies

To immunoprecipitate 14-3-3 antibodies, plasma samples were diluted 10-fold in PBS to 100 μl and supplemented with 20 μl of protein A–coated agarose beads (CST, #9863). After antibody pull-down for 2 h on a rotating wheel at 4 °C, beads were washed, and incubated in 100 μl PBS with 1 μg of the recombinant human 14-3-3 isoforms overnight at 4 °C under constant rotation. After washing and boiling, eluates were analysed by western blotting using polyclonal pan-anti–14-3-3 detection antibody.

Measurement of total IgG and Toxoplasma*-specific IgG*

Total IgG was measured using a ready-to-use ELISA (ZeptoMetrix Corporation, Cat. No. 0801197). The *Toxoplasma*-specific IgG (threshold for positivity $>$6.5 IU/ml) was measured using an automated chemiluminescence immunoassay (Immulite2000 Siemens).

Protein sequence and structure analysis

Amino acid sequences of human 14-3-3γ (NP_036611), 14-3-3ε (NP_006752), 14-3-3ζ (NP_001129174) and secreted *T. gondii* 14-3-3 (BAA25996) were aligned with Clustal Omega (European Bioinformatics Institute). Amino acids containing potential cross-reactive antibody-binding sites between human and the *T. gondii* 14-3-3 isoforms were defined as: identical or of the same category (i.e. acidic/basic, polar/non-polar) between *Toxoplasma* and the respective human isoform, but different amino acid category in the two other isoforms (supplementary Fig. S1, available at *Rheumatology* Online). Positions of candidate amino acids in the respective isoforms were visualized with PyMOL (v. 1.7, Schrödinger LLC) in the following pdb-files: 2B05 (14-3-3γ), 3UAL (14-3-3ε) and 4WRQ (14-3-3ζ).

Histology and semi-quantitative analysis of the inflammatory infiltrate

Temporal artery biopsies (n = 11) from biopsy-proven GCA and large-vessel explants (LVEs) (n = 4: three aortae, one

carotid artery) from two GCA and two TA patients were stained with HE (haematoxylin/eosin), or immunohistochemistry to quantify B cells (anti-CD20, Clone L26; Ventana/Roche 760-2531) and plasma cells (anti-CD138, Clone: B-A38; Ventana/Roche 760-4248) was performed. Inflammation was scored using a 5-point score: 0 for no positive lymphocytes/CD20$^+$ B cells/CD138$^+$ plasma cells; 1 for occasional positive cells; 2 for a moderate number; 3 for a large number; or 4 for a very large number of positive cells [6].

Statistical analysis

Multiple groups were compared using non-parametric group comparison (Kruskal–Wallis test) with Dunn's correction. Spearman ranks correlation was performed to test for a correlation between anti–14-3-3 IgG levels assessed by western blot *vs* multiplexed bead-assay. Chi-square tests were applied to compare clinical manifestations between different groups.

Results

Detection of antibodies against 14-3-3 isoforms in newly diagnosed GCA and control groups

Compared with the cut-off defined in young, healthy volunteers, we detected elevated 14-3-3-specific antibodies against the γ, ε and ζ isoforms in 12, 30 and 30% of GCA, and 0, 67 and 67% of TA patients, respectively (Fig. 1A and supplementary Fig. S2, available at *Rheumatology* Online). Frequency of a positive test (seroprevalence) and the absolute antibody levels were not higher in GCA patients when compared with age-matched inflammatory or non-inflammatory controls. Moreover, antibody levels in five GCA patients with longer-lasting disease were not higher than in recently diagnosed patients (Fig. 1A). Notably, antibody titres were also similar in GCA and controls (supplementary Fig. S3, available at *Rheumatology* Online), and the results were comparable when only including GCA subjects without any prior glucocorticoid treatment. Data from antibody immunoprecipitation assays [4] correlated well with the MFI obtained in the multiplex assay, thus validating our findings (Fig. 1B and C). Notably, binding reactivity of anti–14-3-3-IgG was relatively low, as indicated by comparison with the reactivity of IgG binding with an influenza protein, and showed no increase over the first year after diagnosis (Fig. 1D).

High levels of anti-14-3-3γ, but not ε or ζ, antibodies was associated with latent Toxoplasma *infection*

The concept of molecular mimicry proposes that a pathogen-specific immune response cross-reacts against self-proteins. *Toxoplasma gondii*, a widespread opportunistic parasite causing asymptomatic latent infection in immunocompetent hosts, has been linked to autoimmune diseases, including vasculitis [7]. This parasite secretes a 14-3-3 homologue, and detection of anti–14-3-3 antibodies in patients with recent *Toxoplasma* infection has been reported [8]. Therefore, we next tested whether subjects with high anti–14-3-3 responses were more likely to be *Toxoplasma* seropositive. In the entire cohort, anti–*Toxoplasma*-IgG was detected in 48% (40 of 83 tested). Intriguingly, 14-3-3γ antibody-positive subjects were significantly enriched for *Toxoplasma* seropositivity compared with 14-3-3γ antibody-negative subjects (80% *vs* 40.6%, $P = 0.008$; Fig. 2A). In contrast, when stratified based on antibody-positivity against 14-3-3ε or 14-3-3ζ, no difference was observed (Fig. 2A). All three 14-3-3 isoforms have a sequence similarity of 74–76% to the *Toxoplasma* isoform. Searching for evidence of potential cross-reactivity, we compared the sequences of the different isoforms and mapped amino acids diverging between *Toxoplasma*/14-3-3γ *vs* 14-3-3ε/14-3-3ζ on the 3D protein structure. Indeed, a cluster of three amino acids, conserved between the *Toxoplasma* 14-3-3 and 14-3-3γ protein, was arranged in close proximity to each other (Fig. 2B). No similarly enriched region was detected between *Toxoplasma* 14-3-3 and the other human isoforms (supplementary Fig. S4, available at *Rheumatology* Online). The seroprevalence and the *in silico* structural analysis combined suggested that anti-14-3-3γ responses might, to some extent, be driven by cross-reactive anti–*Toxoplasma*-14-3-3 antibodies.

Are 14-3-3 antibodies the consequence of tissue remodelling in complicating large-vessel inflammation?

Thoracic aortic aneurysm occurs in ∼12% of GCA patients as a late complication [5]. Since autoantibodies can be induced secondarily via antigen release from damaged tissue, and in light of the report of high prevalence of 14-3-3ε and 14-3-3ζ antibodies in subjects with manifest aneurysm [4], we assessed whether these antibodies were associated with clinical manifestations. We found that 71% (10/14) of patients with anti-14-3-3ε who underwent imaging of the aorta (i.e. MRI, PET-CT or CT, which was performed in 38 out of the 52 LLV patients) had a finding compatible with aortitis (Fig. 2C), while this was only the case in 29% (7/24) of those with anti-14-3-3ε below the threshold. Moreover, four out of 52 LVV patients had a stroke, all were anti-14-3-3ε positive, and three were also 14-3-3-ζ positive (Fig. 2D). Other clinical features, including cardiovascular risk factors, jaw claudication, vision disturbances, polymyalgia or inflammation markers were equally distributed (data not shown). Interestingly, B cells and plasma cells, that is, potential sources of autoantibodies, were more abundant in LVEs of patients with aortitis or carotis affection as compared with inflamed temporal artery biopsies (Fig. 2E and F), and tertiary lymph follicles—indicative of a locally induced immune response—were almost exclusively found in the LVE (Fig. 2G).

Discussion

Availability of a specific diagnostic or prognostic biomarker is an unmet need in LVV. Anti-14-3-3 antibodies have been found in LVV patients with aortic aneurysm. Here we tested for such antibodies in GCA and TA patients at the time of diagnosis. We found that antibodies against

FIG. 1 Anti-14-3-3-IgG in newly diagnosed GCA

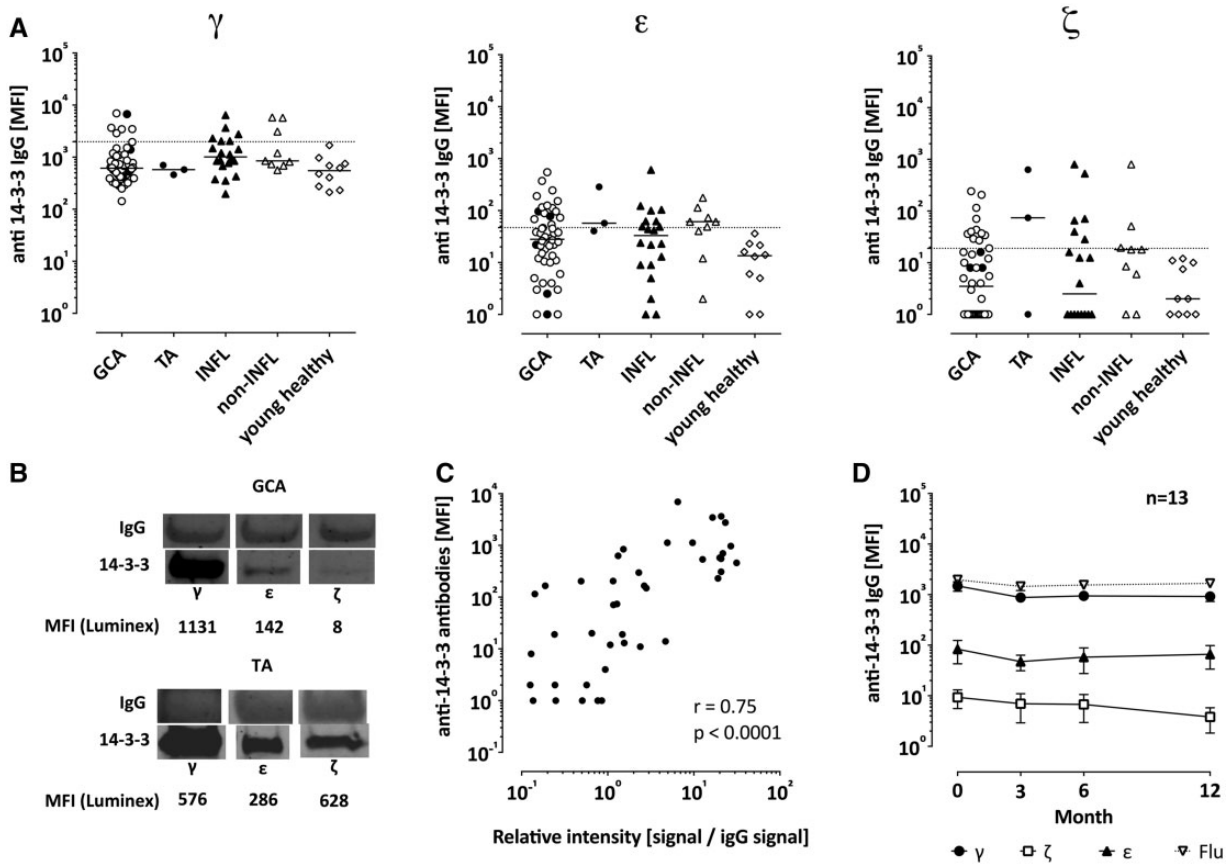

(**A**) Isoform-specific anti-14-3-3-IgG levels [median fluorescence intensity (MFI)] in GCA patients, including some with long-standing disease (closed circles), TA, inflammatory (IFNL), non-inflammatory (non-IFNL) and young healthy controls (*$P < 0.05$). Dotted line indicates positivity cut-off. (**B**) Example western blots from immunoprecipitation of 14-3-3 isoform-specific-IgG from a GCA and a TA patient. (**C**) Correlation with multiplex assay. $n = 42$ measurements (i.e. isoforms γ, ϵ, ζ) in 14 patients. (**D**) Longitudinal anti-14-3-3 and -influenza haemagglutinin-IgG (Flu) in a subset of $n = 13$ anti-14-3-3-IgG-positive GCA patients at diagnosis. TA: Takayasu's arteritis.

14-3-3 isoforms were detectable in LVV patients, but are also present at similar levels and with comparable frequency in age-matched controls, limiting their use as diagnostic biomarkers.

In contrast to the study by Chakravarti *et al.*, our patients were sampled at the time of diagnosis, and only two patients had aortic aneurysm. Thus, our study does not inform whether high anti-14-3-3 IgG levels present early in disease may be involved in subsequent aneurysm formation. However, increased reactivity against 14-3-3ζ and 14-3-3ε proteins in patients with LVV-associated thoracic aortic aneurysms may also be elicited following the release of the respective immunological targets in the setting of severe aortic damage. In this scenario, an inflammatory process would be a prerequisite for autoantibody formation, as Chakravarti *et al.* found no 14-3-3 antibodies in controls with non-inflammatory aneurysm. Although anti-14-3-3 antibodies were not LVV-specific, antibodies targeting 14-3-3ζ and 14-3-3ε were more frequent in patients with aortitis (14-3-3ε) and/or stroke (14-3-3ζ and 14-3-3ε), compatible with a model where 14-3-3 autoantibodies were induced as a consequence of tissue damage. Notably, in conditions associated with destruction of neuronal tissue, substantial amounts of variable 14-3-3 isoforms—including ε, γ and ζ—can be released [9, 10], and 14-3-3 was upregulated in inflamed parts of the aorta [4]. This might directly impact tissue remodelling, because 14-3-3 release influences activity of MMPs [11], which likewise are crucial in LVV pathogenesis [12]. The finding of lymph-follicles in the wall of large arteries further hints at a locally triggered immune response by antigens released in damaged vasculitis-associated tissue. It is possible that other forms of (vascular) tissue damage, such as arteriosclerosis, explain increased anti-14-3-3 antibody levels in age-matched controls. The present study was, however, underpowered to perform these relevant subgroup analyses.

Intriguingly, subjects with antibodies against the 14-3-3γ isoform had a high seroprevalence of *T. gondii* compared with the general population (30–50% *Toxoplasma*

FIG. 2 Clinical associations with 14-3-3 antibody positivity

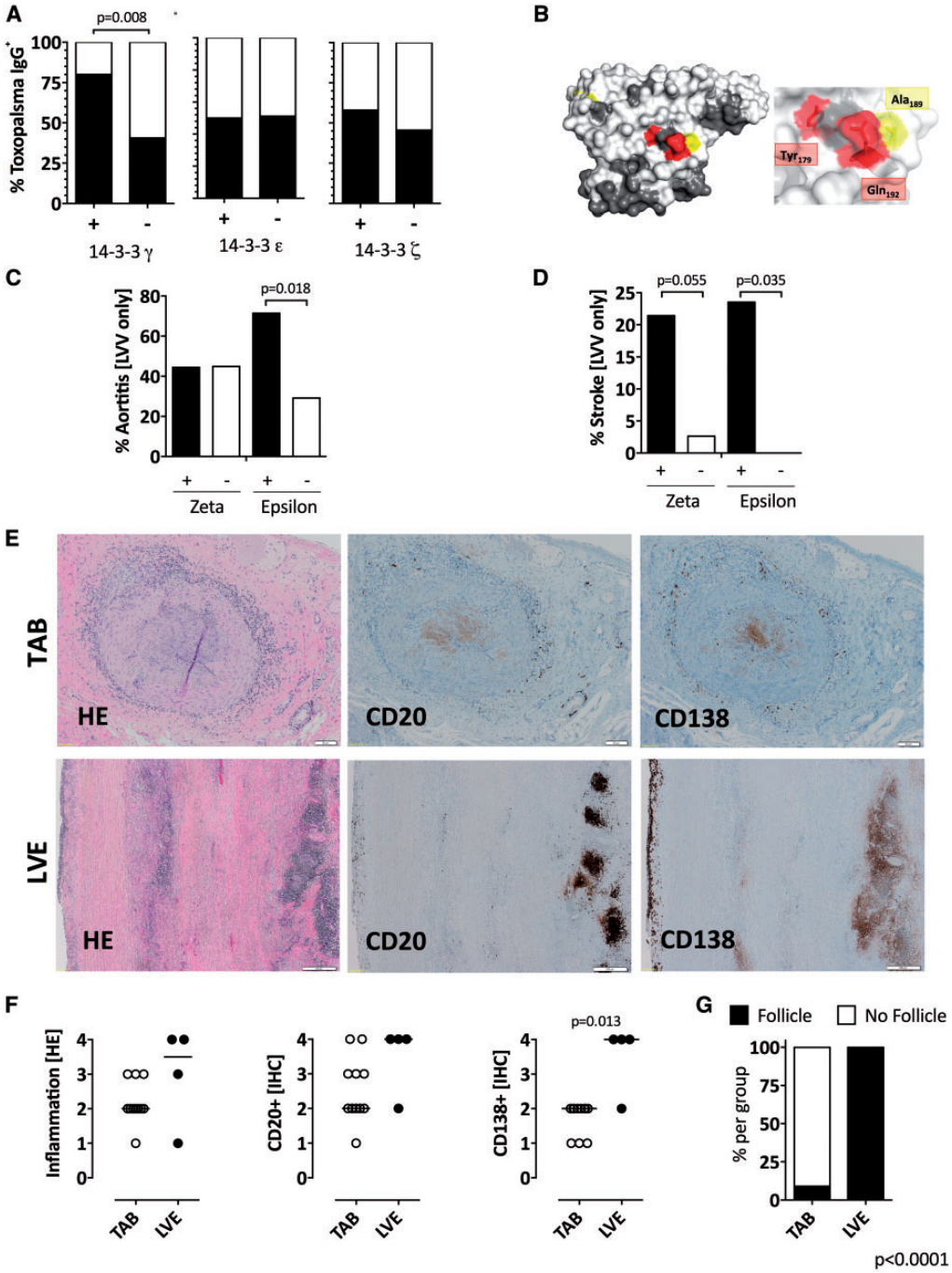

(**A**) *Toxoplasma gondii* seroprevalence in patients with/without 14-3-3 IgG (percentage per group). (**B**) The 14-3-3 crystal structure: 'dark grey' = conserved between isoforms; 'red' = identical and 'yellow' = similar amino-acids only between *Toxoplasma* and human 14-3-3γ. Potential cross-reactive binding-site *Toxoplasma*/human 14-3-3γ is illustrated in higher magnification. Anti-14-3-3-IgG positivity associated with aortitis (**C**) and stroke (**D**) in LVV (percentage with event stratified by anti-14-3-3-IgG positivity/negativity). (**E**) Large-vessel explants (LVEs, $n = 4$) and temporal artery biopsy (TAB, $n = 11$) were compared in HE, B cell (CD20) and plasma cell (CD138) stainings using (**F**) a score from 0 (no inflammation) to 4 (strong inflammation). LVV: large-vessel vasculitis; HE: haematoxylin/eosin.

IgG positive) [13, 14], raising the possibility of cross-reactive antibodies. Indeed, we found a potentially immunogenic region shared between the *Toxoplasma* and the human 14-3-3γ protein—but not the other two isoforms—thus precluding anti-14-3-3γ-IgG as a widely applicable biomarker. Cross-reactivity with other existing 14-3-3 isoforms cannot be excluded based on our data, and may be a general limitation to their use in populations with high *Toxoplasma* seroprevalence.

Whether the presence of 14-3-3ε and/or ζ antibodies precedes aortic aneurysm formation in LVV, and/or may be present in elderly patients with other inflammatory large-vessel disease, including extensive arteriosclerosis, needs to be tested longitudinally in large cohorts. This could validate anti-14-3-3 antibodies as a potential aneurysm biomarker, helping patient stratification for follow-up imaging studies, and possibly indicating patients that might benefit from B cell–depleting strategies in addition to conventional therapy.

Acknowledgements

We thank Christoph Hess and Adrian Egli for their input and critical reading of the manuscript. We thank the physicians of the medical outpatient clinic for their help in the patient care, and the members of the Immunobiology Lab at the Department of Biomedicine for their help in sample processing. M.R. holds a professorship from the Swiss National Science Foundation (PP00P3_144863). M.M. is supported by the Swiss National Science Foundation (PZ00P3_154733).

Funding: This work was supported by the Swiss National Science Foundation [PZ00P3-148000 to C.T.B.].

Disclosure statement: The authors have declared no conflicts of interest.

Supplementary data

Supplementary data are available at *Rheumatology* Online.

References

1 Mohan C, Assassi S. Biomarkers in rheumatic diseases: how can they facilitate diagnosis and assessment of disease activity? BMJ 2015;351:h5079.

2 Berger CT, Wolbers M, Meyer P, Daikeler T, Hess C. High incidence of severe ischaemic complications in patients with giant cell arteritis irrespective of platelet count and size, and platelet inhibition. Rheumatology 2009;48:258–61.

3 Weyand CM, Goronzy JJ. Immune mechanisms in medium and large-vessel vasculitis. Nat Rev Rheumatol 2013;9:731–40.

4 Chakravarti R, Gupta K, Swain M *et al*. 14-3-3 in thoracic aortic aneurysms: identification of a novel autoantigen in large vessel vasculitis. Arthritis Rheumatol 2015;67:1913–21.

5 Kermani TA, Warrington KJ, Crowson CS *et al*. Large-vessel involvement in giant cell arteritis: a population-based cohort study of the incidence-trends and prognosis. Ann Rheum Dis 2013;72:1989–94.

6 van der Geest KS, Abdulahad WH, Chalan P *et al*. Disturbed B cell homeostasis in newly diagnosed giant cell arteritis and polymyalgia rheumatica. Arthritis Rheumatol 2014;66:1927–38.

7 Shapira Y, Agmon-Levin N, Selmi C *et al*. Prevalence of anti-Toxoplasma antibodies in patients with autoimmune diseases. J Autoimmun 2012;39:112–6.

8 Assossou O, Besson F, Rouault JP *et al*. Characterization of an excreted/secreted antigen form of 14-3-3 protein in *Toxoplasma gondii* tachyzoites. FEMS Microbiol Lett 2004;234:19–25.

9 Shiga Y, Wakabayashi H, Miyazawa K, Kido H, Itoyama Y. 14-3-3 protein levels and isoform patterns in the cerebrospinal fluid of Creutzfeldt–Jakob disease patients in the progressive and terminal stages. J Clin Neurosci 2006;13:661–5.

10 Hsich G, Kenney K, Gibbs CJ, Lee KH, Harrington MG. The 14-3-3 brain protein in cerebrospinal fluid as a marker for transmissible spongiform encephalopathies. N Engl J Med 1996;335:924–30.

11 Kilani RT, Maksymowych WP, Aitken A *et al*. Detection of high levels of 2 specific isoforms of 14-3-3 proteins in synovial fluid from patients with joint inflammation. J Rheumatol 2007;34:1650–7.

12 Rodriguez-Pla A, Bosch-Gil JA, Rossello-Urgell J *et al*. Metalloproteinase-2 and -9 in giant cell arteritis: involvement in vascular remodeling. Circulation 2005;112:264–9.

13 Jacquier P, Nadal D, Zuber P, Eckert J. Seroprevalence of specific antibodies to *Toxoplasma gondii* in the general swiss population – a seroepidemiologic study from Canton Zurich. Schweiz Med Wschr 1995;125:S23–8.

14 Jones JL, Kruszon-Moran D, Wilson M *et al*. *Toxoplasma gondii* infection in the United States: seroprevalence and risk factors. Am J Epidemiol 2001;154:357–65.

Supplementary Data

Supplementary Table S1: Patient Characteristics

	GCA	long-lasting GCA	TA	INFL	non-INFL	young healthy
Patients, n	43	5	3	20	9	10
Age, years, median (range)	75 (56-91)	71 (63-75)	31 (19-53)	63 (49-86)	72 (59-76)	29 (25-38)
Sex, female, n (%)	25 (58)	5 (100)	3 (100)	11(55)	3 (33)	3 (30)
PDN treated samples, n (%)	20 (46)	5 (100)	2 (66)	3 (15)	1 (11)	0 (0)
Days on PDN, median (range)	0 (0-38)	Years	Years	0 (0-17)	0 (0-18)	ND
Histology[a] done, n (%)	39 (91)	4 (80)	2 (67)	9 (44)	2 (22)	ND
Histologically confirmed[b], n (%)	30/39 (77)	3/4 (75)	2/2 (100)	0/9 (0)	0/2 (0)	ND
CRP in mg/l, median (range)	63 (10-364)	86 (9-184)	8.6[c]	71 (4-152)	1.5 (0.3-3)	ND
ESR in mm/h, median (range)	76 (14-120)	86 (20-98)	56[c]	61 (10-120)	8 (1-24)	ND
active PMR	16 (37)	1 (20)	0 (0)	13 (65)	0 (0)	0 (0)

[a] includes temporal artery biopsies and large vessel explants; [b] n= biopsy positives of those who had a biopsy. [c] CRP and ESR at time of study blood draw only available for 1/3, but these were in stable disease for >6 months. TA: Takayasu arteritis; INFL: inflammatory control; non-INFL: non-inflammatory control; PDN: prednisone; ND: not done

Supplementary Table 2: Diagnoses of disease controls

Inflammatory Controls (n=20)	**n cases**
PMR / atypical PMR	12
Periaortitis / Aortitis	2
ANCA-associated Vasculitis	1
Inflammatory Syndrome	1
Interstitial Pneumopathy/-itis	1
Tooth infection and abscess	1
Metastatic prostate cancer	1
Infection & chronic neck pain	1
Non-inflammatory Controls (n=9)	
chronic pain disorder	3
Non-inflammatory shoulder pain	2
Tendinopathy	1
cardioembolic AION	1
non-inflammatory stroke	1
Check-up	1

AION: anterior ischemic optic neuropathy

Supplementary Figure S1: Linear alignment of the amino acid sequences of the human and *Toxoplasma gondii* 14-3-3 isoforms

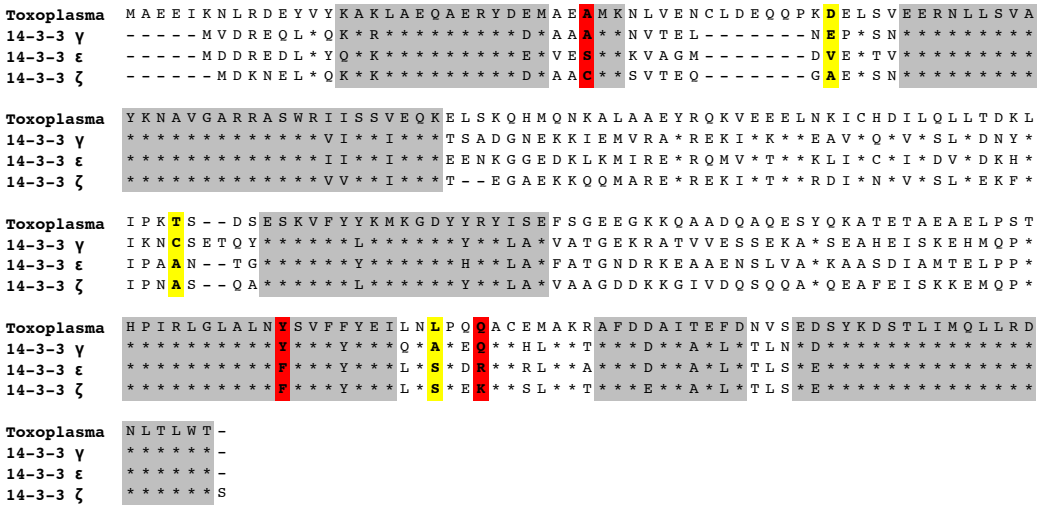

Multiple sequence alignment of *Toxoplasma gondii* 14-3-3 and the human γ, ε and ζ isoforms is shown. Amino acids identical between all four proteins are depicted with an asterisk. Amino acids of interest are shown for the comparison *Toxoplasma* / 14-3-3γ. The color code corresponds to the coloring used in *Figure 2B*: conserved regions are shown in grey; Amino acids being identical between *Toxoplasma* and 14-3-3γ but having a different class in 14-3-3ε and -ζ are highlighted in red. Those being biochemically similar (i.e. in terms of charge, polarization, etc…) between *Toxoplasma* and 14-3-3γ (e.g. D and E, two acidic amino acids) but having a different class in 14-3-3ε and -ζ are shown in yellow.

Supplementary Figure S2: Seroprevalence of 14-3-3 antibodies was comparable between LVV and controls.

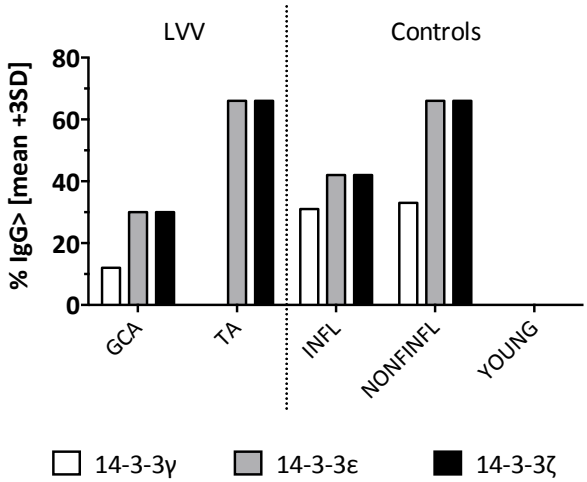

An antibody level above mean+3SD of the young healthy group was considered as positive. TA patients had no 14-3-3γ antibodies but 2/3 had antibodies against one of the other isoforms.

Supplementary Figure S3: Anti-14-3-3 antibody titers are not higher in LVV compared to age-matched controls.

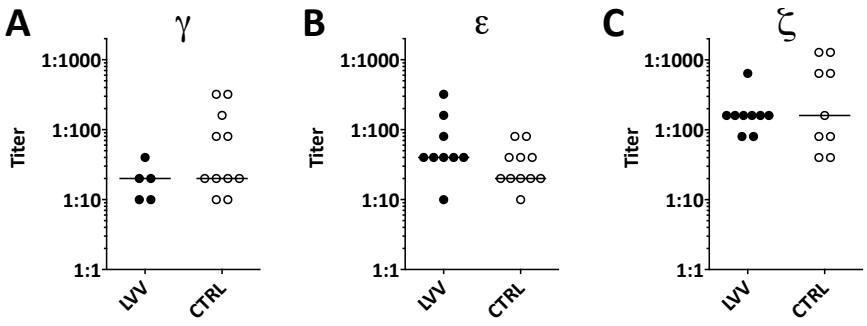

Twofold serial dilutions of plasma of patients with high 14-3-3 antibodies against (**A**) 14-3-3γ, (**B**) 14-3-3ε and (**C**) 14-3-3ζ were performed to determine the titer. Positivity was defined as mean+3SD of the 10 young healthy controls. To increase the power, GCA and TA patients were merged to a LVV group and all controls were merged to a control group. LVV: large vessel vasculitis; CTRL: control

Supplementary Figure S4: Conservation visualization of the different human and Toxoplasma 14-3-3 isoforms

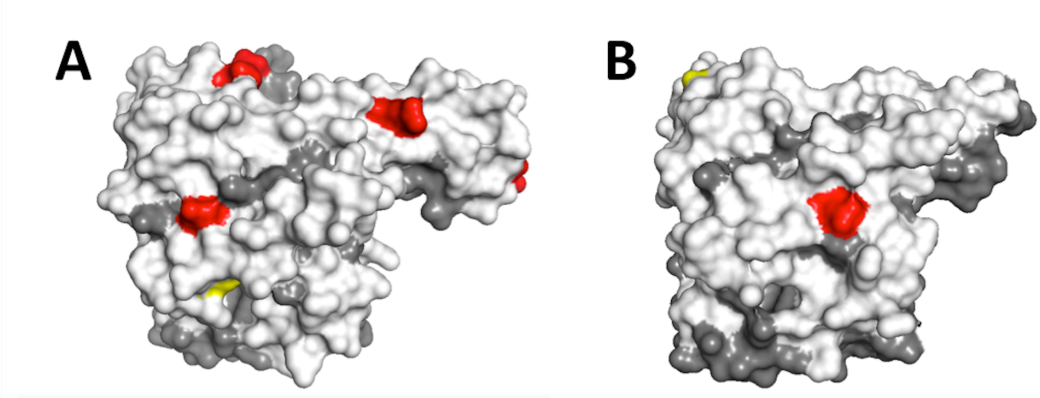

The crystal structure of the human 14-3-3ε (**A**) and human 14-3-3ζ protein (**B**) are shown from the same perspective. Specific regions were color-coded analog to Figure 2B: Surface stained in dark grey depicts conserved regions. Amino acids are highlighted in color, when they are identical (red) or similar (same amino acid class, yellow) in *Toxoplasma* 14-3-3 and 14-3-3ε, but different in 14-3-3γ and -ζ (**A**) or identical in in *Toxoplasma* 14-3-3 and 14-3-3ζ, but different in 14-3-3γ and -ε respectively (**B**).

Discussion

Antigen-specific responses in GCA

A straightforward way to investigate Th1 cell reactivity against specific antigens is to measure IFN-γ production upon exposure to antigen presented on APC. Among other pathogens, *Varicella zoster virus* (VZV) has been implicated in GCA pathogenesis [155]. When PBMC were directly exposed to unprocessed self-proteins, IFN-γ production was extremely high, indicating TCR-independent activation. This prompted us to use a two-step protocol were we pre-incubated PBMC (including APC) with antigen over night, washed the cells and added them to autologous PBMC on anti-IFN-γ coated EliSpot plates. The investigated antigens were recombinant VZV Glycoprotein E, shown to be highly immunogenic [162], a vaccine preparation against VZV (Varilrix), an influenza vaccine (Fluarix) or SEB (staphylococcal enterotoxin B) as positive controls and 5 pools of aortic wall-derived proteins as a source of autoantigen.

The most informative procedure would have been to interrogate TA-derived T cells in the EliSpot assay. Indeed, it has been shown that T cell clonotypes are present in the inflamed TA that react towards GCA-TA extracts but not towards control extracts [148]. These assays were done on *in vitro* expanded T cells that migrated out of the TA. Such an approach is not applicable to larger screens in a GCA cohort or as a potential test in the clinic. Peripheral blood EliSpots on the other hand are broadly used in the clinic and in clinical trials to test for previous antigen encounter including VZV [163]. Compared to age-matched inflammatory disease controls or healthy controls, we did not find an increase in the number of autoantigen- or VZV-specific T cells in newly diagnosed GCA. GCA patients were rather hyporesponsive towards certain antigens. This could potentially be due to the context of an acute systemic inflammation. We also cannot exclude that VZV- or arterial wall-specific T cells were exhausted (e.g. due to repeated *in vivo* exposure), but we would have expected increased responses in at least some patients if these antigens were relevant to GCA pathogenesis.

Our TCR-centered approach therefore was chosen to zoom right into the inflamed tissue compartment and bears the potential to help elucidating the nature of the antigen targeted by specific T cells in the TA. Given the distinct distribution of clones in the TA compared to bulk $CD4^+$ T cells, we potentially have missed disease-relevant clones in our peripheral T cell EliSpot. Since we found at least one strongly expanded T cell clone

in every donor, this gives the opportunity to match the corresponding TCR alpha chain sequence based on its frequency when also sequencing the TCR alpha chain repertoire. This will enable us to reveal the sequence of the complete TCR which then could be transfected into TCRαβ-deficient Jurkat T cells [164]. These transgenic T cell lines can be used as reporter cell lines to test peptide libraries for reactivity against antigens in an HLA-matched background.

While we did not find evidence for any expanded public T cell clones, it is possible that shared antigen-specific T cells are present nevertheless. A slightly altered CDR3-region might still recognize the same epitope. To investigate enriched and potentially shared CDR3-motifs, we will genotype MHC class II of the subjects from the TA biopsy study and further mine our TCR data by using the GLIPH algorithm [165]. GLIPH clusters CDR3-regions with similar or identical enriched motifs relevant to binding the peptide or specific HLA-alleles into groups. The TCRs within these groups may be strongly enriched for binding the same antigen, thereby enhancing the TCR repertoire data and informing further antigen screens.

Based on the histopathology, there is no evidence for substantial involvement of a humoral immune response in GCA. One group reported reduced number of B cell subsets in the periphery and increased serum levels of BAFF, a B cell survival factor [166,167]. Nevertheless, efforts have been undertaken to investigate binding of autoantibodies in GCA by either cDNA library screening or 2D-proteomics, which may have a use as a simple diagnostic or prognostic tool. Reactivity against a series of intracellular proteins has been reported, many of them matrix proteins such as vinculin or lamin A/C [168,169]. The most convincing data stems from a group reporting elevated concentrations of antibodies targeting isoforms of 14-3-3 protein in LVV-patients undergoing surgical aortic aneurysm repair [170]. 14-3-3 isoforms are phospho-serin/threonine-binding proteins involved in a very broad range of cellular processes [171]. Given the fact that most of the previously reported antibody targets are very abundant intracellular proteins, we hypothesized that the observed reactivity was rather due to a secondary immune response reflecting tissue damage.

After testing for antibody binding to 14-3-3 via bead-based immunoassay, we found reactivity against all three reported 14-3-3 isoforms (γ, ε, ζ). However, the binding levels were similarly distributed between the LVV-group and the control groups. Interestingly, the frequency of patients with aortitis and stroke was significantly higher in those

positive for anti-14-3-3 ε antibodies, hinting at an immune response following tissue damage. Indeed, elevated levels of extracellular, i.e. potentially immunogenic 14-3-3 isoforms have been reported for several inflammatory and necrotizing diseases [170,172–174], in one case also coincident with autoantibody prevalence [172]. Patients with aortitis also showed considerable infiltration of plasma cells and presence of tertiary lymph follicles, consistent with a locally induced immune response.

The highest antibody levels were found against the γ-isoform. We hypothesized that these antibodies are present due to molecular mimicry; they are targeting a pathogen-derived protein but are cross-reactive to a self-protein. The frequent opportunistic protozoan parasite *Toxoplasma gondii* seemed to be a promising candidate, being also able to secrete a homologous form of 14-3-3 [175]. Indeed, individuals seropositive for *T. gondii* were significantly more frequent among the anti-γ-positive (but not ε- or ζ-positive). Also, we found a potential epitope that is identical between the protozoan 14-3-3 and human 14-3-3-γ, but not ε or ζ.

Taken together, we found evidence for antigen-specific T cell proliferation in all investigated arteries based on dominant T cell clones. Defining the types of antigen targeted and investigating potentially shared antigens is the goal of our future research. Being interested in autoreactive B cells as biomarkers, we found that antibodies targeting 14-3-3 isoforms are not suitable to diagnose GCA.

Concluding discussion

The focus of this thesis are cross-reactive immune responses. Cross-reactive immune cells are originally selected against one epitope, but are also able to recognize similar epitopes. An optimal influenza vaccine should induce selection of B cells with the capacity to produce broadly neutralizing antibodies against a wide range of strains and ideally even against other serotypes. While initially not investigating cross-reactivity in the strict sense (i.e a single epitope), we found that vaccine responses against the whole hemagglutinin protein are to a certain extent cross-reactive to similar strains. However, in the case of a H3N2 strain that emerged several years after the vaccination cohort was collected, we described a single point mutation altering an epitope on the HA head by removal of a glycan. This mutation resulted in escape from a large proportion of the antibodies binding to the HA without the mutation, revealing the vulnerability of the vaccine-induced immune response. Moreover, it supports that cross-reactive antibodies should ideally bind to functionally indispensable structures of the protein, thereby restricting viral escape to a minimum.

In GCA, and autoimmunity in general, cross-reactive T cells have been suggested to contribute to the immunopathology. Specifically, infection was proposed as a trigger of autoimmune responses by molecular mimicry of host proteins or bystander activation of T cells resulting in tissue targeting. In GCA, these assumptions were so far only based on detection of viral DNA and proteins at the site of infection and epidemiological inferences. We aimed at investigating GCA-specific T cell reactivity against self-protein using protein extracts from aortic wall proteins that could have been further characterized to define the targeted peptide sequences. In peripheral blood, however, we found no evidence for increased T cell reactivity towards host proteins. By investigating 14-3-3 autoantibodies in GCA patients, we could confirm their presence but not their use for diagnosing GCA in the clinic. Interestingly, however, we established a link in the general population between reactivity towards 14-3-3-γ and previous infection with *Toxoplasma gondii*. This protozoan secretes a 14-3-3-γ homolog, hereby suggesting molecular mimicry.

Summing up, cross-reactivity is an inherent feature of the adaptive immune response. Organisms have evolved measures to control negative cross-reactive effects leading to autoimmunity. But humans have not yet been able to develop a cross-protective influenza vaccine.

References

1. Takaba, H. & Takayanagi, H. The Mechanisms of T Cell Selection in the Thymus. *Trends Immunol.* **38,** 805–816 (2017).
2. Nemazee, D. Mechanisms of central tolerance for B cells. *Nat. Rev. Immunol.* **17,** 281 (2017).
3. Sakaguchi, S., Yamaguchi, T., Nomura, T. & Ono, M. Regulatory T Cells and Immune Tolerance. *Cell* **133,** 775–787 (2008).
4. Victora, G. D. & Nussenzweig, M. C. Germinal Centers. *Annu. Rev. Immunol.* **30,** 429–457 (2012).
5. Carson, M. J., Dosse, J. M., Melchior, B., Schmid, C. D. & Ploix, C. C. CNS immune privilege : hiding in plain sight. *Immunol. Rev.* **October,** 48–65 (2006).
6. Steinman, R. M. & Nussenzweig, M. C. Avoiding horror autotoxicus: the importance of dendritic cells in peripheral T cell tolerance. *Proc. Natl. Acad. Sci. U. S. A.* **99,** 351–8 (2002).
7. Matzaraki, V., Kumar, V., Wijmenga, C. & Zhernakova, A. The MHC locus and genetic susceptibility to autoimmune and infectious diseases. *Genome Biol.* **18,** (2017).
8. Carmona, F. D. *et al.* A Large-Scale Genetic Analysis Reveals a Strong Contribution of the HLA Class II Region to Giant Cell Arteritis Susceptibility. *Am. J. Hum. Genet.* **96,** 565–580 (2015).
9. Kyvik, K. O., Green, A. & Beck-Nielsen, H. Concordance rates of insulin dependent diabetes mellitus: a population based study of young Danish twins. *BMJ* **311,** 913 LP-917 (1995).
10. Fujinami, R. S. & Oldstone, M. B. A. Amino Add Homology Between the Encephalitgenic Site of Myelin Basic Protein and Virus: Mechanism for Autoimmunity. *Science (80-.).* **230,** 1043–1045 (1985).
11. McClain, M. T. *et al.* Early events in lupus humoral autoimmunity suggest initiation through molecular mimicry. *Nat. Med.* **11,** 85 (2004).
12. Fujinami, R. S., Herrath, M. G. Von, Christen, U. & Whitton, J. L. Molecular Mimicry , Bystander Activation , or Viral Persistence : Infections and Autoimmune Disease Molecular Mimicry , Bystander Activation , or Viral Persistence : Infections and Autoimmune Disease. *Clin. Microbiol. Rev.* **19,** 80–94 (2006).
13. Vanderlugt, C. J. & Miller, S. D. Epitope Spreading. *Curr. Opin. Immunol.* **8,** 831–836 (2004).
14. Padovan, E. *et al.* Expression of two T cell receptor α chains: dual receptor T cells. *Science (80-.).* **262,** 422–24 (1993).
15. Davodeau, F. *et al.* Dual T cell receptor b chain expression on human T lymphocytes. *J.Exp.Med.* **181,** 1391–1398 (1995).
16. Cusick, M. F., Libbey, J. E. & Fujinami, R. S. Molecular mimicry as a mechanism of autoimmune disease. *Clin. Rev. Allergy Immunol.* **42,** 102–111 (2012).
17. Wucherpfennig, K. W. & Strominger, J. L. Molecular mimicry in T cell-mediated autoimmunity: Viral peptides activate human T cell clones specific for myelin basic protein. *Cell* **80,** 695–705 (1995).
18. Dyer, M. J. S. *et al.* Immunoglobulin heavy chain locus chromosomal translocations in B-cell precursor acute lymphoblastic leukemia: Rare clinical curios or potent genetic drivers? *Blood* **115,** 1490–1499 (2010).
19. Jung, D. & Alt, F. W. Unraveling V(D)J Recombination: Insights into Gene Regulation. *Cell* **116,** 299–311 (2004).
20. Karasuyama, B. H. & Melchers, F. The Proteins Encoded by the VpreB and X5 Pre-B Cell-specific Genes Can Associate with Each Other and with IA Heavy Chain. *J. Exp. Med.* **172,** 969–972 (1990).

21. Lebien, T. W. & Tedder, T. F. ASH 50th anniversary review B lymphocytes : how they develop and function. *Am. Soc. Hematol.* **112,** 1570–1580 (2008).
22. Loder, F. *et al.* B cell development in the spleen takes place in discrete steps and is determined by the quality of B cell receptor-derived signals. *J. Exp. Med.* **190,** 75–89 (1999).
23. Sörman, A., Zhang, L., Ding, Z. & Heyman, B. How antibodies use complement to regulate antibody responses. *Mol. Immunol.* **61,** 79–88 (2014).
24. Stavnezer, J. & Schrader, C. E. Ig heavy chain class switch recombination: mechanism and regulation. *J. Immunol.* **193,** 5370–5378 (2015).
25. Bruhns, P. & Friederike, J. Mouse and human FcR effector functions. *Immunol. Rev.* **268,** 25–51 (2015).
26. WHO. Influenza fact sheet. *2018* at <http://www.who.int/en/news-room/fact-sheets/detail/influenza-(seasonal)>
27. Mesin, L., Di Niro, R., Thompson, K. M., Lundin, K. E. A. & Sollid, L. M. Long-Lived Plasma Cells from Human Small Intestine Biopsies Secrete Immunoglobulins for Many Weeks In Vitro. *J. Immunol.* **187,** 2867–2874 (2011).
28. Nair, H. *et al.* Global burden of respiratory infections due to seasonal influenza in young children: A systematic review and meta-analysis. *Lancet* **378,** 1917–1930 (2011).
29. Meltzer, M. I., Cox, N. J. & Fukuda, K. The economic impact of pandemic influenza in the United States: Priorities for intervention. *Emerg. Infect. Dis.* **5,** 659–671 (1999).
30. Lu 1994 - The influenza virus NS1 protein- a novel inhibitor of pre-mRNA sphcmg.pdf.
31. Nayak, D. P., Balogun, R. A., Yamada, H., Zhou, Z. H. & Barman, S. Influenza virus morphogenesis and budding. *Virus Res.* **143,** 147–161 (2009).
32. Samji, T. Influenza A: Understanding the viral life cycle. *Yale J. Biol. Med.* **82,** 153–159 (2009).
33. Rogers, G. N. & Paulson, J. C. Receptor determinants of human and animal influenza virus isolates: Differences in receptor specificity of the H3 hemagglutinin based on species of origin. *Virology* **127,** 361–373 (1983).
34. Skehel, J. J. & Wiley, D. C. Receptor Binding and Membrane Fusion in Virus Entry: The Influenza Hemagglutinin. *Annu. Rev. Biochem.* **69,** 531–569 (2000).
35. Pinto, L. H., Holsinger, L. J. & Lamb, R. A. Influenza virus M2 protein has ion channel activity. *Cell* **69,** 517–528 (1992).
36. Shi, Y., Wu, Y., Zhang, W., Qi, J. & Gao, G. F. Enabling the 'host jump': structural determinants of receptor-binding specificity in influenza A viruses. *Nat. Rev. Microbiol.* **12,** 822–831 (2014).
37. Boulo, S., Akarsu, H., Ruigrok, R. W. H. & Baudin, F. Nuclear traffic of influenza virus proteins and ribonucleoprotein complexes. *Virus Res.* **124,** 12–21 (2007).
38. Deng, T., Vreede, F. T. & Brownlee, G. G. Different De Novo Initiation Strategies Are Used by Influenza Virus RNA Polymerase on Its cRNA and Viral RNA Promoters during Viral RNA Replication. *J. Virol.* **80,** 2337–2348 (2006).
39. Engelhardt, O., Smith, M. & Fodor, E. Association of the influenza A virus RNA-dependent RNA polymerase with cellular RNA polymerase II. *J. Virol.* **79,** 5812–5818 (2005).
40. Plotch, S. J., Bouloy, M., Ulmanen, I. & Krug, R. M. A unique cap(m7GpppXm)-dependent influenza virion endonuclease cleaves capped RNAs to generate the primers that initiate viral RNA transcription. *Cell* **23,** 847–858 (1981).
41. Poon, L. L., Pritlove, D. C., Fodor, E. & Brownlee, G. G. Direct evidence that the poly(A) tail of influenza A virus mRNA is synthesized by reiterative copying of a U track in the virion RNA template. *J. Virol.* **73,** 3473–6 (1999).
42. Matsuoka, Y. *et al.* A comprehensive map of the influenza A virus replication cycle. *BMC Syst. Biol.* **7,** 1 (2013).

43. Palese, P., Tobita, K., Ueda, M. & Compans, R. W. Characterization of temperature sensitive influenza virus mutants defective in neuraminidase. *Virology* **61,** 397–410 (1974).
44. Lazarowitz, S. G., Goldberg, A. R. & Choppin, P. W. Proteolytic Cleavage by Plasmin of the HA Polypeptide of Influenza Virus: Host Cell Activation of Serum Plasminogen. *Virology* **56,** 172–180 (1973).
45. Brandenburg, B. *et al.* Mechanisms of Hemagglutinin Targeted Influenza Virus Neutralization. **8,** (2013).
46. *ICTV 9th Report: Negative Sense RNA Viruses*. (2011).
47. Osterhaus G.F. Rimmelzwaan, B.E.E. Martina, T.M. Besterbroer, R.A.M. Fouchier, A. D. M. E. Influenza B virus in seals. *Science (80-.).* **288,** 1051–1053 (2000).
48. Guo, Y. J., Jin, F. G., Wang, P., Wang, M. & Zhu, J. M. Isolation of influenza C virus from pigs and experimental infection of pigs with influenza C virus. *J Gen Virol* **64 (Pt 1),** 177–182 (1983).
49. Cycle, R. & Comparisons, S. Evolution and Ecology of Influenza A Viruses. *Genet. Anal.* **56,** 152–179 (1992).
50. Reperant, L. A., Kuiken, T. & Osterhaus, A. D. M. E. Adaptive pathways of zoonotic influenza viruses: From exposure to establishment in humans. *Vaccine* **30,** 4419–4434 (2012).
51. Short, K. R. *et al.* One health, multiple challenges: The inter-species transmission of influenza A virus. *One Heal.* **1,** 1–13 (2015).
52. Garten, R. J., Davis, C. T. & Russell, C. A. Antigenic and Genetic Characteristics of the Early Isolates of Swine-Origin 2009 A(H1N1) Influenza Viruses Circulating in Humans. *Science (80-.).* **325,** 197–201 (2009).
53. Traubenberger, J. K. & Kash, J. C. Influenza Virus Evolution, Host Adaptation and Pandemic Formation. *NIH Public Access* **7,** 440–451 (2010).
54. Wahlgren, J. Influenza A viruses: an ecology review. *Infect. Ecol. Epidemiol.* **1,** 6004 (2011).
55. Assaad, F. A., Brès, P. & Chi-Ming, C. A revision of the system of nomenclature for influenza viruses: a WHO Memorandum. *Bull. World Health Organ.* **58,** 585–591 (1980).
56. Shu, Y. & Mccauley, J. GISAID : Global initiative on sharing all influenza data – from vision to reality. *Eurosurveillance* **22,** (2017).
57. CDC. How Flu spreads. (2017). at <https://www.cdc.gov/flu/about/disease/spread.htm>
58. Killingley, B. & Nguyen-Van-Tam, J. Routes of influenza transmission. *Influenza Other Respi. Viruses* **7,** 42–51 (2013).
59. Pang, I. K. & Iwasaki, A. Inflammasomes as mediators of immunity against influenza virus. *Trends Immunol.* **32,** 34–41 (2011).
60. Wang, J. *et al.* NF- B RelA Subunit Is Crucial for Early IFN- Expression and Resistance to RNA Virus Replication. *J. Immunol.* **185,** 1720–1729 (2010).
61. Jayasekera, J. P., Vinuesa, C. G., Karupiah, G. & King, N. J. C. Enhanced antiviral antibody secretion and attenuated immunopathology during influenza virus infection in nitric oxide synthase-2-deficient mice. *J. Gen. Virol.* **87,** 3361–3371 (2006).
62. GeurtsvanKessel, C. H. *et al.* Both conventional and interferon killer dendritic cells have antigen-presenting capacity during influenza virus infection. *PLoS One* **4,** (2009).
63. Kamphorst, A. O., Guermonprez, P., Dudziak, D. & Nussenzweig, M. C. Route of Antigen Uptake Differentially Impacts Presentation by Dendritic Cells and Activated Monocytes. *J. Immunol.* **185,** 3426–3435 (2010).
64. Mandelboim, O. *et al.* Recognition of haemagglutinins on virus-infected cells by NKp46 activates lysis by human NK cells. *Nature* **409,** 1055–1060 (2001).
65. Mazanec, M. B., Kaetzel, C. S., Lamm, M. E., Fletcher, D. & Nedrud, J. G. Intracellular

neutralization of virus by immunoglobulin A antibodies. *Proc. Natl. Acad. Sci. U. S. A.* **89,** 6901–6905 (1992).
66. Jayasekera, J. P., Moseman, E. A. & Carroll, M. C. Natural Antibody and Complement Mediate Neutralization of Influenza Virus in the Absence of Prior Immunity. *J. Virol.* **81,** 3487–3494 (2007).
67. Potter, C. W. & Oxford, J. S. Determinants of immunity to influenza infection in man. *Br. Med. Bull.* **35,** 69–75 (1979).
68. Hobson, D., Curry, R. L., Beare, A. S. & Ward-Gardner, A. The role of serum haemagglutination-inhibiting antibody in protection against challenge infection with influenza A2 and B viruses. *J. Hyg. (Lond).* **70,** 767–777 (1972).
69. Leon, P. E. *et al.* Optimal activation of Fc-mediated effector functions by influenza virus hemagglutinin antibodies requires two points of contact. *Proc. Natl. Acad. Sci.* **113,** 5944–5951 (2016).
70. Gotch, F., McMichael, a, Smith, G. & Moss, B. Identification of viral molecules recognized by influenza-specific human cytotoxic T lymphocytes. *J. Exp. Med.* **165,** 408–416 (1987).
71. Jameson, J., Cruz, J. & Ennis, F. a. Human cytotoxic T-lymphocyte repertoire to influenza A viruses. *J. Virol.* **72,** 8682–8689 (1998).
72. Wang, M. *et al.* CTL epitopes for influenza A including the H5N1 bird flu; genome-, pathogen-, and HLA-wide screening. *Vaccine* **25,** 2823–2831 (2007).
73. Sridhar, S. *et al.* Cellular immune correlates of protection against symptomatic pandemic influenza. *Nat. Med.* **19,** 1305–1312 (2013).
74. CDC. Seasonal Influenza Vaccine Supply for the U.S. 2017-2018 Influenza Season. (2017). at <https://www.cdc.gov/flu/about/qa/vaxsupply.htm>
75. DiazGranados, C. A., Denis, M. & Plotkin, S. Seasonal influenza vaccine efficacy and its determinants in children and non-elderly adults: a systematic review with meta-analyses of controlled trials. *Vaccine* **31,** 49–57 (2012).
76. Bedford, T. *et al.* Integrating influenza antigenic dynamics with molecular evolution. *Elife* **2014,** 1–26 (2014).
77. Ito, T. *et al.* Differences in sialic acid-galactose linkages in the chicken egg amnion and allantois influence human influenza virus receptor specificity and variant selection. *J. Virol.* **71,** 3357–3362 (1997).
78. Wu, N. C. *et al.* A structural explanation for the low effectiveness of the seasonal influenza H3N2 vaccine. *PLoS Pathog.* **13,** 1–17 (2017).
79. Zost, S. J. *et al.* Contemporary H3N2 influenza viruses have a glycosylation site that alters binding of antibodies elicited by egg-adapted vaccine strains. *Proc. Natl. Acad. Sci.* **144,** 12578–12583 (2017).
80. Garretson, T. A., Petrie, J. G., Martin, E. T., Monto, A. S. & Hensley, S. E. Identification of human vaccinees that possess antibodies targeting the egg-adapted hemagglutinin receptor binding site of an H1N1 influenza vaccine strain. *Vaccine* 1–7 (2018). doi:10.1016/j.vaccine.2018.05.086
81. Francis Jr., T. On the Doctrine of Original Antigenic Sin. *Proc. Am. Philos. Soc.* **104,** 572–578 (1960).
82. Henry, C., Palm, A. K. E., Krammer, F. & Wilson, P. C. From Original Antigenic Sin to the Universal Influenza Virus Vaccine. *Trends Immunol.* **39,** 70–79 (2018).
83. Hoskins, T.W.; Davies, J.R.; Smith, J.; Miller, C.L.; Allchin, A. Assessment of inactivated influenza-A vaccine after three outbreaks of influenza A at Christ's Hospital. *Lancet* **1,** 33–5 (1979).
84. Keitel, W. A., Cate, T. R., Couch, R. B., Huggins, L. L. & Hess, K. R. Efficacy of repeated annual immunization with inactivated influenza virus vaccines over a five year period. *Vaccine* **15,** 1114–1122 (1997).
85. Skowronski, D. M. *et al.* Serial vaccination and the antigenic distance hypothesis: Effects on influenza vaccine effectiveness during A(H3N2) epidemics in Canada, 2010-2011 to 2014-2015. *J. Infect. Dis.* **215,** 1059–1069 (2017).

86. Wiley, D. C. & Skehel, J. J. The Structure and Function of the Hemagglutinin Membrane Glycoprotein of Influenza Virus. *Annu. Rev. Biochem.* **56,** 365–94 (1987).
87. Wiley, D. C., Wilson, I. A. & Skehel, J. J. Structural identification of the antibody-binding sites of Hong Kong influenza haemagglutinin and their involvement in antigenic variation. *Nature* **289,** 373–378 (1981).
88. Gerhard, W., Yewdell, J., Frankel, M. E. & Webster, R. Antigenic structure of influenza virus haemagglutinin defined by hybridoma antibodies. *Nature* **290,** 713–717 (1981).
89. Skehel, J. J. *et al.* A carbohydrate side chain on hemagglutinins of Hong Kong influenza viruses inhibits recognition by a monoclonal antibody. *Cell* **81,** 1779–1783 (1984).
90. Koel, B. F. *et al.* Substitutions Near the Receptor Binding Site Determine Major Antigenic Change During Influenza Virus Evolution. *Science (80-.).* **342,** 976–979 (2013).
91. Wu, N. C. *et al.* High-throughput profiling of influenza A virus hemagglutinin gene at single-nucleotide resolution. *Sci. Rep.* **4,** 1–8 (2014).
92. Wu, N. C. *et al.* A complex epistatic network limits the mutational reversibility in the influenza hemagglutinin receptor-binding site. *Nat. Commun.* **9,** (2018).
93. Wilson, I. C. N. Structural Basis of Immune Recognition of Influenza Virus Hemagglutinin. *Annu. Rev. Immunol.* **Vol. 8,** 737–787 (1990).
94. Kendal, A. P., M. S. Pereira, and J. J. S. *Concepts and procedures for laboratory-based influenza surveillance*. (U.S. Dept. of Health and Human Services, Washington, D.C., 1982).
95. Hobson, D., Curry, R. L., Beare, A. S. & Ward-Gardner, A. The role of serum haemagglutination-inhibiting antibody in protection against challenge infection with influenza A2 and B viruses. *J Hyg* **70,** 767–777 (1972).
96. Rowe, T. *et al.* Detection of antibody to avian influenza a (H5N1) virus in human serum by using a combination of serologic assays. *J. Clin. Microbiol.* **37,** 937–943 (1999).
97. Angeloni, S., Dunbar, S., Garcia, C. & Stone, V. *xMAP® Cookbook, 3rd Edition, Luminex Corporation*. (2016).
98. Roberts, C. *et al.* Development of a human papillomavirus competitive luminex immunoassay for 9 HPV types. *Hum. Vaccines Immunother.* **10,** 2168–2174 (2014).
99. Pickering, J. W. *et al.* A multiplexed fluorescent microsphere immunoassay for antibodies to pneumococcal capsular polysaccharides. *Am. J. Clin. Pathol.* **117,** 589–596 (2002).
100. Wang, J. *et al.* Multi-dimensional measurement of antibody-mediated heterosubtypic immunity to influenza. *PLoS One* **10,** 1–27 (2015).
101. Neher, R. A. & Bedford, T. nextflu: real-time tracking of seasonal influenza virus evolution in humans. *Bioinformatics* **31,** 3546–3548 (2015).
102. Smith, D. J. Mapping the Antigenic and Genetic. *Science (80-.).* **305,** 371–376 (2004).
103. Lapedes, A. & Farber, R. The geometry of shape space: Application to influenza. *J. Theor. Biol.* **212,** 57–69 (2001).
104. Kim, J. H. *et al.* Prior infection with influenza virus but not vaccination leaves a long-term immunological imprint that intensifies the protective efficacy of antigenically drifted vaccine strains. *Vaccine* **34,** 495–502 (2016).
105. Campbell, J. I. *et al.* Comparative Effectiveness of Induction Therapy for Human Immunodeficiency Virus-Associated Cryptococcal Meningitis: A Network Meta-Analysis. *Ofid* **2,** 1–8 (2015).
106. Fonville, J. M. *et al.* Antibody landscapes after influenza virus infection or vaccination. *Science* **346,** 996–1000 (2014).

107. Andrews, S. F. *et al.* High preexisting serological antibody levels correlate with diversification of the influenza vaccine response. *J. Virol.* **89,** 3308–17 (2015).
108. Andrews, S. F. *et al.* Immune history profoundly affects broadly protective B cell responses to influenza. *Sci Transl Med* **7,** (2015).
109. Nikolaj, B., Thomas, S., Ramneek, G., Steen, G. & Søren, B. Prediction of post-translational glycosylation and phosphorylation of proteins from the amino acid sequence. *Proteomics* **4,** 1633–1649 (2004).
110. Tate, M. D. *et al.* Playing hide and seek: How glycosylation of the influenza virus hemagglutinin can modulate the immune response to infection. *Viruses* **6,** 1294–1316 (2014).
111. Barnes, C. O. *et al.* Structural characterization of a highly-potent V3-glycan broadly neutralizing antibody bound to natively-glycosylated HIV-1 envelope. *Nat. Commun.* **9,** (2018).
112. Sterner, E., Flanagan, N. & Gildersleeve, C. Perspectives on Anti-Glycan Antibodies Gleaned from Development of a Community Resource Database. *ACS Chem. Biol.* **11,** 1773–1783 (2016).
113. Bardelli, M. *et al.* Ex Vivo Analysis of Human Memory B Lymphocytes Specific for A and B Influenza Hemagglutinin by Polychromatic Flow-Cytometry. *PLoS One* **8,** (2013).
114. Yang, H. *et al.* Structure and receptor binding preferences of recombinant human A(H3N2) virus hemagglutinins. *Virology* **477,** 18–31 (2015).
115. Baden, L. R. *et al.* First-in-Human Randomized Controlled Trial of Mosaic HIV-1 Immunogens Delivered via a Modified Vaccinia Ankara Vector. *J. Infect. Dis.* **217,** (2018).
116. Esposito, S. *et al.* Safety and immunogenicity of a 13-valent pneumococcal conjugate vaccine compared to those of a 7-valent pneumococcal conjugate vaccine given as a three-dose series with routine vaccines in healthy infants and toddlers. *Clin. Vaccine Immunol.* **17,** 1017–1026 (2010).
117. CDC. Selecting Viruses for the Seasonal Influenza Vaccine. (2016).
118. Manini, I. *et al.* Egg-Independent Influenza Vaccines and Vaccine Candidates. *Vaccines* **5,** 18 (2017).
119. Wrammert, J. *et al.* Rapid cloning of high-affinity human monoclonal antibodies against influenza virus. *Nature* **453,** 667–71 (2008).
120. Margine, I. *et al.* H3N2 Influenza Virus Infection Induces Broadly Reactive Hemagglutinin Stalk Antibodies in Humans and Mice. *J. Virol.* **87,** 4728–4737 (2013).
121. Corti, D. *et al.* Heterosubtypic neutralizing antibodies are produced by individuals immunized with a seasonal influenza vaccine. *J. Clin. Invest.* **120,** 1663–1673 (2010).
122. Agatic, G. *et al.* A Neutralizing Antibody Selected from. *Science* **333,** 850–856 (2011).
123. DiLillo, D. J., Tan, G. S., Palese, P. & Ravetch, J. V. Broadly neutralizing hemagglutinin stalk–specific antibodies require FcγR interactions for protection against influenza virus in vivo. *Nat. Med.* **20,** 143 (2014).
124. Lu, Y., Welsh, J. P. & Swartz, J. R. Production and stabilization of the trimeric influenza hemagglutinin stem domain for potentially broadly protective influenza vaccines. **111,** 125–130 (2014).
125. Apetri, A. *et al.* A stable trimeric influenza hemagglutinin stem as a broadly protective immunogen. **349,** (2015).
126. Wrammert, J. *et al.* Broadly cross-reactive antibodies dominate the human B cell response against 2009 pandemic H1N1 influenza virus infection. *J. Exp. Med.* **208,** 181–193 (2011).
127. Ellebedy, A. H. *et al.* Induction of broadly cross-reactive antibody responses to the influenza HA stem region following H5N1 vaccination in humans. *Proc. Natl. Acad.*

Sci. **111,** 13133–13138 (2014).
128. Grant, E. J., Quinõnes-Parra, S. M., Clemens, E. B. & Kedzierska, K. Human influenza viruses and CD8+T cell responses. *Curr. Opin. Virol.* **16,** 132–142 (2016).
129. He, W. *et al.* Molecular Basis of Live-Attenuated Influenza Virus. *PLoS One* **8,** 1–9 (2013).
130. Berthoud, T. K. *et al.* Potent CD8+T-cell immunogenicity in humans of a novel heterosubtypic influenza a vaccine, MVA-NP+M1. *Clin. Infect. Dis.* **52,** 1–7 (2011).
131. Lillie, P. J. *et al.* Preliminary assessment of the efficacy of a T-cell-based influenza vaccine, MVA-NP+M1, in humans. *Clin. Infect. Dis.* **55,** 19–25 (2012).
132. Pleguezuelos, O. *et al.* A synthetic influenza virus vaccine induces a cellular immune response that correlates with reduction in symptomatology and virus shedding in a randomized phase Ib live-virus challenge in humans. *Clin. Vaccine Immunol.* **22,** 828–835 (2015).
133. Arteritis, G. & Rheumatica, P. Giant-Cell Arteritis and Polymyalgia Rheumatica. *Ann. Intern. Med.* **139,** 505–516 (2003).
134. Weyand, C. M., Ph, D., Goronzy, J. J. & Ph, D. Medium- and Large-Vessel Vasculitis. *N. Engl. J. Med.* **349,** 160–169 (2003).
135. Salvarani, C., Gabriel, S., O'Fallon, W. & Hunder, G. Epidemiology of polymyalgia rheumatica in Olmsted County Minnesota 1970 - 1991. *Arthritis Rheum* **38,** 369–73 (1995).
136. Epidemiologic, A. & Analysis, H. An Epidemiologic and Histopathologic Analysis. **37,** 1007–1012 (1994).
137. Kobayashi, S. *et al.* Clinical and epidemiologic analysis of giant cell (temporal) arteritis from a nationwide survey in 1998 in Japan: The first government-supported nationwide survey. *Arthritis Rheum.* **49,** 594–598 (2003).
138. Hunder, G. G., Bloch, D. A. & Michel, B. A. The American College of Rheumatology 1990 Criteria for the Classification of Giant Cell Arteritis. *Arthritis Rheum.* **33,** 1122–1128 (1990).
139. PathPedia. Giant cell (temporal) arteritis. (2018). at <http://www.pathpedia.com/education/eatlas/histopathology/blood_vessels/giant_cell_(temporal)_arteritis.aspx>
140. Ma-Krupa, W. Activation of Arterial Wall Dendritic Cells and Breakdown of Self-tolerance in Giant Cell Arteritis. *J. Exp. Med.* **199,** 173–183 (2004).
141. Weyand, C. M. & Goronzy, J. J. Immune mechanisms in medium and large-vessel vasculitis. *Nat. Rev. Rheumatol.* **9,** 731–740 (2013).
142. Deng, J., Younge, B. R., Olshen, R. A., Goronzy, J. J. & Weyand, C. M. Th17 and th1 T-cell responses in giant cell arteritis. *Circulation* **121,** 906–915 (2010).
143. Piggott, K. *et al.* Blocking the NOTCH pathway inhibits vascular inflammation in large-vessel vasculitis. *Circulation* **123,** 309–318 (2011).
144. Zhang, H. *et al.* Immunoinhibitory checkpoint deficiency in medium and large vessel vasculitis. *Proc. Natl. Acad. Sci.* **114,** 970–979 (2017).
145. Greenbaum, J. *et al.* Functional classification of class II human leukocyte antigen (HLA) molecules reveals seven different supertypes and a surprising degree of repertoire sharing across supertypes. *Immunogenetics* **63,** 325–335 (2011).
146. Carmona, F. D., González-Gay, M. a. & Martín, J. Genetic component of giant cell arteritis. *Rheumatol. (United Kingdom)* **53,** 6–18 (2014).
147. Weyand, C. M. *et al.* Distinct vascular lesions in giant cell arteritis share identical T cell clonotypes. *J. Exp. Med.* **179,** 951–60 (1994).
148. Martinez-Taboada, V., Hunder, N. N. H., Hunder, G. G., Weyand, C. M. & Goronzy, J. J. Recognition of tissue residing antigen by T cells in vasculitic lesions of giant cell arteritis. *J. Mol. Med.* **74,** 695–703 (1996).
149. Weyand, C. M. *et al.* Vascular dendritic cells in giant cell arteritis. *Ann. N. Y. Acad. Sci.* **1062,** 195–208 (2005).

150. Deng, J. *et al.* Toll-like receptors 4 and 5 induce distinct types of vasculitis. *Circ. Res.* **104,** 488–495 (2009).
151. Pryshchep, O., Ma-Krupa, W., Younge, B. R., Goronzy, J. J. & Weyand, C. M. Vessel-specific toll-like receptor profiles in human medium and large arteries. *Circulation* **118,** 1276–1284 (2008).
152. Wolinsky, H. & Glagov, S. Nature of species differences in the medial distribution of aortic vasa vasorum in mammals. *Circ. Res.* **20,** 409–421 (1967).
153. Gabriel, S. the Role of Parvovirus B19 in the Pathogenesis of Giant Cell Arteritis. *Arthritis Rheumatol.* **42,** 1255–1258 (1999).
154. Wagner, A. D. *et al.* Detection of chlamydia pneumoniae in giant cell vasculitis and correlation with the topographic: Arrangement of tissue-infiltrating dendritic cells. *Arthritis Rheum.* **43,** 1543–1551 (2000).
155. Gilden, D. *et al.* Prevalence and distribution of VZV in temporal arteries of patients with giant cell arteritis. *Neurology* **84,** 1948–1955 (2015).
156. Helweg-Larsen, J., Tarp, B., Obel, N. & Baslund, B. No evidence of parvovirus B19, Chlamydia pneumoniae or human herpes virus infection in temporal artery biopsies in patients with giant cell arteritis. *Rheumatology.(Oxford)* **41,** 445–449 (2002).
157. Procop, G. W., Eng, C. & Clifford, A. Varicella Zoster Virus and Large Vessel Vasculitis, the Absence of an Association. **2,** 228–238 (2017).
158. Samson, M. *et al.* Th1 and Th17 lymphocytes expressing CD161 are implicated in giant cell arteritis and polymyalgia rheumatica pathogenesis. *Arthritis Rheum.* **64,** 3788–3798 (2012).
159. Robins, H. S. *et al.* Comprehensive assessment of T-cell receptor β-chain diversity in αβ T cells. *Blood* **114,** 4099–4107 (2010).
160. Carlson, C. S. *et al.* Using synthetic templates to design an unbiased multiplex PCR assay. *Nat. Commun.* **4,** 1–9 (2013).
161. Lefranc, M. P. *et al.* IMGT, the international ImMunoGeneTics database. *Nucleic Acids Res* **27,** 209–212 (1999).
162. Haumont, M. *et al.* Purification, characterization and immunogenicity of recombinant varicella-zoster virus glycoprotein gE secreted by Chinese hamster ovary cells. *Virus Res.* **40,** 199–204 (1996).
163. Levin, M. J. *et al.* Decline in Varicella-Zoster Virus (VZV)–Speci c Cell-Mediated Immunity with Increasing Age and Boosting with a High-Dose VZV Vaccine. *J. Infect. Dis.* **188,** 1336–1244 (2003).
164. Schub, A., Schuster, I. G., Hammerschmidt, W. & Moosmann, A. CMV-Specific TCR-Transgenic T Cells for Immunotherapy. *J. Immunol.* **183,** 6819–6830 (2009).
165. Glanville, J. *et al.* Identifying specificity groups in the T cell receptor repertoire. *Nature* **547,** 94–98 (2017).
166. van der Geest, K. S. M. *et al.* Disturbed B cell homeostasis in newly diagnosed giant cell arteritis and polymyalgia rheumatica. *Arthritis Rheumatol. (Hoboken, N.J.)* **66,** 1927–38 (2014).
167. van der Geest, K. S. M. *et al.* Serum markers associated with disease activity in giant cell arteritis and polymyalgia rheumatica. *Rheumatology* **54,** 1397–1402 (2015).
168. Schmits, R., Kubuschok, B., Schuster, S., Preuss, K.-D. & Pfreundschuh, M. Analysis of the B cell repertoire against autoantigens in patients with giant cell arteritis and polymyalgia rheumatica. *Clin. Exp. Immunol.* **127,** 379–85 (2002).
169. Régent, A. *et al.* Identification of target antigens of anti-endothelial cell and anti-vascular smooth muscle cell antibodies in patients with giant cell arteritis: a proteomic approach. *Arthritis Res. Ther.* **13,** R107 (2011).
170. Chakravarti, R., Gupta, K. & Swain, M. 14-3-3 in Thoracic Aortic Aneurysms. *Arthritis Rheumatol.* **67,** 1913–1921 (2015).
171. Morrison, D. K. The 14-3-3 proteins: integrators of diverse signaling cues that

impact cell fate and cancer development. *Trends Cell Biol.* **19,** 16–23 (2009).
172. Kilani, R. T. *et al.* Detection of high levels of 2 specific isoforms of 14-3-3 proteins in synovial fluid from patients with joint inflammation. *J. Rheumatol.* **34,** 1650–1657 (2007).
173. Maksymowych, W. P. *et al.* 14-3-3 Autoantibodies: Diagnostic Use in Early Rheumatoid Arthritis. *J. Rheumatol.* **42,** (2015).
174. Hamlin, C. *et al.* A comparison of tau and 14-3-3 protein in the diagnosis of Creutzfeldt-Jakob disease. *Neurology* **79,** 547–552 (2012).
175. Assossou, O. Characterization of an excreted/secreted antigen form of 14-3-3 protein in Toxoplasma gondii tachyzoites. *FEMS Microbiol. Lett.* **234,** 19–25 (2004).

Abbreviations

AID	Activation-induced cytidine deaminase
APC	Antigen-presenting cell
ADCC	Antibody-dependent cellular cytotoxicity
ADCP	Antibody-dependent cellular phagocytosis
BAFF	B cell activating factor
BCR	B cell receptor
BER	Base-excision repair
bnAb	broadly neutralizing antibody
CCL	Chemokine ligand
CDR3	Complementarity-determining region 3
DC	Dendritic cell
DSB	Double-strand break
DZ	Dark zone (of GC)
EBNA1	Epstein-Barr nuclear antigen 1
EBV	Epstein-Barr virus
ELISA	Enzyme-linked immunosorbent assay
EliSpot	Enzyme-linked immunospot
ER	Endoplasmatic reticulum
Fab	Fragment antigen-binding (of antibody)
Fc	Fragment crystallizable (of antibody)
FDA	(US) Food and drug administration
FDC	Follicular dendritic cell
FFPE	Formalin-fixed, paraffin-embedded
Gal	Galactose
GC	Germinal center
GCA	Giant cell arteritis
GISAID	Global initiative on sharing all influenza data
GlcNAc	N-Acetylglucosamin
GLIPH	Grouping of lymphocyte interactions by paratope hotspots
GM-CSF	Granulocyte-macrophage colony-stimulating factor
HA	Hemagglutinin

HAI	Hemagglutination inhibition
HBVP	Hepatitis B virus polymerase
HLA	Human leukocyte antigen
HPAIV	Highly pathogenic avian influenza virus
IFN	Interferon
IL	Interleukin
IMGT	Immunogenetics (information system)
LAL	*Limulus* amoebocyte lysate
LPAIV	Low pathogenic avian influenza virus
LPS	Lipopolysaccharide
LVV	Large vessel vasculitis
LZ	Light zone (of GC)
MBP	Myelin basic protein
MDCK	Madin-Darby canine kidney (cells)
MFI	Median fluorescence intensity
MHC	Major histocompatibility complex
MMP	Matrix metalloproteinase
MMR	Mismatch repair
moDC	Monocyte-derived dendritic cell
mTEC	Medullary thymic epithelial cell
NA	Neuraminidase
NHEJ	Non-homologous end joining
NK	Natural killer (cell)
NP	Nucleoprotein
OCT	Optimal cutting temperature (resin)
PBMC	Peripheral blood mononuclear cells
PDB	Protein data bank
PMR	Polymyalgia rheumatica
RACE	Rapid amplification of cDNA-ends
RAG	Recombination-activating gene
ROS	Reactive oxygen species
RBS	Receptor-binding site
RdRp	RNA-dependent RNA polymerase
RNP	Ribonucleoprotein
RPMI	Roswell Park Memorial Institute (medium)
SA	Sialic acid

SCID	Severe combined immunodeficiency
SEB	Staphylococcal enterotoxin B
SHM	Somatic hypermutation
SLE	Systemic lupus erythematosus
TA	Temporal artery
TCR	T cell receptor
TNF	Tumor necrosis factor
UNG	Uracil DNA glycosylase
VE	Vaccine efficacy
VSMC	Vascular smooth muscle cell
VZV	*Varicella zoster virus*
WHO	World health organization

Acknowledgments

I would like to thank my supervisor Christoph Berger for having the trust in me to start his own research group. His ideas could probably keep a lab five times as big busy, but together we could focus on what was most interesting.

The small Berger group would not be the same with all the students I had the honor to supervise. Simon, I promise that we will finally publish your work after it has aged like a good wine! Anne, thank you for being such an eager and kind Master student, it was a pleasure. And thank you Julia for bearing with my sudden mood deteriorations, I am impressed that you will continue the story of the lab.

While not on the Berger salary list, my deep gratitude goes to Victor, our unbelievably patient bioinformatician of trust. This is not less valid for Dirk in Amsterdam: It was great to generate some nasty viruses with you!

Of course, I want to acknowledge the Recher and Mehling start-up groups completing the lab. The range of emotions and decibels created by you was astonishing. I will miss you!

My gratitude goes to the members of my committee, Christian Brander, Primo Schär and Christoph Hess. They were not only helpful by providing good ideas but also in keeping me focused on what was feasible.

I apologize to everyone that deserves to be acknowledged but is not listed here.

Last but not least, I want to thank Claudi and my family for being wonderful persons. Without you, I might have quitted this endeavor, as research can be tough and nonrewarding.

Appendix

Measurement of LPS levels and bacteria-specific antibody responses in GCA

Introduction

Given the importance of TLR4-engagement to induce transmural infiltration of $CD4^+$ T cells in an experimental transplantation model, we hypothesized that TLR4 ligands are available in increased amount in GCA patients and may be involved in the arterial breakdown of tolerance. LPS, bacterial endotoxins, are the main TLR4 ligands. In humans, LPS can enter the blood stream if the integrity of the gastrointestinal tract is disrupted. Reduced gastrointestinal barrier function has been reported in elderly people [1]. Therefore, we tested whether GCA patients have higher LPS in the blood stream that may activate the vascular DCs and contribute to the initiation process of the disease.

Methods

Plasma was diluted 1:10 and protein-LPS interaction reduced by adding 0.2% Pyrosperse™. After heat-inactivation (30 min. at 85°C), samples were diluted to 1:100 and divided into duplicates of "real" and "spiked" (with 50 pg/ml of LPS from *E. coli*, L3012, Sigma Aldrich, St. Louis, MO, USA) samples. LPS levels were determined with a chromogenic kinetic LAL assay (LAL Kinetic-QCL™, 50-650, Lonza, Basel, Switzerland) and calculated using WinKQCL™ software (Lonza). Effective concentrations (c) were determined with the following formula:

$$c_{effective} = (c_{spiked} - c_{real}) / 50\ pg/mL * c_{real}$$

All procedures were carried out with endotoxin-free water and plastic ware.

To generate monocyte-derived dendritic cells (moDC), monocytes were enriched from PBMC by adherence to a flat-bottom plate for 2 hours. These were then cultured for 5 days in the presence of 1000 U/ml of GM-CSF and IL-4 in RPMI medium supplemented with 1.5% autologous heat-inactivated human plasma (37°C, 5% CO_2). Afterwards, moDCs were treated with/without 200 pg/mL of LPS for 24 hours and activation was assessed by flow cytometry. Anti-human antibodies: CD11c (APC, clone BU15, 21487116, ImmunoTools, Friesoythe, Germany), CD14 (PerCP, clone TuK4, MHCD1431, Invitrogen, Carlsbad, CA, USA), CD14 (FITC, clone MOP9, 345784), CD83 (PE, clone HB15e, 556855), CD86 (PE-Cy5, clone B70/B7-2, 555659), HLA-DR (PE, clone L243,

347401); all BD biosciences, Franklin Lakes, NJ, USA and CD209 (FITC, clone 9E9A8, Biolegend, San Diego, CA, USA).

Bacterial FACS was performed as described previously [2]. The following species were obtained from the clinical microbiology department at the Basel university hospital: *Escherichia coli, Bacteroides fragilis, Enterococcus faecalis, Staphylococcus epidermidis* and *Propionibacterium acnes.* Anti-human antibodies: IgG (Alexa Fluor 647, polyclonal, 309-605-008) and IgA (FITC, polyclonal, 309-095-011), both Jackson ImmunoResearch, West Grove, PA, USA. Bacteria-specific IgG- and IgA-concentrations were corrected for total plasma IgG and IgA, as defined by ELISA (Human IgG/IgA ELISA kit, 801182/801197, ZeptoMetrix Corporation, Buffalo, NY, USA).

LPS-levels are elevated in GCA patient plasma

LPS-levels were significantly elevated in GCA-patients at time point of diagnosis compared to age-matched controls, including also subjects with GCA-like inflammatory disease (PMR) (**Figure 14A**). Moreover, we could show that an LPS concentration of 200 pg/mL (median concentration in the GCA group) was sufficient to induce activation of monocyte-derived dendritic cells (moDC) *in vitro* (see **Figure 14B**).

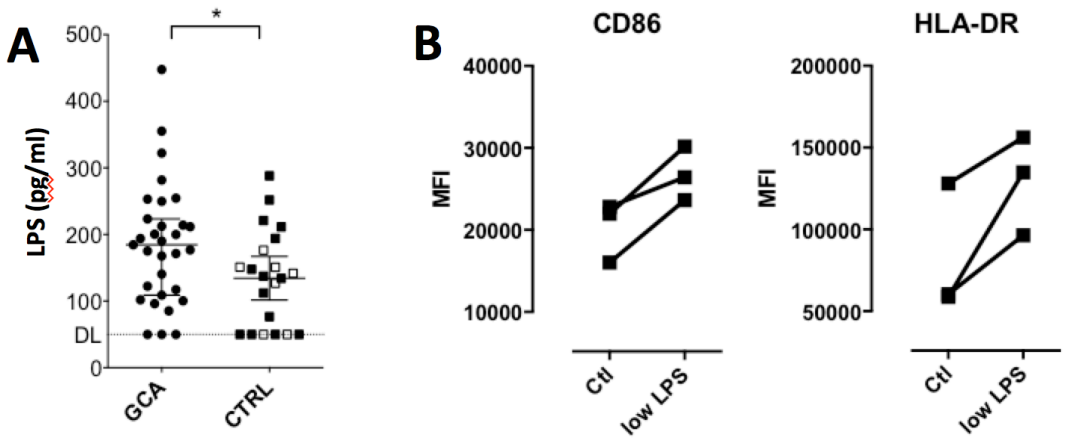

Figure 14: Plasma LPS levels are increased in GCA patients and suffice to activate moDCs *in vitro*. A) Plasma LPS-concentrations, as defined by LAL-assay, are shown for GCA-patients and controls (open squares: PMR-patients) at time point of diagnosis. DL: Assay detection limit. Mann-Whitney U test was applied to compare group distributions, * $p<0.05$. **B)** moDCs were treated with 200 pg/mL of LPS (approx. median LPS-level in GCA-group) and assessed by flow cytometry. Median fluorescence intensity (MFI) is shown for the activation markers CD86 and HLA-DR. moDCs are gated as doublet-negative $CD11c^+/CD14^-/CD209^+$.

The presence of increased systemic levels of LPS in GCA-patients indicated a certain degree of gram-negative bacterial transfer. We thus decided to measure the abundance of plasma IgG- and IgA-antibodies against the two common gram-negative, commensal intestinal bacteria *Escherichia coli* and *Bacteroides fragilis*. The gram-positive gut bacterium *Enterococcus faecalis* served as a negative control. Diluted bacteria were directly exposed to human plasma. While both IgG- and IgA-antibodies could be detected against all bacterial species, none of them were significantly more frequent in the GCA-patients compared to controls (data not shown).

Discussion

By using the LAL-assay, we could detect elevated levels of LPS in the plasma of GCA-patients. LPS is a potent activator of dendritic cells and vascular DC activation seems to be an early event in GCA pathogenesis. The measured LPS-concentrations are sufficient to activate mature moDCs; whether this holds true for vascular DCs and whether LPS is present in vascular walls at these concentrations is difficult to determine.

We investigated bacterial translocation from the intestinal tract as a possible reason for the elevated LPS concentrations observed. While we did not find differences between patients and controls in antibodies targeting *Escherichia coli* and *Bacteroides fragilis*, but this might be different with other gram-negative bacteria. It is not feasible though to screen for antibodies against the whole series of bacterial species that might possibly colonize the gut. Therefore, an approach would be to investigate the gut microbiota in patients and age-matched donors for species differences. This could be accomplished e.g. by direct 16S rRNA-sequencing [3]. The GCA-related microbiota could then be tested using the bacterial FACS approach.

References

1. Steele, A. K. *et al.* Contribution of intestinal barrier damage, microbial translocation and HIV-1 infection status to an inflammaging signature. *PLoS One* **9,** (2014).
2. Balmer, M. L. *et al.* The liver may act as a firewall mediating mutualism between the host and its gut commensal microbiota. *Sci. Transl. Med.* **6,** (2014).
3. Rosselli, R. *et al.* Direct 16S rRNA-seq from bacterial communities: A PCR-independent approach to simultaneously assess microbial diversity and functional activity potential of each taxon. *Sci. Rep.* **6,** 1–12 (2016).

Manuscript 4

Stress-Induced In Vivo Recruitment of Human Cytotoxic Natural Killer Cells Favors Subsets with Distinct Receptor Profiles and Associates with Increased Epinephrine Levels

PLOS ONE

RESEARCH ARTICLE

Stress-Induced *In Vivo* Recruitment of Human Cytotoxic Natural Killer Cells Favors Subsets with Distinct Receptor Profiles and Associates with Increased Epinephrine Levels

Marc B. Bigler[1], Simon B. Egli[1], Cédric M. Hysek[2], Gideon Hoenger[3], Laurent Schmied[4], Fabian S. Baldin[5], Florian A. Marquardsen[5], Mike Recher[5,6], Matthias E. Liechti[2]*, Christoph Hess[3,6], Christoph T. Berger[1,6]*

1 Translational Immunology, Dep. of Biomedicine, University Hospital Basel, Basel, Switzerland, **2** Clinical Pharmacology, Dep. of Internal Medicine, University Hospital Basel, Basel, Switzerland, **3** Immunobiology Lab, Dep. of Biomedicine, University Hospital Basel, Basel, Switzerland, **4** Immunotherapy Laboratory, Department of Biomedicine, University Hospital Basel, Basel, Switzerland, **5** Immunodeficiency Lab, Dep. of Biomedicine, University Hospital Basel, Basel, Switzerland, **6** Medical Outpatient Clinic, Dep. of Internal Medicine, University Hospital Basel, Basel, Switzerland

* christoph.berger@usb.ch (CTB); matthias.liechti@usb.ch (MEL)

Citation: Bigler MB, Egli SB, Hysek CM, Hoenger G, Schmied L, Baldin FS, et al. (2015) Stress-Induced *In Vivo* Recruitment of Human Cytotoxic Natural Killer Cells Favors Subsets with Distinct Receptor Profiles and Associates with Increased Epinephrine Levels. PLoS ONE 10(12): e0145635. doi:10.1371/journal.pone.0145635

Editor: Eric Vivier, INSERM- CNRS- Univ. Méditerranée, FRANCE

Received: August 21, 2015

Accepted: December 7, 2015

Published: December 23, 2015

Data Availability Statement: All relevant data are within the paper and its Supporting Information files.

Funding: The work was supported by the Swiss National Science Foundation (SNSF, www.snf.ch) to CTB (PZ00P3-148000), CH (SNSF 310030_153059), and ML (SNSF 320030_149493). MR holds a professorship from the Swiss National Science Foundation (PP00P3_144863). The funders had no role in study design, data collection and analysis, decision to publish, or preparation of the manuscript.

Abstract

Background

Acute stress drives a 'high-alert' response in the immune system. Psychoactive drugs induce distinct stress hormone profiles, offering a sought-after opportunity to dissect the *in vivo* immunological effects of acute stress in humans.

Methods

3,4-methylenedioxymethamphetamine (MDMA), methylphenidate (MPH), or both, were administered to healthy volunteers in a randomized, double-blind, placebo-controlled cross-over-study. Lymphocyte subset frequencies, natural killer (NK) cell immune-phenotypes, and changes in effector function were assessed, and linked to stress hormone levels and expression of CD62L, CX3CR1, CD18, and stress hormone receptors on NK cells.

Results

MDMA/MPH > MDMA > MPH robustly induced an epinephrine-dominant stress response. Immunologically, rapid redistribution of peripheral blood lymphocyte-subsets towards phenotypically mature NK cells occurred. NK cytotoxicity was unaltered, but they expressed slightly reduced levels of the activating receptor NKG2D. Preferential circulation of mature NK cells was associated with high epinephrine receptor expression among this subset, as well as expression of integrin ligands previously linked to epinephrine-induced endothelial detachment.

Competing Interests: The authors have declared that no competing interests exist.

Conclusion

The acute epinephrine-induced stress response was characterized by rapid accumulation of mature and functional NK cells in the peripheral circulation. This is in line with studies using other acute stressors and supports the role of the acute stress response in rapidly mobilizing the innate immune system to counteract incoming threats.

Introduction

The response of the body to stress consists in the complex integration of endocrine, neuro-cognitive and immunologic adaptations [1]. Chronic persistent stress has been linked to suppressed immune function and increased susceptibility to infections and cancer [1–4], while acute stress induces a fight-or-flight reaction, tuned to rapidly respond to injury and subsequent entry of infectious agents into the organism. Acute stress-induced changes in the immune system thus plausibly aim at accelerating wound repair, help prevent infections, and should occur very rapidly [1].

In contrast to adaptive immunity, the innate immune response is optimized to immediately respond to pathogens without need for prior cognate exposure. Natural Killer (NK) cells represent 5–15% of all lymphocytes in the peripheral blood and are important in the defense against viruses and tumors. Based on their CD56 surface expression-density they can by divided into cytotoxic $CD56^{dim}$ NK cells (roughly 90%), and the immunomodulatory $CD56^{bright}$ NK cells (approximately 10% of NK in the peripheral blood). Circulating cytotoxic $CD56^{dim}$ NK cells detect virally infected or malignantly transformed cells. Their activation results in target cell lysis and the secretion of cytokines [5]. Previous studies found a strong increase of circulating NK cells upon stress, suggesting a potential role for NK cells in this context [6].

Stress hormones, including glucocorticoids and catecholamines, are key modulators of stress-induced immune-dysregulation [7, 8]. However, inter-individual differences in the endocrine responses often hinder subtle stress-associated immunologic alterations to become apparent. Thus, a well-controlled experimental model triggering a homogeneous endocrine stress response should allow to better study how stress impacts the immune system.

3,4-Methylenedioxymethamphetamine (MDMA, "ecstasy") and methylphenidate (MPH, "Ritalin®") are widely used psychoactive substances that induce an endocrine and cardiovascular stress response that has been extensively studied [9–12]. Previous murine and human studies suggested that MDMA impacts both the innate and the adaptive immune responses [13, 14]. Data regarding the effect of MPH on the immune system are sparse. Both drugs result in an increase in norepinephrine levels, i.e. have sympathomimetic effects. While MDMA enhances serotonergic neurotransmission [15] and increases cortisol levels [11], MPH elevates dopamine concentrations but has no serotonergic effects [16], and does not increase cortisol levels [11]. Thus, both MDMA and MPH share sympathomimetic and psychostimulant effects, yet with distinct hormone profiles.

Here we used drug-induced stress to test its effects on the human immune system. Specifically, we studied stress hormone-mediated recruitment of NK cell subsets in the context of a randomized, double-blind, placebo-controlled clinical trial of subjects receiving MDMA and/or MPH.

Materials and Methods

Clinical study

Healthy subjects (n = 12, mean age 24.9 years, 8 female, 4 male) from a pharmacological study (NCT01465685) on the effects of single-dose MDMA (125 mg), MPH (60 mg) or a

combination of the two drugs were tested for the effects of the drugs on the immune system. Characteristics of the study and the participants have previously been published [12]. All subjects provided written informed consent. The study was approved by the ethics committee of the canton of Basel, Switzerland (EKBB 228/11) and conducted in accordance with the Declaration of Helsinki. All subjects received each drug condition once in a double-blind, placebo-controlled, crossover design with four experimental test sessions (placebo–placebo, MPH–placebo, placebo–MDMA, and MPH–MDMA). Drugs were taken orally. Washout periods between two conditions were at least 10 days. All blood draws were performed via an indwelling intravenous catheter placed in an antecubital vein and the baseline blood draw was at 8 am for all study subjects. Peripheral blood mononuclear cells (PBMC) were isolated using Lymphoprep™ (Axis-Shield, Oslo, Norway) density centrifugation and cryopreserved until use, in order to be able to measure all study timepoints (i.e. conditions) for each subject on the same day. The cardiovascular stress response (systolic blood pressure and heart rate) was repeatedly recorded and plasma levels of norepinephrine, epinephrine, dopamine and cortisol were determined before and 2h after drug administration [12].

Flow cytometry based immunophenotyping

PBMC were immunophenotyped using the following antibodies: CD3-PerCP (UCHT1), CD4-APC (OKT4), CD18-PE (TS1/18), CD19-PE (HIB19), NKG2D-APC (1D11), CX3CR1-FITC (2A9-1, all Biolegend), CD3-Pacific Blue (UCHT1), CD8-FITC (HIT8a), CD16-PE-Cy5 (3G8), CD56-PE, -Alexa Fluor 647 or -PE-Cy7 (B159), CD69-FITC (FN50) (all BD Biosciences), CD62L-FITC (LT-TD180) (ImmunoTools), GCR-Alexa Fluor 488 (D8H2) (Cell Signaling Technology) and ADRB2 pure (S364, RayBiotech). The antibody against ADRB2 was coupled to R-phycoerythrin (RPE) in house using the ABSelect BSA Removal Kit to clean and concentrate the pure ADRB2 antibody followed by fluorochrome coupling with the Lightning-Link® R-Phycoerythrin Conjugation Kit according to manufacturer's instructions (Innova Biosciences).

All stainings were performed as surface-stainings for 30 min. at 4°C, with exception of the intracellular GCR staining that was performed in whole blood according to a standard ICS protocol (Cell Signaling Technology). All sample acquisitions were performed on an Accuri™ C6 (immune cell subsets and NK function) or a LSRFortessa™ (NK receptor phenotyping) flow cytometer (BD Biosciences).

NK cell *in vitro* stimulation assays

NK cell function was assessed by IFNγ production and degranulation (CD107a) as an indirect marker of cytotoxicity [17]. NK cells were stimulated with K562 cells by co-culture of 10^6 PBMC at a 10:1 effector-to-target ratio as previously described [18]. Following 30 min. of pre-incubation, cells were incubated during 4 hours in the presence of Brefeldin A (Biolegend) at 0.5 μg/mL, Monensin (Golgi-Stop™, BD Biosciences) at 0.3 μg/mL and anti-CD107a-APC (H4A3) (BD Bioscience). Cells were then surface-stained using anti-CD3 PerCP and anti-CD56 PE followed by intracellular staining for IFNγ using Cytofix/Cytoperm™ (BD Biosciences) and anti-IFNγ-FITC (4S.B3) (Biolegend). For experiments testing the impact of stress hormones on NKG2D expression *in vitro*, cells were incubated for 3 h in serum-free RPMI 1640 (Life Technologies) in the presence of cortisol (Sigma) at 280 ng/mL, epinephrine (Sintetica) at 50 pg/mL, or a combination of both and NKG2D mean fluorescence intensity (MFI) was assessed.

Hormone receptor quantification on NK cell subsets using real-time RT PCR

The β2-adrenergic receptor (ADRB2) and the glucocorticoid receptor (GCR) expression on NK cell subsets were quantified by real-time PCR. $CD56^{bright}$ and $CD56^{dim}$ NK cells were sorted on a FACSAria™ III (BD Bioscience) and RNA was extracted using the QIAamp® RNA Blood Mini Kit (Qiagen). Genomic DNA was removed and first-strand cDNA was generated by means of GoScript™ Reverse Transcription System (Promega). RT-PCR was performed with GoTaq® qPCR Master Mix in duplicates in a 7500 Fast Real-Time PCR System (Applied Biosystems) using the following primers (Microsynth, Switzerland): ADRB2: 5'-ACAGGGGAGCAGAGTG GATA-3' and 3'- ACAGTACCTTGATGGCCCAC-5' and GCR: 5'-TGGGGACTCTGAACTTC CCTG-3' and 3'- CTGTTGTTGCTGTTGAGGAGC-5' (Complete primer list available in S1 Protocol). The amplification process consisted of polymerase activation at 95°C for 10 min., 45 cycles with 15 s of denaturation at 95°C and 1 min. of annealing and elongation at 60°C and a final elongation step for 1 min. at 60°C. For all samples signals were detected between cycles 24 and 35. Two reference genes (GADPH and PKG1) were used for relative quantification. A more detailed description of the qPCR protocol is available in S1 Protocol.

Data analysis and statistics

All flow cytometry data was analyzed blinded for the drug condition using FlowJo Software (Version X 10.0.7). Gating strategies for the analyses are shown in the supporting information (S2 Fig and S3 Fig). Statistical analyses and data visualization was performed using Prism software (Prism 6.0, Graphpad). Group comparisons were performed using t-tests or Kruskal Wallis tests followed by Dunn's comparisons. Correlation analyses were performed using Spearman Rank tests.

Results and Discussion

Drug-induced cardiovascular stress responses associate with an increased proportion of peripheral Natural killer cells

The cardiovascular response and stress hormone levels in the peripheral blood can indicate stress. MDMA, MPH, and the combination of the two drugs induced an increase in systolic blood pressure (SBP) and heart rate peaking three hours after drug administration (Fig 1A and 1B). Details to the cardiovascular response in the study subjects have been reported previously [12]. The MDMA/MPH combination induced the strongest increase in SBP, and MPH alone induced a SBP increase of lower magnitude than the conditions that included MDMA (Fig 1A). Contrarily, the heart rate was highest in treatment conditions including MPH (Fig 1B). Since these differences might be linked to different stress hormone profiles induced by the different treatments, levels of cortisol and catecholamines were analyzed and compared with levels measured in placebo treated study subjects. Hormone levels two hours after drug administration (i.e. at their peak) were compared to the baseline blood draws, which were all performed at 8 am. All active drug conditions resulted in a comparable, albeit non-significant increase of norepinephrine at 2 hours (*data not shown*). The most striking difference between the drug conditions was an increase in cortisol concentration upon exposure to MDMA ($p < 0.001$) or MDMA/MPH ($p < 0.0001$) compared to placebo or MPH alone (Fig 1C). Cortisol levels fell in the placebo and MPH condition, consistent with known circadian changes in cortisol, given the timing of the blood draws, all starting at 8 am [19]. The increase in epinephrine concentrations was higher in individuals exposed to MDMA/MPH ($p < 0.0001$) than in those exposed to MDMA alone ($p < 0.01$) and lowest in participants after MPH intake alone,

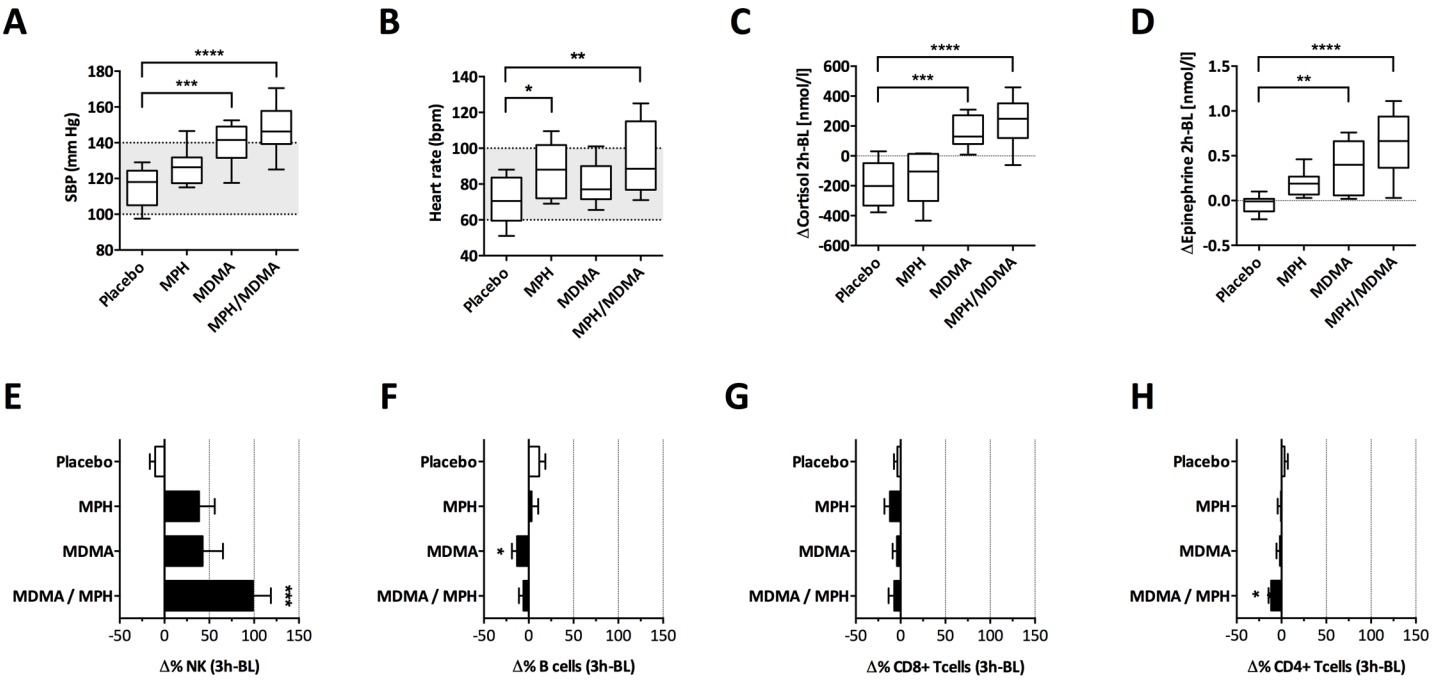

Fig 1. Drug-induced stress induces a pronounced cardiovascular responses and NK cell recruitment. (A) Systolic blood pressure (SBP) in mmHg and (B) heart rate (HR) in beats per minute (bpm) are shown three hours (i.e. one hour after the stress hormone peak) post-adminstration of the study drug (n = 12). The grey shaded area indicates the normal values. Serum cortisol (C) and epinephrine (D) levels were measured before and two hours post drug administration and the difference from baseline was calculated. Box plots indicate median and IQR, whiskers indicate range. (E-H) Lymphocyte subset distribution 3 hours after drug administration was examined (n = 12). Percent change from baseline level to three hours post administration (Δ%) was calculated for each lymphocyte subset. Mean Δ% and S.E.M is shown for the four main lymphocyte subsets: (E) NK cells ($CD3^-$ $CD56^+$), (F) B cells ($CD3^-$ $CD19^+$), (G) CD8 cytotoxic T cells ($CD3^+$ $CD8^+$) and (H) CD4 T helper cells ($CD3^+$ $CD4^+$). Kruskal-Wallis test with Dunn's correction to test for multiple comparisons was used (*p<0.05, **p<0.01, ***p<0.001, ****p<0.0001).

doi:10.1371/journal.pone.0145635.g001

suggesting an additive effect of MDMA and MPH on the epinephrine stress response (Fig 1D). The cardiovascular stress response (i.e. HR increase and SBP increase) correlated with both, the epinephrine (HR: p = 0.0035, r = 0.42; SBP: p = 0.0001, r = 0.53), and cortisol increase (HR: p = 0.0001, r = 0.53; SBP p<0.0001, r = 0.71). Together, the findings suggest that the study conditions resulted in distinct cardiovascular and endocrine stress response profiles.

Acute stress has been linked to a recruitment of NK cells to the peripheral blood in various models [6]. To test whether the same applies to pharmacological stress induced by MDMA, MPH or their combination, we monitored the change in lymphocyte subset-distribution at baseline and three hours after drug administration. This time-point was chosen based on the stress hormone level peak that occurs around 2–3 hours after drug-intake [11]. We then calculated the percentage change in T cells (CD4+ and CD8+), B cells and NK cells compared to the baseline distribution (gating strategy is depicted in S2 Fig). The most striking observation was a dramatic increase of NK cells within the lymphocyte compartment that was most pronounced upon exposure to combination treatment of MDMA and MPH ($p < 0.001$ Fig 1E). The other immune cell subsets were variably decreased (Fig 1F–1H). Pacifici *et al.* also reported a comparable and rapid increase of total NK cells in MDMA treated subjects, which was however not further investigated [14, 20–22]. To enable an immediate response to any threat it is plausible that early stress-induced adaptations act through cell redistribution, and preferentially impact innate immunity that can unfold much more rapidly [6, 23].

Because this rapidly occurring redistribution of lymphocyte subsets suggested stress hormone-mediated effects, we next correlated stress hormone levels (2 hours post administration)

with the individual NK cell increase, irrespective of the treatment. NK cell increase correlated with the change in epinephrine levels ($p = 0.0049$, $r = 0.44$; S1A Fig), but not with the change of cortisol or norepinephrine (S1B and S1C Fig). Dopamine was only very weakly (median 0.03 nmol/L, IQR -0.03–0.09) and inconstantly increased following any drug administration and the change in dopamine levels showed no correlation with the change in NK cell frequencies (data not shown). Similarly, we found no correlation between drug induced neuropsychological effects -namely changes in activity or emotional excitability- and NK cell redistribution. Taken together, this hinted at a more pronounced role of epinephrine in NK cell redistribution.

Stress enriches for circulating cytotoxic NK cells with unaltered effector functions and activation state

Given their strong relative increase upon drug-induced stress, we performed a more detailed analysis of the specific NK cell subsets and their functionality. Although both cytotoxic ($CD56^{dim}$) and immunomodulatory ($CD56^{bright}$) NK cell subsets increased, the most pronounced effect was detected for $CD56^{dim}$ NK cells upon the combined drug stimulation (Fig 2A). This indicated that $CD56^{dim}$ NK cells were recruited preferentially upon stress. The stronger correlation between the change in $CD56^{dim}$ NK cells and the alteration in epinephrine levels ($p = 0.004$, $r = 0.45$, Fig 2B), as compared to the correlation with change in cortisol levels (Fig 2C, $p = 0.041$, $r = 0.31$), further supported this notion. In contrast, we did not detect any correlation of $CD56^{bright}$ NK cells and hormone levels (*data not shown*). Interestingly, the shift in the NK cell subsets did not translate into enhanced NK effector functions against target cells (Fig 2D). Previous studies variably associated acute stress with enhanced [6], or decreased NK cell activity [24, 25], which could relate to different assay conditions (e.g. not including human plasma in the culture media, cryopreservation [26]), some of which were, however, inevitable in order to test all samples from a donor simultaneously with the same target cell conditions. Reduced function has moreover been attributed to glucocorticoid-induced epigenetic changes, which we might have missed by testing NK function within three hours post-stressor [27].

Drug-induced stress consistently associated with a moderate, but significant lower per-cell expression (i.e. mean fluorescence intensity; MFI) of NKG2D, an NK cell activating receptor recognizing stress-induced proteins (Fig 2E). This decrease was limited to $CD56^{dim}$ NK cells, and NKG2D on bulk T cells was slightly increased (*data not shown*). NKG2D expression on $CD56^{dim}$ NK cells was inversely correlated with the change in epinephrine levels (Fig 2F, $p < 0.0001$, $r = -0.59$), compared to an again more moderate effect of cortisol (Fig 2G, $p = 0.036$, $r = -0.32$). This $NKG2D^{low}$ phenotype might reflect a safety measure preventing an overshooting NK stimulation that would result in excessive immunopathology [28–31]. Due to sample availability, we could however not address this hypothesis experimentally. Treatment of NK cells with synthetic epinephrine and cortisol *in vitro* dampened NK function, as expected from the literature [32]. Yet, this NK cell inhibition was independent of NKG2D expression, as NKG2D was only reduced inconstantly (i.e. six of eleven healthy donors) and showed no correlation with NK function. Moreover, a reduction in NK function was also observed against 721.221 target cells not expressing NKG2D ligands (data not shown). Together, this indicates that the $NKG2D^{low}$ phenotype results from mobilization of these NK cells rather than from a receptor down-modulation by direct hormone effects.

Inherent expression differences of key surface receptors may explain preferential recruitment of $CD56^{dim}$ NK cells

Our immunophenotypic data suggested that drug-induced stress associated with the preferential recruitment of cytotoxic NK cells without substantially affecting their function. Thus, we

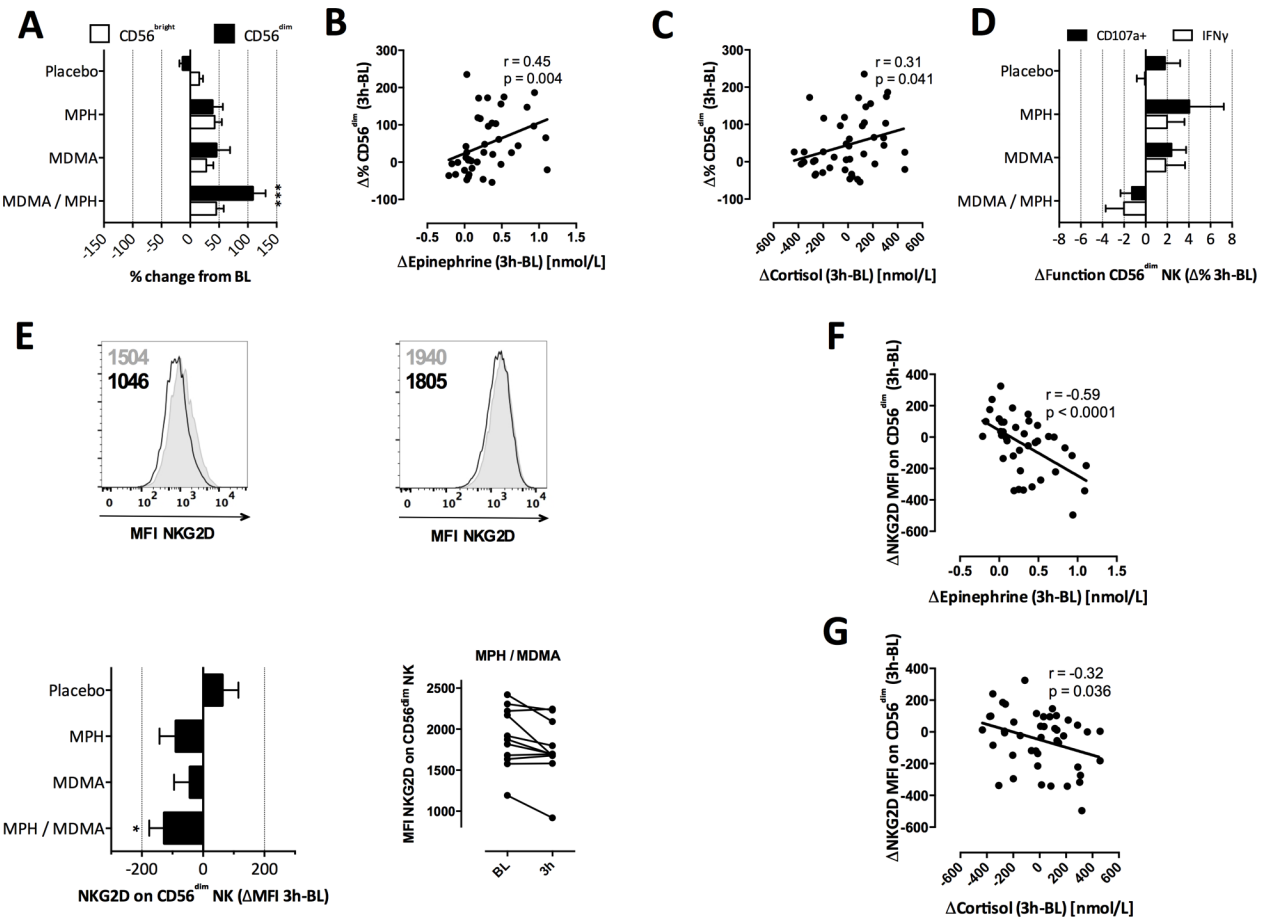

Fig 2. Unaltered NK function but reduced NKG2D expression upon drug-induced stress. (A) Percent change in the two NK cell subsets was calculated and expressed as mean + S.E.M. (B,C) The percent change of $CD3^-$ $CD56^{dim}$ NK cells was correlated to the change in serum epinephrine (B) and cortisol (C) levels 2 hours p.a. in all drug categories together (n = 44). (D) NK function against K562 target cells was assessed. Changes in $IFN\gamma^+$ or $CD107a^+$ (degranulation) $CD56^{dim}$ NK cells are shown for each drug category as absolute change in percentage (n = 11, mean + S.E.M). (E) Example histograms of NKG2D MFI before (grey) and after (black) MPH / MDMA treatment are shown for a donor with a strong (left) and weak (right) response (upper panels). The numbers indicate the MFI. Absolute change in the MFI of NKG2D expression (n = 12, mean + S.E.M) is displayed for each drug condition (lower left panel). NKG2D MFI at baseline and 3 hours p.a. is shown separately for all subjects for the condition with a significant difference to placebo (MPH / MDMA) (lower right panel). The absolute change in MFI of NKG2D was correlated to serum epinephrine (F) and cortisol (G) levels irrespective of drug treatment (n = 44). Spearman correlation and nonlinear fit were applied for correlation analyses and Kruskal-Wallis test was applied for all group comparisons. *P < 0.05, **P < 0.01, ***P < 0.001.

doi:10.1371/journal.pone.0145635.g002

next aimed at defining molecular differences between $CD56^{dim}$ and $CD56^{bright}$ NK cell subsets that may explain the preferential recruitment of the $CD56^{dim}$ subset. First, we assessed the expression-profile of receptors previously linked to epinephrine-mediated lymphocyte redistribution, namely high expression of the fractalkine receptor CX3CR1 and low expression of CD62L [33], in five healthy untreated individuals. The flow cytometry gating strategies are shown in the supporting information (S3 Fig). Indeed, we found that the $CD56^{dim}$ subset expressed very high levels of CX3CR1 (Fig 3A), but low levels of CD62L (Fig 3B). This expression profile was inverse in the $CD56^{bright}$ subset (CX3CR1, $p < 0.0001$; CD62L, $p = 0.001$). In contrast, CD18, an integrin known to bind to ICAMs and thereby enhancing NK cell migration [34] was slightly more expressed on the $CD56^{dim}$ NK subset ($p = 0.008$, Fig 3C). Next, we assessed mRNA and protein levels of the β2-adrenergic receptor (ADRB2) and glucocorticoid receptor (GCR), i.e. the receptor for epinephrine and cortisol respectively, in the two NK cell

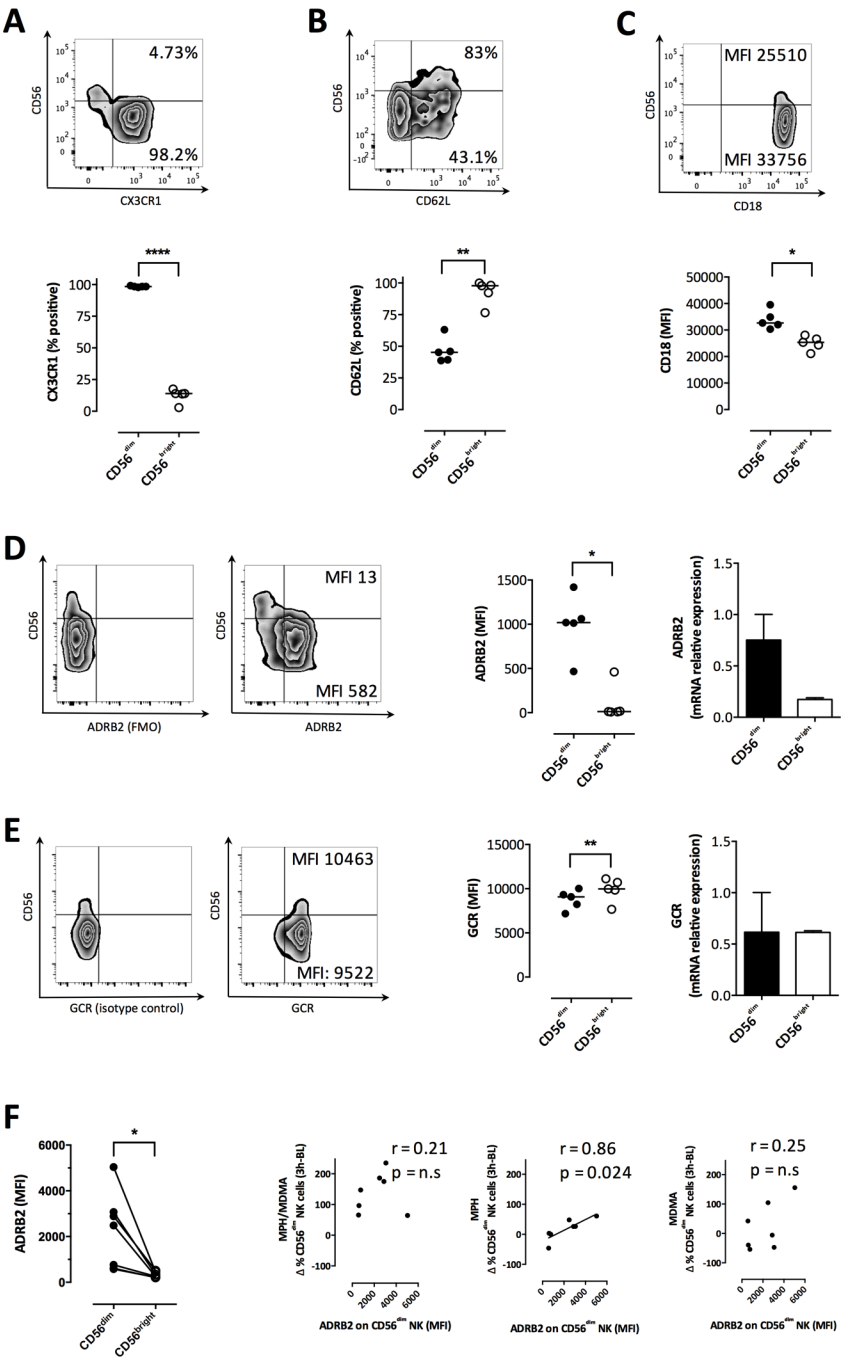

Fig 3. Preferential recruitment of CD56^{dim} NK cells depends on distinct hormone and migration receptor expression profiles. Expression of three receptors important in cell adhesion and migration were assessed by flow cytometry. (A-C) Example stainings gated on CD3$^-$ CD56$^+$ lymphocytes are shown for CX3CR1 (A), CD62L (B) and CD18 (C). The frequency (A, B) or MFI (C) of receptor expression on CD56^{bright} and CD56^{dim} is indicated (upper panels). Data on freshly derived PBMCs from five healthy, unstressed donors are summarized (A-C lower panels). (D, E) Expression of the epinephrine receptor (ADRB2) (D) and the glucocorticoid receptor (GCR) (E) were assessed on CD3$^-$ CD56$^+$ lymphocytes by flow cytometry. Isotype control stainings for ADRB2 and GCR are shown, followed by an example staining (left panels). The MFI of the two subsets is indicated for CD56^{bright} (upper right corner) and CD56^{dim} NK cell subsets (lower right corner). Flow cytometric data of the aforementioned five donors is summarized for CD56^{bright} and CD56^{dim} NK cells (middle panels). Differential ADRB2 and GCR expression on the two NK cell subsets were also confirmed on mRNA level by measuring relative hormone receptor expression on sorted CD56^{dim} (n = 3) and CD56^{bright} NK cells (n = 2) by qPCR (right panels). (F) Differential expression of ADRB2 on CD56^{bright} and

CD56^{dim} NK cells was confirmed in study participants 1 hour after placebo treatment (left panel, n = 7). ADRB2 expression was correlated to the increase in NK cell percentage upon drug administration. Paired t tests were applied for all group comparisons and Spearman correlation and nonlinear fit for correlation analyses. *P < 0.05, **P < 0.01, ****P < 0.0001.

doi:10.1371/journal.pone.0145635.g003

subsets. Both qPCR- and flow cytometry-based quantification indicated higher expression of the ADRB2 among CD56^{dim}, compared to the CD56^{bright}, NK cells (p = 0.019 for MFI, Fig 3D). In contrast, the GCR was lower expressed in CD56^{dim} NK cells (p = 0.005 for MFI, Fig 3E). Taken together, and in line with the correlation analyses of the *in vivo* data, this was suggestive that the CD56^{dim} subset was able to respond more vigorously to epinephrine.

Interestingly, we observed that ADRB2 abundance varied considerably between individuals (Fig 3D). Therefore, we next tested whether the individual ADRB2 receptor expression on NK cells might have determined the increase of NK cells *in vivo* in the clinical study. We first confirmed the inter-individual and NK subset-specific variability of ARDB2 expression in seven subjects included in the clinical stress study (Fig 3F). Importantly, the individual ADRB2 expression was stable over time, as the same donors showed comparable levels on separate study days (*data not shown*). Taking advantage of the distinct hormone changes induced by the different drug conditions (Fig 1C and 1D), epinephrine effects were analyzed by correlating the change in NK cells and altered ADRB2 expression in the presence (MDMA or MDMA/MPH group) or absence (MPH) of a concomitant cortisol increase. We found a very strong correlation between an increase of NK cells and ADRB2 expression in the MPH group (p = 0.02, r = 0.86), i.e. in absence of a cortisol response. Similar trends, albeit much weaker, were seen in the other groups (Fig 3F), suggesting that cortisol might contribute to NK cell distribution in these conditions.

Together, our findings pointed at an important role of epinephrine in the early changes in the NK cell compartment. Interestingly, in the absence of a cortisol response and at low epinephrine levels (i.e. the MPH treatment condition), NK cell redistribution correlated almost perfectly with the expression level of the beta-adrenergic receptor. This is in line with a model of selective catecholamine-dependent regulation of NK cell adhesion to the endothelia [24], as supported by studies using beta-adrenergic blockade suggesting catecholamines as master regulators of early stress effects on the immune system [35].

Conclusion

Stress was observed to induce an enrichment of CD56^{dim} NK cells in the peripheral blood, which associated with a strong epinephrine response. These NK cells expressed a receptor profile that would enable them to rapidly re-distribute to a site of injury or infection, where this cytotoxic subset could contribute to pathogen defense and wound healing. Differences in hormone receptor expression might explain differences in the magnitude of individual stress responses. The insights gained from this controlled clinical trial setting, using standardized stressors that consistently induced distinct stress hormone profiles, support that, in humans, NK cells can be recruited through epinephrine dependent mechanisms, which may be beneficial e.g. in leukemia or cancer therapy [36]. Our study thus adds a rationale to interventions that increase endogenous epinephrine levels (i.e. physical activity, MDMA etc. . .) currently explored e.g. as adjunctive cancer treatments.

Supporting Information

S1 Fig. Correlation of NK cell increase with serum hormone levels. Absolute change in NK percentage 3 hours after drug administration was correlated to change in concentrations of

epinephrine (A), cortisol (B) and norepinephrine (C) 2 hours post treatment. Spearman correlation and nonlinear fit were applied.
(TIFF)

S2 Fig. Gating strategy to define lymphocyte and NK cell subsets and to assess NKG2D expression and IFNγ and CD107a production in NK cell subsets. The top row shows the gating in order to distinguish B cells, CD4+ and CD8+ T cells. A second panel was used to detect NK cells, further subdividing them into CD56 dim and CD56 bright NK cells and analyzing IFNγ and CD107a production (**2**, middle row, data is shown for CD56 dim). A third panel was designed to detect NKG2D expression (**3**, CD314, bottom middle) and a last one to stain for the glucocorticoid receptor (**4**, bottom right) on NK subsets. In grey, full stainings are shown whereas in white, an FMO staining is depicted for NKG2D and an isotype control for GCR. All data was acquired on an Accuri C6 (Becton Dickinson).
(TIFF)

S3 Fig. Gating strategy for the analysis of adhesion and hormone receptor expression on NK cell subsets. NK cells were defined by CD16 and CD56 expression on single, live CD3- cells (upper row). The first panel stained for ADRB2 and CD62L on NK cell subsets whereas the second panel stained for CX3CR1 and CD18. Example stainings on CD56dim NK cells are shown in dark grey while isotype control (ADRB2) or fluorescence minus one controls (FMO, for CD62L, CX3CR1 and CD18) are shown in light grey. All data was acquired on an LSRFortessa flow cytometer (Becton Dickinson).
(TIFF)

S1 Protocol. Detailed RT-PCR protocol for the hormone receptor analysis incl. a complete list of the primers used.
(DOCX)

Acknowledgments

The authors declare no conflict of interest. We thank the clinical pharmacology team for conducting the clinical study and the members of the Immunobiology Lab at the Department of Biomedicine for their help in processing the blood samples.

Author Contributions

Conceived and designed the experiments: MBB SBE LS MEL CTB. Performed the experiments: MBB SBE LS CMH FSB FAM. Analyzed the data: MBB SBE FSB FAM CTB. Contributed reagents/materials/analysis tools: GH CH MR. Wrote the paper: MBB MEL CH MR CTB.

References

1. Glaser R, Kiecolt-Glaser JK. Stress-induced immune dysfunction: implications for health. Nat Rev Immunol. 2005; 5(3):243–51. Epub 2005/03/02. doi: nri1571 [pii] doi: 10.1038/nri1571 PMID: 15738954.
2. Cohen S, Tyrrell DA, Smith AP. Psychological stress and susceptibility to the common cold. N Engl J Med. 1991; 325(9):606–12. Epub 1991/08/29. doi: 10.1056/NEJM199108293250903 PMID: 1713648.
3. Pedersen A, Zachariae R, Bovbjerg DH. Influence of psychological stress on upper respiratory infection—a meta-analysis of prospective studies. Psychosomatic medicine. 2010; 72(8):823–32. Epub 2010/08/19. doi: PSY.0b013e3181f1d003 [pii] doi: 10.1097/PSY.0b013e3181f1d003 PMID: 20716708.
4. Reiche EM, Nunes SO, Morimoto HK. Stress, depression, the immune system, and cancer. The Lancet Oncology. 2004; 5(10):617–25. Epub 2004/10/07. doi: S1470204504015979 [pii] doi: 10.1016/S1470-2045(04)01597-9 PMID: 15465465.

5. Lanier LL. NK cell recognition. Annu Rev Immunol. 2005; 23:225–74. Epub 2005/03/18. doi: 10.1146/annurev.immunol.23.021704.115526 PMID: 15771571.
6. Segerstrom SC, Miller GE. Psychological stress and the human immune system: a meta-analytic study of 30 years of inquiry. Psychological bulletin. 2004; 130(4):601–30. doi: 10.1037/0033-2909.130.4.601 PMID: 15250815; PubMed Central PMCID: PMC1361287.
7. Ashcraft KA, Hunzeker J, Bonneau RH. Psychological stress impairs the local CD8+ T cell response to mucosal HSV-1 infection and allows for increased pathogenicity via a glucocorticoid receptor-mediated mechanism. Psychoneuroendocrinology. 2008; 33(7):951–63. Epub 2008/07/29. doi: S0306-4530(08)00099-1 [pii] doi: 10.1016/j.psyneuen.2008.04.010 PMID: 18657369.
8. Padgett DA, Glaser R. How stress influences the immune response. Trends Immunol. 2003; 24(8):444–8. Epub 2003/08/12. doi: S147149060300173X [pii]. PMID: 12909458.
9. Joyce PR, Donald RA, Nicholls MG, Livesey JH, Abbott RM. Endocrine and behavioral responses to methylphenidate in normal subjects. Biological psychiatry. 1986; 21(11):1015–23. PMID: 3741917.
10. Mas M, Farre M, de la Torre R, Roset PN, Ortuno J, Segura J, et al. Cardiovascular and neuroendocrine effects and pharmacokinetics of 3, 4-methylenedioxymethamphetamine in humans. J Pharmacol Exp Ther. 1999; 290(1):136–45. PMID: 10381769.
11. Seibert J, Hysek CM, Penno CA, Schmid Y, Kratschmar DV, Liechti ME, et al. Acute Effects of 3,4-Methylenedioxymethamphetamine and Methylphenidate on Circulating Steroid Levels in Healthy Subjects. Neuroendocrinology. 2014. doi: 10.1159/000364879 PMID: 24903002.
12. Hysek CM, Simmler LD, Schillinger N, Meyer N, Schmid Y, Donzelli M, et al. Pharmacokinetic and pharmacodynamic effects of methylphenidate and MDMA administered alone or in combination. The international journal of neuropsychopharmacology / official scientific journal of the Collegium Internationale Neuropsychopharmacologicum. 2014; 17(3):371–81. doi: 10.1017/S1461145713001132 PMID: 24103254.
13. Boyle NT, Connor TJ. Methylenedioxymethamphetamine ('Ecstasy')-induced immunosuppression: a cause for concern? British journal of pharmacology. 2010; 161(1):17–32. doi: 10.1111/j.1476-5381.2010.00899.x PMID: 20718737; PubMed Central PMCID: PMC2962814.
14. Pacifici R, Pichini S, Zuccaro P, Farre M, Segura M, Ortuno J, et al. Paroxetine inhibits acute effects of 3,4-methylenedioxymethamphetamine on the immune system in humans. Journal of Pharmacology and Experimental Therapeutics. 2004; 309(1):285–92. doi: 10.1124/Jpet.103.061374 PMID: WOS:000220481900035.
15. Hysek CM, Simmler LD, Nicola VG, Vischer N, Donzelli M, Krahenbuhl S, et al. Duloxetine inhibits effects of MDMA ("ecstasy") in vitro and in humans in a randomized placebo-controlled laboratory study. PLoS One. 2012; 7(5):e36476. doi: 10.1371/journal.pone.0036476 PMID: 22574166; PubMed Central PMCID: PMC3344887.
16. Simmler LD, Wandeler R, Liechti ME. Bupropion, methylphenidate, and 3,4-methylenedioxypyrovalerone antagonize methamphetamine-induced efflux of dopamine according to their potencies as dopamine uptake inhibitors: implications for the treatment of methamphetamine dependence. BMC research notes. 2013; 6:220. doi: 10.1186/1756-0500-6-220 PMID: 23734766; PubMed Central PMCID: PMC3679734.
17. Alter G, Malenfant JM, Altfeld M. CD107a as a functional marker for the identification of natural killer cell activity. J Immunol Methods. 2004; 294(1–2):15–22. PMID: 15604012.
18. Cosgrove C, Berger CT, Kroy DC, Cheney PC, Ghebremichael M, Aneja J, et al. Chronic HCV infection affects the NK cell phenotype in the blood more than in the liver. PLoS One. 2014; 9(8):e105950. doi: 10.1371/journal.pone.0105950 PMID: 25148254; PubMed Central PMCID: PMC4141847.
19. Scheiermann C, Kunisaki Y, Frenette PS. Circadian control of the immune system. Nat Rev Immunol. 2013; 13(3):190–8. doi: 10.1038/nri3386 PMID: 23391992; PubMed Central PMCID: PMC4090048.
20. Pacifici R, Zuccaro P, Farre M, Pichini S, Di Carlo S, Roset PN, et al. Immunomodulating activity of MDMA. Ann Ny Acad Sci. 2000; 914:215–24. PMID: WOS:000171939100021.
21. Pacifici R, Zuccaro P, Farre M, Pichini S, Di Carlo S, Roset PN, et al. Effects of repeated doses of MDMA ("ecstasy") on cell-mediated immune response in humans. Life Sciences. 2001; 69(24):2931–41. doi: 10.1016/S0024-3205(01)01373-X PMID: WOS:000172063600011.
22. Pacifici R, Zuccaro P, Farre M, Pichini S, Di Carlo S, Roset PN, et al. Cell-mediated immune response in MDMA users after repeated dose administration—Studies in controlled versus noncontrolled settings. Ann Ny Acad Sci. 2002; 965:421–33. PMID: WOS:000177157600038.
23. Dhabhar FS. Enhancing versus Suppressive Effects of Stress on Immune Function: Implications for Immunoprotection versus Immunopathology. Allergy, asthma, and clinical immunology: official journal of the Canadian Society of Allergy and Clinical Immunology. 2008; 4(1):2–11. doi: 10.1186/1710-1492-4-1-2 PMID: 20525121; PubMed Central PMCID: PMC2869337.

24. Benschop RJ, Oostveen FG, Heijnen CJ, Ballieux RE. Beta(2)-Adrenergic Stimulation Causes Detachment of Natural-Killer-Cells from Cultured Endothelium. European Journal of Immunology. 1993; 23 (12):3242–7. doi: 10.1002/Eji.1830231230 PMID: WOS:A1993MM68900029.

25. Schedlowski M, Hosch W, Oberbeck R, Benschop RJ, Jacobs R, Raab HR, et al. Catecholamines modulate human NK cell circulation and function via spleen-independent beta 2-adrenergic mechanisms. Journal of immunology. 1996; 156(1):93–9. PMID: 8598500.

26. Gotlieb N, Rosenne E, Matzner P, Shaashua L, Sorski L, Ben-Eliyahu S. The misleading nature of in vitro and ex vivo findings in studying the impact of stress hormones on NK cell cytotoxicity. Brain, behavior, and immunity. 2015; 45:277–86. doi: 10.1016/j.bbi.2014.12.020 PMID: 25546569; PubMed Central PMCID: PMC4342306.

27. Bush KA, Krukowski K, Eddy JL, Janusek LW, Mathews HL. Glucocorticoid receptor mediated suppression of natural killer cell activity: Identification of associated deacetylase and corepressor molecules. Cellular Immunology. 2012; 275(1–2):80–9. doi: 10.1016/J.Cellimm.2012.02.014 PMID: WOS:000304509400012.

28. Wiemann K, Mittrucker HW, Feger U, Welte SA, Yokoyama WM, Spies T, et al. Systemic NKG2D down-regulation impairs NK and CD8 T cell responses in vivo. J Immunol. 2005; 175(2):720–9. Epub 2005/07/09. doi: 175/2/720 [pii]. PMID: 16002667.

29. Abdul-Careem MF, Mian MF, Yue G, Gillgrass A, Chenoweth MJ, Barra NG, et al. Critical role of natural killer cells in lung immunopathology during influenza infection in mice. J Infect Dis. 2012; 206(2):167–77. doi: 10.1093/infdis/jis340 PMID: 22561366.

30. Crosby EJ, Goldschmidt MH, Wherry EJ, Scott P. Engagement of NKG2D on bystander memory CD8 T cells promotes increased immunopathology following Leishmania major infection. PLoS Pathog. 2014; 10(2):e1003970. doi: 10.1371/journal.ppat.1003970 PMID: 24586170; PubMed Central PMCID: PMC3937277.

31. Baeriswyl V, Wodnar-Filipowicz A, Kalberer CP. The effect of silencing NKG2D through RNA interference on receptor functions in interleukin-2-activated human natural killer cells. Haematologica. 2006; 91(11):1538–41. PMID: 17043026.

32. Callewaert DM, Moudgil VK, Radcliff G, Waite R. Hormone specific regulation of natural killer cells by cortisol. Direct inactivation of the cytotoxic function of cloned human NK cells without an effect on cellular proliferation. FEBS Lett. 1991; 285(1):108–10. PMID: 2065773.

33. Dimitrov S, Lange T, Born J. Selective mobilization of cytotoxic leukocytes by epinephrine. J Immunol. 2010; 184(1):503–11. doi: 10.4049/jimmunol.0902189 PMID: 19949113.

34. Somersalo K, Carpen O, Saksela E, Gahmberg CG, Nortamo P, Timonen T. Activation of natural killer cell migration by leukocyte integrin-binding peptide from intracellular adhesion molecule-2 (ICAM-2). J Biol Chem. 1995; 270(15):8629–36. PMID: 7721764.

35. Hanke ML, Powell ND, Stiner LM, Bailey MT, Sheridan JF. Beta adrenergic blockade decreases the immunomodulatory effects of social disruption stress. Brain, behavior, and immunity. 2012; 26 (7):1150–9. doi: 10.1016/j.bbi.2012.07.011 PMID: 22841997; PubMed Central PMCID: PMC3506115.

36. Venstrom JM, Pittari G, Gooley TA, Chewning JH, Spellman S, Haagenson M, et al. HLA-C-dependent prevention of leukemia relapse by donor activating KIR2DS1. N Engl J Med. 2012; 367(9):805–16. doi: 10.1056/NEJMoa1200503 PMID: 22931314; PubMed Central PMCID: PMC3767478.

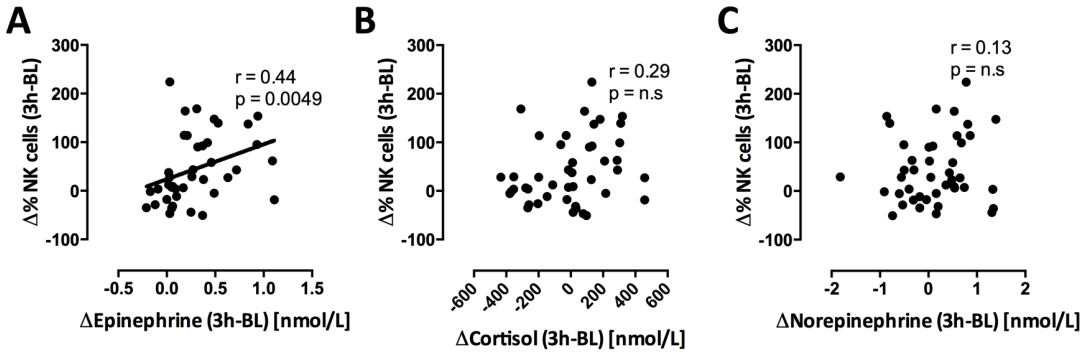

S1 Fig. Correlation of NK cell increase with serum hormone levels. Absolute change in NK percentage 3 hours after drug administration was correlated to change in concentrations of epinephrine (A), cortisol (B) and norepinephrine (C) 2 hours post treatment. Spearman correlation and nonlinear fit were applied.

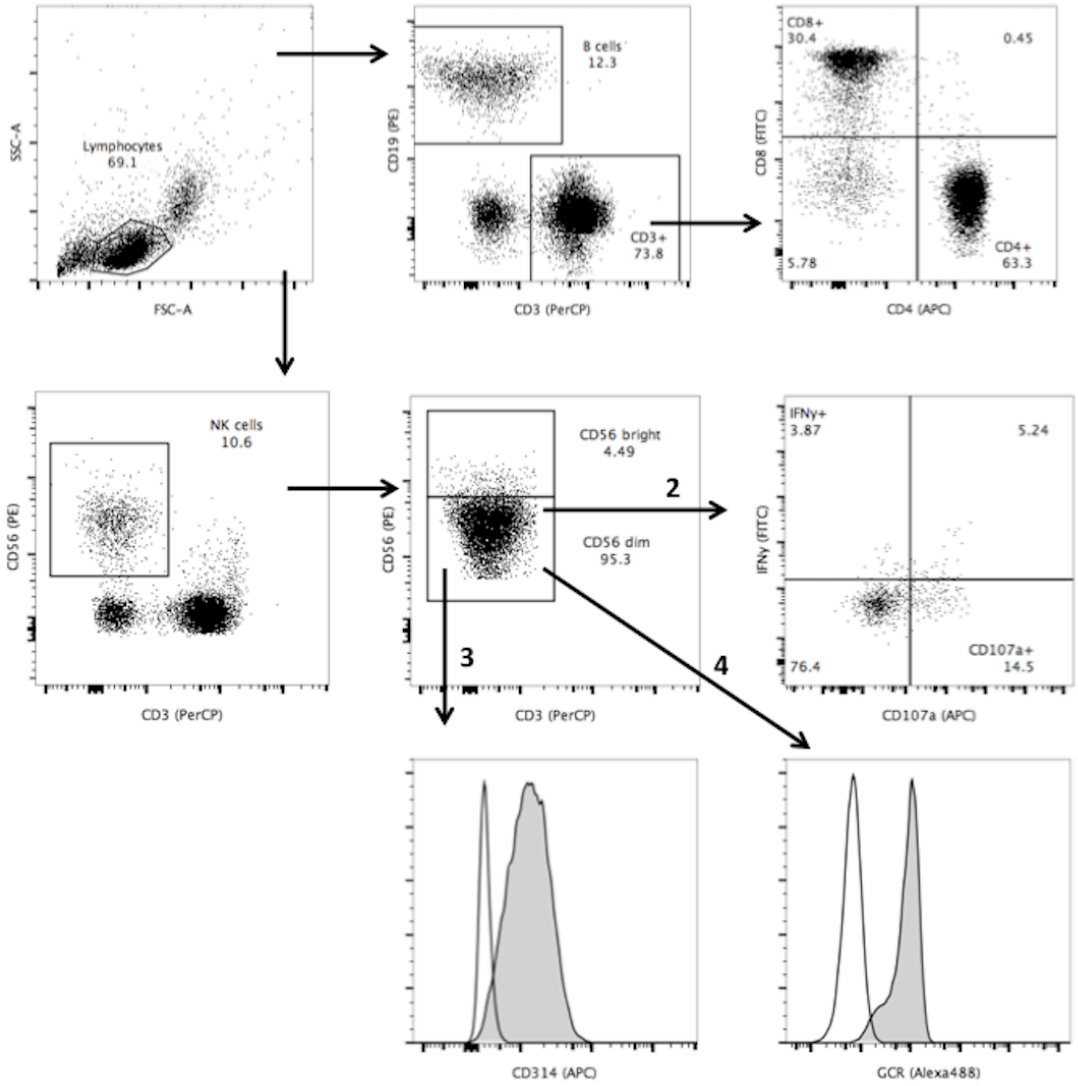

S2 Fig. Gating strategy to define lymphocyte and NK cell subsets and to assess NKG2D expression and IFNγ and CD107a production in NK cell subsets. The top row shows the gating in order to distinguish B cells, CD4+ and CD8+ T cells. A second panel was used to detect NK cells, further subdividing them into CD56 dim and CD56 bright NK cells and analyzing IFNγ and CD107a production (2, middle row, data is shown for CD56 dim). A third panel was designed to detect NKG2D expression (3, CD314, bottom middle) and a last one to stain for the glucocorticoid receptor (4, bottom right) on NK subsets. In grey, full stainings are shown whereas in white, an FMO staining is depicted for NKG2D and an isotype control for GCR. All data was acquired on an Accuri C6 (Becton Dickinson).

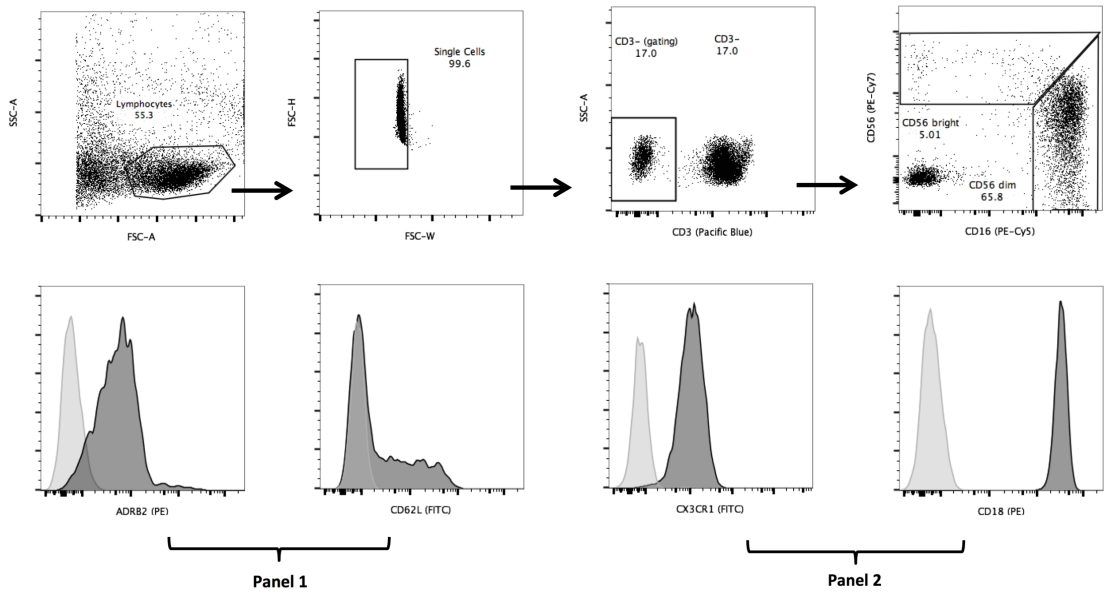

S3 Fig. Gating strategy for the analysis of adhesion and hormone receptor expression on NK cell subsets. NK cells were defined by CD16 and CD56 expression on single, live CD3- cells (upper row). The first panel stained for ADRB2 and CD62L on NK cell subsets whereas the second panel stained for CX3CR1 and CD18. Example stainings on CD56dim NK cells are shown in dark grey while isotype control (ADRB2) or fluorescence minus one controls (FMO, for CD62L, CX3CR1 and CD18) are shown in light grey. All data was acquired on an LSRFortessa flow cytometer (Becton Dickinson).

SUPPLEMENTARY METHODS

Primers for real-time RT PCR

All primers were designed with Primer3 software in a way to create amplicons spanning exon-exon junctions wherever possible (except for ADRB2 and ACTB). We also aimed for maximal isoform coverage with help of the Ensembl database. Primers were ordered at Microsynth Switzerland.

Symbol	Forward primer	Reverse Primer	Product length
ADRB2	ACAGGGGAGCAGAGTGGATA	ACAGTACCTTGATGGCCCAC	104 bp
GCR	TGGGGACTCTGAACTTCCCTG	CTGTTGTTGCTGTTGAGGAGC	111 bp
ACTB	CGAGCACAGAGCCTCGCCTT	CATCATCCATGGTGAGCTGGCG	70 bp
GADPH	TCTTCTTTTGCGTCGCCAGCC	CCCAATACGACCAAATCCGTTGA	87 bp
PKG1	GTTGACCGAATCACCGACCT	GTCGACTCTCATAACGACCCG	115 bp
HPRT	ATGGACAGGACTGAACGTCT	TCCAGCAGGTCAGCAAAGAA	113 bp

Hormone receptor expression using real-time RT PCR

NK cells were enriched from PBMC using the magnetic beads based NK enrichment kit (Miltenyi Biotec) according to the manufacturer's instructions. $CD56^{bright}$ and $CD56^{dim}$ NK cells were then sorted on a FACSAria III (BD Bioscience) and RNA was extracted using the QIAamp RNA Blood Mini Kit (Qiagen). Up to 1 µg of extracted RNA was treated with 1 unit of DNAse I (Promega) to remove genomic DNA. Immediately afterwards, first-strand cDNA was generated by means of GoScript™ Reverse Transcription System according to manufacturer's protocol (Promega) using random hexamer primers and a $MgCl_2$ concentration of 3 mM. RT-PCR reactions (20 µl) contained variable amounts of template cDNA (5 µl), 2x GoTaq Probe qPCR Master Mix (10 µl), nuclease-free water (3 µl) and 500 nM forward and reverse primers each (2 µl). Reactions were run in duplicates in a 7500 Fast Real-Time PCR System (Applied Biosystems). The amplification process consisted of polymerase activation at

95°C for 10 minutes, 45 cycles with 15 s of denaturation at 95°C and 1 minute of annealing and elongation at 60°C and a final elongation step for 1 minute at 60°C. Specificity of all primer pairs was confirmed with melt curves, efficiencies (E) were calculated with a standard curve of four serial dilution points according to the following formula:

$$E = 10^{(-\frac{1}{slope})}$$

For normalization, suitable reference genes had to be found. This was done by application of the GeNorm algorithm [40] for assessing the most stable expression in four potential reference genes in five samples. The two best reference genes (GADPH and PKG1) were used for relative quantification by application of the following formula:

$$NRQ = \frac{E^{\Delta Cq,goi,goi}}{\sqrt{E^{\Delta Cq,GADPH,GADPH} * E^{\Delta Cq,PKG1,PKG1}}}$$

where NRQ is normalized relative quantity, Cq is cycle of quantification and goi is gene of interest.